No. NYO-7828

Carnegie Institute of Technology

Department of Physics

STRAIN AMPLITUDE DEPENDENT INTERNAL DAMPING EFFECTS IN ALUMINUM AND MAGNESIUM SINGLE CRYSTALS

Robert Harry Chambers

NYO-7828

STRAIN AMPLITUDE DEPENDENT INTERNAL DAMPING EFFECTS IN ALUMINUM AND MAGNESIUM SINGLE CRYSTALS

by

Robert Harry Chambers

September 7, 1957

Carnegie Institute of Technology
Pittsburgh, Pennsylvania

AT(30-1)-1193

Issued September 7, 1957

II

TABLE OF CONTENTS

		Page
ABSTRACT		i
ACKNOWLEDGEMENTS		ii
PART I		
INTRODUCTION AND THEORY		
A.	Background	2
B.	Koehler Model	5
C.	Nowick Model	6
D.	Weertman Model	10
E.	Granato-Lücke Model	13
PART II		
EXPERIMENTAL CONSIDERATIONS		
A.	Method of exciting and detecting specimen oscillation	16
B.	Apparatus detail	18
C.	Measurement of the effective Young's modulus and the decrement	22
D.	Pickup calibration by quartz dummy specimen assembly	25
E.	Furnace construction, temperature measurement and control	27
F.	Oscillator and frequency measurement	28

III

Page

PART III

PREPARATION AND NON-ACOUSTICAL OBSERVATIONS OF CRYSTALS

A. The magnesium crystals 30

B. The aluminum crystals 31

C. Attaching the magnetic discs 34

PART IV

DATA

A. Amplitude dependence of decrement and Young's modulus at room temperature 35

B. Temperature dependence of the amplitude independent decrement and modulus 42

C. Temperature dependence of the amplitude dependent decrement and modulus 44

D. Time dependence 48

PART V

INTERPRETATION

A. Granato-Lücke Model parameters 54

B. Temperature dependence of the amplitude independent decrement and modulus 59

C. Temperature dependence of the amplitude dependent decrement and modulus 63

D. Time dependence 67

CONCLUSIONS 71

REFERENCES 72

APPENDIX 77

FIGURES

IV

UNCLASSIFIED

ABSTRACT

Internal damping and relative Young's modulus measurements were made of single crystals of four nines pure aluminum and magnesium and single crystals of zone refined aluminum in the kilocycle range. Particular attention was placed on strain amplitude dependent effects; measurements were made from room temperature to 400°C at strain amplitudes from 10^{-7} to 10^{-5} and as a function of thermal and mechanical history. Time dependent effects were studied in some detail, and a correlation was made with these effects and certain anomalies in the amplitude dependent behavior. The amplitude dependent effects were described in terms of the pinned dislocation model of Granato and Lücke. It was concluded that this model can explain the above findings if it is assumed that the active dislocation density is of the order of 1/10 to 1/100 of the total dislocation density. It is believed that the time dependent effects can be attributed to the redistribution of the point-type imperfection atmosphere surrounding the dislocations.

IV

ACKNOWLEDGEMENTS

The author wishes to thank Professor R. Smoluchowski for his encouragement and assistance throughout the course of this work.

The author is grateful to the National Carbon Company for its generous financial aid in the form of a fellowship during the early part of this work and to the Atomic Energy Commission for its support during the past year.

The author also wishes to extend his sincere thanks to the following people:

L. Vassamillet for his x-ray studies and helpful discussions

J. Hall for his calibration studies

L. Couling of the Dow Chemical Company for the magnesium samples

The Aluminum Company of America for the aluminum ingots

H. S. Ingham of the Metallizing Engineering Company for his help in the spray bonding of the magnesium samples

W. A. Tiller for the zone refining of the aluminum ingots

A. Seeger, G. Schoek, A. Granato, K. Lücke, and J. Weertman for helpful discussions

I. M. Chambers for the preparation of the figures.

Finally, the author wishes to thank his wife most sincerely for help in preparing the manuscript and typing of this thesis.

Part I

INTRODUCTION AND THEORY NYO-7828

Of increasing importance in solid state physics today is the study of crystal lattice defects. These lattice defects may be classified by specifying the dimensionality of the defect: the point-type defect - missing, misplaced, or outsized atoms; the line defect - the dislocation (see Appendix); and the surface-type defect - certain dislocation arrays, intra- and inter-crystalline boundaries.

The measurements reported here are believed to represent information which can profitably be interpreted in terms of an interaction between defects from two of these classes, namely, the point defect and the dislocation. Conversely, if the interpretation is valid, then the model that has been chosen to interpret the data should provide a useful basis for further study of these defects.

Internal damping (or internal friction) refers to the dissipation of energy which accompanies the motion of any solid which is set into oscillation even though the solid may be completely mechanically and acoustically decoupled from its surroundings. A convenient measure of internal damping, and the one used here, is called the decrement δ

$$\delta = \Delta W/2W$$

where ΔW is the energy dissipated in taking the solid through a stress cycle and W is the elastic energy stored in the solid when the strain is a maximum in the cycle.

The internal damping effects which form the substance of the present study refer to 1) the dependence of the damping and the Young's modulus of a

crystal upon the amplitude of oscillation, the temperature of the measurement, and the thermal and mechanical history of the crystal; and 2) certain time dependent effects which involve the dependence of the state of the solid on the presence of the mechanical oscillations.

A. BACKGROUND

Much work on damping problems in Metals (1, 2) has been done on polycrystalline material measured at frequencies ranging from fractions of a cycle to several thousands of cycles per second and at strain amplitudes in excess of 10^{-5}. Most of these experiments are notable in that they exhibit linear characteristics; that is, there is little or no dependence of damping on the amplitude of oscillation. The theory of Zener (1), based on the flow of macroscopic thermoelastically induced heat currents, and linear relaxation mechanisms (2) such as the viscous flow of complex internal (grain) boundaries, stress-induced atomic rearrangements, or phase changes in certain types of lattices seem to explain most of the linear damping phenomena found in the above-mentioned experiments.

There have been, however, a number of damping experiments (3 - 23) in metals beginning with T. A. Read's systematic study of copper and zinc single crystals in the kilocycle frequency range (3,4,5) that show non-linear (strain amplitude dependent) phenomena. These experiments show that both the decrement and the Young's modulus are strongly dependent on the magnitude of the oscillating strain amplitude; moreover, both quantities obey the same amplitude dependence with the ratio of the change in the decrement to the change in the modulus being the order of unity. Since attempts to interpret these experiments in terms of intrinsically linear models have not been productive, it appears that the experiments showing

non-linear behavior represent an entirely different class of damping phenomena from those classed as linear relaxation mechanisms.

There are other features which set the non-linear experiments apart from the linear ones. The non-linear damping appears to be relatively frequency independent (11, 35) while linear damping shows characteristic relaxation-type frequency dependence (2). The non-linear damping is also associated with measurements made in relatively pure material and at low (10^{-8} to 10^{-5}) oscillating strain amplitudes; while linear behavior, on the other hand, is associated with higher (10^{-5}) amplitudes and generally less pure substances. In fact, by increasing the impurity level, a specimen which exhibits non-linear characteristics may change to one showing only linear behavior (22). Damping in crystals exhibiting non-linear behavior is greatly increased by small applied external stresses (3 - 8,10,14) while annealing reduces the damping (3 - 5,7,8,10,12). In general, extreme sensitivity to externally applied stresses, static or oscillating, is a characteristic of these non-linear damping phenomena.

Thus the mechanism responsible for non-linear damping must in some way be intimately related to those parameters which determine the mechanical state of the metal and which can be influenced by very small applied stresses.

In 1934, Taylor, Polanyi, Orowan, and others (24,25,26) proposed the line-like atomic defect called the dislocation to explain the ease with which plastic flow occurs in metals. Six years later in 1940 T. A. Read (3) suggested that dislocation motion was an adequate mechanism to account qualitatively for many of the observed features of the non-linear damping and modulus change.

More of the evidence connecting internal damping in single crystals with the presence of dislocations was found by T. A. Read in 1941 (4,5). His observations showed a large increase in damping with prior application of static stress and subsequent decrease of the damping to very low values by high temperature annealing. He also showed that there was a dependence of damping on orientation in hexagonal zinc where plastic flow by slip occurs only along the basal planes.

Another phenomenon that Read observed was the difference in the damping behavior between the metals zinc and copper. Zinc was found to exhibit definite time dependence: the decrement increased as the result of the oscillations that were necessary to make the measurement and decreased with time when the crystal was left undisturbed. Copper showed none of these time effects. The differences between zinc and copper were attributed to the difference in melting temperatures of the two metals; thus room temperature represented a higher effective temperature for zinc than for copper. Time effects in zinc were discussed in terms of dislocation mobility involving a balance between the numbers created by the vibrations and the numbers lost by migration out of the crystal.

In 1948 (27) Cottrell showed that point-type imperfections can interact strongly enough with dislocations to impede their motion and thus affect significantly a number of the plastic properties of crystalline materials.

Later (1950) T. A. Read suggested (29) that the essential difference between the time dependent behavior of zinc and copper probably lies in the different diffusion rates of foreign atoms in the two metals at room temperature - the foreign atoms diffusing to and influencing the motion of the dislocations.

In 1950 both Koehler and Nowick (28,30) proposed dislocation models to explain non-linear damping. Both of these models recognize that in addition

to dislocations, point-type imperfections are important to the understanding of these phenomena. Recently, Weertman (33) and Granato and Lücke (36,37) have constructed more elaborate dislocation-point imperfection models. These models will be discussed in the following sections.

B. THE KOEHLER MODEL

Koehler's model (30) considers a metal to contain long lines of dislocations held down or "pinned" at intervals along the lines either by other intersecting dislocations or point-type imperfections. The interaction with the point-type imperfections is assumed to be given by the Cottrell elastic binding (27). The resolved shear component of a stress applied to the specimen causes the segments between the pinning points to bow out in the slip plane (see Fig. 1). The pinning points are assumed to remain immobile during the time of application of the stress because the diffusion jump time for most pinning points is generally larger than the period of the applied stress.

An internal damping experiment would then consist of applying a rapidly alternating stress to the specimen making the pinned dislocation lines vibrate like an elastic string held at points along its length. As the maximum value of applied stress increases, the Cottrell binding force will be exceeded at some places along the line and the dislocation torn loose from the pinning points resulting in a sudden displacement of the dislocation line during the first and third quarter of each cycle. Koehler assumed that during the second and fourth quarter of each cycle, the dislocations were repinned.

Since (31) a displacement of a dislocation means that more total strain results from a given applied stress than would otherwise occur if the dislocation were either not present or considered immobile, the dislocation

displacement is equivalent to a decrease in the effective Young's modulus. The depinning mechanism can then account, at least qualitatively, for the amplitude dependence of Young's modulus. Koehler also assumed that the motion of a dislocation is damped according to an interaction with the lattice which gives a velocity dependent retarding force. In Koehler's model, then, the amplitude dependent depinning mechanism would result in an amplitude dependent damping since depinning would allow more dislocation length to move at higher amplitudes and, hence, dissipate more energy.

A direct consequence of assuming that the damping force is velocity dependent is that the damping will depend in some manner on the frequency of oscillation. The details of the frequency dependence vary with the particular model chosen.

Koehler applied his model to measurements of single crystal copper and lead by Marx (12) and found that the magnitude of the damping predicted from estimates made by Eshelby (31), Leibfried (53), and Nabarro (54) of the intrinsic lattice damping constant was about 100 times smaller than that needed to give the magnitude observed. Marx (35) found evidence that the damping increases only slightly with increasing frequency in copper crystals.

C. THE NOWICK MODEL

A. S. Nowick (28) also made damping and modulus measurements in single crystal copper in the kilocycle range. His data had the typical non-linear characteristics noted previously; in addition, he found that the ratio r of the modulus change to the decrement change which Read had found to be independent of amplitude was independent of frequency and temperature as well.

In Nowick's attempt to explain non-linear damping phenomena, he examined two formal mechanisms: A) a non-linear relaxation mechanism which because it is a relaxation mechanism is frequency dependent; and B) a non-linear static

hysteresis mechanism which is frequency independent. He showed that mechanism A predicts different frequency dependence for the modulus change than for the decrement change and also that the ratio r defined above is dependent on temperature. Both of these results contradicted his data, but the hysteresis mechanism did not; furthermore, the particular hysteresis mechanism that he used predicted the value of the ratio r to be between 0 and 4, which was verified by his data.

Any static hysteresis-based mechanism must stand or fall on a determination of whether the damping phenomena concerned is frequency dependent. Some of Read's data seems to show a frequency dependence; Nowick's did not. Other authors find mutually contradictory evidence for this dependence. Nowick pointed out, however, that since non-linear experiments generally were made by resonant techniques, different frequencies could only be obtained by going to higher harmonics; and this meant measuring, in effect, different parts of the crystal because the maxima in the standing wave pattern must shift position with different harmonics. Variations, therefore, in dislocation density along the specimen could cause an apparent frequency dependency where none may in fact exist.

The following phenomenological approach to damping problems is also due to Nowick (2): Suppose a solid is subjected to an oscillating stress τ given by the real part of $\tau_o e^{i\omega t}$, where ω is the angular frequency of oscillation and t is time. Consider that a maximum principal strain in the oscillating solid is composed of two parts: S_e - the elastic component and S_p - the plastic or non-elastic component. Suppose also that in this body the non-elastic component S_p lags in phase behind the elastic component S_e. Complex notation will be used to express components with their phases so that S_p is given by

$$S_p = S_p' - i S_p''$$

where S_p' is that component of S_p which is in phase with S_e, and S_p'' is the component lagging 90° behind S_e. The total strain S_o is then given by

$$S_o = S_e + S_p$$

or

$$S_o = S_e + S_p' - iS_p'' \qquad [1.1]$$

If the non-elastic components do not exist, the stress and strain are assumed to be related by the elastic relation

$$\tau = YS \qquad [1.2]$$

where there exists the periodic sinusoidal solutions

$$\tau = \tau_o e^{i\omega t} \qquad [1.3]$$

and

$$S = S_o e^{i\omega t} = S_e e^{i\omega t} \qquad [1.4]$$

If the non-elastic strain components do exist, [1.3] and [1.4] will not be solutions to [1.2]. If the non-elastic components are non-linear functions of the stress, [1.2] will be a non-linear equation with [1.3] and [1.4] replaced by Fourier series solutions. Simple approximation solutions to [1.2] may be obtained by standard techniques employed in solving non-linear equations (32) for the condition that both non-elastic components of strain are small by comparison to the elastic component. These approximate solutions are

$$\tau = \tau_o e^{i\omega t} \qquad [1.3']$$

$$S = (S_e + S_p' - iS_p'')e^{i\omega t} \qquad [1.4']$$

where [1.3'] and [1.4'] are regarded as the fundamental Fourier components, and the higher order components are ignored. The lag angle ϕ is then given by

$$\phi = S_p''/S_e \qquad [1.5]$$

Furthermore, from the definition of the decrement δ given on page 1,

$$\delta = \pi\phi . \qquad [1.6]$$

The dynamic modulus is defined as

$$Y' \equiv \frac{\tau_o}{S_e + S'_p}$$

If $S'_p \ll S_e$,

$$Y' = Y(1 - S'_p / S_e) \qquad [1.7]$$

or defining the modulus change $\Delta Y = Y' - Y$,

$$-\Delta Y/Y = S'_p / S_e . \qquad [1.8]$$

The decrement is thus proportional to the out-of-phase component of the non-elastic strain, and the modulus change is proportional to the in-phase non-elastic component.

Combining [1.3'] and [1.4'] by eliminating the parameter ωt yields (again for S'_p and S''_p small) a quasi-linear stress-strain hysteresis loop. To the approximation that the first Fourier component is an adequate solution, this loop is an ellipse with major axis having a slope proportional to the dynamic modulus Y' given by [1.7] above. The area contained within the loop is, of course, equal to ΔW, the energy dissipated per cycle.

It can be seen from the above considerations that almost all the essential features of damping phenomena are contained in the knowledge of the form of the dependence of the non-elastic strain components on the total stress and in whether the hysteresis loop is dependent on the frequency.

Nowick interpreted his static hysteresis mechanism in terms of the hysteretic displacement of dislocations. Dislocation lines are considered to be pinned at low total strain amplitudes and progressively unpin with increased amplitudes as in the Koehler model. Nowick's model does not assume that the dislocations become repinned to the same pinning points on the return quarter cycle, however; he assumes that as they unpin, they move rapidly to other potential minima near by.

Since this model makes no use of a velocity dependent damping force and since the time required for the dislocation displacement to occur is considered

to be negligible compared with the period of oscillation used in most experiments, it meets the requirements of a static hysteresis model. Nowick did not extend his model to find an expression for the amplitude dependence of the decrement and modulus change; he did, however, consider the reasons for the observed dependence of these quantities on temperature. The pinning point population and, hence, the form of the relations between the amplitude and the non-elastic strains were postulated to depend on a Boltzmann factor: the fraction of available pinning sites left unoccupied was taken to be proportional to $\exp(-V/KT)$ where V is the interaction energy between solute atoms and the dislocation. The value he obtained for V was 0.062 eV for the interaction in copper; this is believed to be of the correct order of magnitude for most soluble solutes in copper.

D. THE WEERTMAN MODEL

Weertman and Salkowitz (19) obtained much detailed damping data at kilocycle frequencies in lead and lead alloy single crystals. Their lead data was characterized by a large zero amplitude decrement and the typical non-linear amplitude dependence of the modulus and decrement.

The model (33) used to explain this data was a modification of Nowick's non-linear static hysteresis mechanism. The pinning feature was abandoned since Cottrell binding calculations indicated that the solutes in lead could not interact strongly enough with dislocations at temperatures encountered in their work (27°C and up).

In place of pinning, a collective long-range interaction with solute atoms was used based on a solution-hardening model due to Mott and Nabarro (55). By relinquishing the concept of pinning, the Weertman model emphasizes the explanation of the amplitude independent region of damping and provides an

analytical expression for its value:

$$\delta_o = \frac{0.02 N \lambda b \mu}{\sigma_M} \qquad [1.9]$$

where δ_o is the zero amplitude decrement, N the total active dislocation density, λ the average distance between impurity atoms that interact with the dislocation, b the Burger's vector, μ the shear modulus of the lattice, and σ_M is the average retarding stress on the dislocation due to the random array of impurity atom stress fields calculated from the theory of Mott and Nabarro. The relation [1.9] does produce values for δ_o that generally give the correct order of magnitude, especially if it is assumed that not all the dislocations that are estimated to be in a crystal are participating in the damping process.

Weertman (34) also extended his model to explain the zero amplitude damping at high temperatures. The work of Pittenger (13), Birnbaum and Levy (18), Beshers (20), Kamentsky (21), and the present research all indicate that at temperatures above 100°C the zero amplitude damping in most metals rises very rapidly, showing only a slight tendency to saturate at the highest temperatures.

Weertman's high temperature model assumes that the nodal intersections formed by intersecting dislocations remain fixed during the internal damping measurement. Upon application of stress, the dislocation length between the intersectional nodes bows out in the slip plane reaching an equilibrium position determined by the balance between the force due to the shear component of the applied stress and the dislocation line tension. The dislocation line moves through a random distribution of point stress fields due to the dissolved unsegregated impurities. Weertman considers the motion of such a dislocation to be made up of a series of jumps made by short, coherent subsections of the line to new low energy positions. Each elementary

jump advances the whole line a certain average distance. Thus the line as a whole may respond to an applied stress only by moving in jumps into discrete energy wells; the energy of the bottom of each well increases for wells farther removed from the zero stress equilibrium position.

The height of the energy barriers separating the wells will depend on the applied stress in such a way that thermally activated jumps of the sub-lengths are more probable in directions that a free dislocation would move under the same stress. With this model, Weertman sets up a rate equation the solution of which is similar to the equation of motion of an inertialess elastic string undergoing forced oscillations and damped by a velocity dependent retarding force whose damping coefficient B is temperature dependent. The form of his solution is

$$\delta = A\Lambda \frac{B\omega}{C^2 + B^2\omega^2} \qquad [1.10]$$

where δ is the decrement, Λ the dislocation density, ω the angular frequency, C the dislocation line elastic restoring force, and A a constant depending on the properties of the lattice.

The relation [1.10] predicts a peak in the decrement as the temperature is raised; however, in the experiments that have been performed at low amplitudes, the temperature could not be raised high enough to find the peak. By performing experiments at lower frequencies, the peak temperature can be lowered; but it is difficult to do experiments at low enough amplitudes for low frequencies. The above mechanism is wiped out at the amplitude usually employed in low frequency damping experiments. [1.10] reduces to

$$\delta = \delta_1 \exp(-Q/KT) \qquad [1.11]$$

for temperatures on the low side of the peak. Both Q and δ_1 can be determined by Weertman's analysis. Comparison of the activation energies Q obtained by the above-mentioned investigators with that predicted by Weertman's formula

indicates that his value lies consistently below the observed values by about 20 to 50 per cent where the mechanism should be applicable.

E. THE GRANATO-LÜCKE MODEL

The most extensive effort to construct a dislocation model that can be compared quantitatively with damping data was undertaken by A. Granato and K. Lücke (36,37).

They took as a starting point the Koehler pinned, velocity damped dislocation model described in Section B. To obtain quantitative results, they considered in detail the action of an applied shear stress on a pinned dislocation. Consider Fig. 2. A dislocation of length L_N is shown held at its extremities by nodal intersections with other dislocations. Pinning points are distributed along the length of the dislocation, dividing it into loops which have lengths ℓ ranging from one lattice spacing to a maximum of nearly L_N. The average of this distribution of loop length is designated as L_c. With the application of a shear stress, the loops bow out in the slip plane (the plane of the paper) as is shown in A. Opposite A is plotted the resolved shear stress vs. the shear strain contributed by the displacement of the bowed-out dislocation. If the stress were released at this point, the line would return elastically to the equilibrium position under the restoring force produced by the line tension of the dislocation. B shows a depinning event where the applied shear stress has exceeded the pinning point binding force at a pinning point which is flanked by two long loop lengths. Once the line has started to break loose, the rest breaks away catastrophically as is shown in C. Breakaway is thus nucleated by a chance "weak" configuration of two long loop lengths placed side by side. The effect of breakaway is to increase the dislocation strain irreversibly

for now the freed loop has a smaller restoring force and will return over a different path in the stress-strain diagram (D, E) on the second quarter cycle. It is assumed that the dislocation will be retrapped by the pinning points, and similar events will occur on the third and fourth quarters with the signs of the stress and displacement reversed.

A hysteresis loop is generated by this elementary breakaway process; also on the average the "modulus" is lowered when breakaway occurs. It is seen from this model that as long as the applied stress amplitude does not exceed a certain value determined by the parameters - pinning binding force, number of pinning points, distribution of pinning points, and the dislocation network length L_N - damping due only to intrinsic velocity damping and a small modulus change is predicted. When the breakaway stress is exceeded, a large increase in damping and modulus, both of hysteretic origin, is obtained.

Granato and Lücke then calculate the effects of all the active network length in the crystal by making the following assumptions: 1) All the network lengths L_N are the same size; 2) At resolved shear stresses below breakaway, the loop lengths ℓ are distributed according to the Koehler relation (30)

$$N(\ell)d\ell = \frac{\Lambda}{L_c^2} e^{-\frac{\ell}{L_c}} d\ell \quad , \quad 0<\ell<L_N$$

where $N(\ell)d\ell$ is the number of loops with lengths between ℓ and $\ell + d\ell$; L_c is the average loop length; Λ is the total length per unit volume of the dislocation segments taking part in the breakaway process. As the resolved shear stress exceeds breakaway, the distribution function $N(\ell)$ changes to $N_1'(\ell)$ for the first quarter of the cycle and to $N_2'(\ell)$ for the second quarter of the cycle where

$$N_1'(\ell)d\ell = \begin{cases} \frac{\Lambda}{L_c^2} e^{-\frac{\ell}{L_c}} K(\mathcal{L}, L_c, L_N)d\ell & 0 \le \ell < \mathcal{L} \\ \Lambda \frac{\delta(\ell - L_N)}{L_N} F\, d\ell & \mathcal{L} \le \ell < L_N \end{cases}$$

where $\mathcal{L} \propto \frac{f_m}{\sigma}$, fm is the Cottrell binding force, σ is the applied stress, F is the fraction of the network lengths in which the catastrophic breakaway has occurred, and K is determined by the conditions that the length of line lost from the exponential distribution is gained by the delta distribution. In the second quarter cycle when the stress is decreasing, there is no change in the distribution of stress because the loops return elastically. Thus $N_2'(\ell)d\ell$ is the same as $N_1'(\ell)d\ell$ corresponding to the largest stress obtained during the first quarter cycle. Fig. 3 shows how $N_1'(\ell)$ changes with increasing resolved shear stress σ and also how the total dislocation strain S_T depends on σ. In A the stress has just exceeded breakaway, and the number of completely depinned network lengths is beginning to increase. In B further increases in stress begin to depopulate completely the shorter pinned loops, and in C the stress has reached such a value that nearly all the network lengths are unpinned.

Having found the equation of the hysteresis loop as a function of stress amplitude in terms of the parameters of the model, an application of the linearization techniques discussed in Section C yields the relations given in Fig. 4 for the amplitude dependent decrement and modulus change.

Since velocity dependent intrinsic damping is also assumed, the model must predict a frequency dependence; it turns out to be relatively insignificant in the kilocycle range but becomes important in the megacycle region when dislocation resonance effects occur.

Granato and Lücke have examined in considerable detail most of the available data that shows non-linear behavior in terms of their model and find reasonable fit by assuming plausable values for some of the more inaccessible parameters, e.g., L_N.

Part II

EXPERIMENTAL CONSIDERATIONS

A. METHOD OF EXCITING AND DETECTING SPECIMEN OSCILLATION

A resonant bar technique is used to measure the decrement and effective Young's modulus. The method used to excite the specimen into longitudinal oscillation and then to detect the oscillation appears to have first been reported by Wegel and Walther in 1935 (40). Subsequently, other investigators have used substantially the same technique of making measurements of damping and Young's modulus at temperatures up to 500°C (13). As used in the present experiment, this method consists of supporting the bar-shaped specimen horizontally on wires placed at the center of gravity of the bar (see Fig. 7). Longitudinal standing waves are induced in the bar by means of a telephone-type electromagnetic exciting unit which superposes a DC magnetic field on a variable AC magnetic field. The theory of this kind of driving unit is found in (41). Since the specimen is non-magnetic, the force coupling between the bar and the electromagnet was provided by a thin magnetic disc cemented to the end of the bar. The specimen oscillation is detected by means of a variable reluctance magnetic pickup; the variable component of the magnetic circuit is another magnetic disc cemented to the pickup end of the specimen. The alternating voltage developed in the pickup coils is measured by an electronic voltmeter; it is also amplified and displayed on a scope. Generally, this output signal is the sum of 1) voltage induced in the pickup coils as the result of the moving magnetic disc, of 2) air coupling to the pickup coils - the exciting magnetic field as the source; and of 3) air coupling to the pickup coils - external background fields as the source. Since only the specimen signal is desired, 2) and 3)

should be eliminated; 2) can be practically removed by taking the signal from the exciting unit and retarding its phase 180°, adjusting its amplitude, and then feeding it into the pickup circuit thereby cancelling out the undesired component. The cancellation was accomplished by the procedure indicated in the block diagram shown in Fig. 5 where, by manipulating in space two oppositely wound auxiliary coils, each in series with the exciting and pickup coils, cancellation could be effected. Both 2) and 3) were reduced considerably by surrounding the pickup coil with a high frequency eddy current shield. Aluminum sheet 1/8" thick proved to be effective for this purpose. Once a reasonably pure specimen signal was obtained, it was important to know whether a given change in the specimen oscillation amplitude was accompanied by a proportional change in output voltage; i.e., how linear was the pickup. It was also necessary to be able to calibrate the output signal, i.e., to find out what maximum strain corresponded to a given output voltage. Of course, if the maximum strain in the specimen and the mode of oscillation is known, the distribution of strains can be determined.

Both the linearity and the calibration of the pickup was established by substituting a quartz piezoelectric assembly for the specimen. The details of the piezoelectric assembly are discussed later in Section B. The essential features were as follows: A dummy of the specimen as regards to size and approximate fundamental resonant frequency was used. The same magnetic discs were attached to the dummy as were attached to the specimen. Reproducible geometry with respect to exciting unit, pickup, and specimen was maintained. The piezoelectric dummy output voltage was related in a known way through the piezoelectric and elastic constants of the quartz to the maximum strain amplitude in the dummy. By comparing the piezoelectric

output with the electromagnetic pickup output, a calibration was made (see Section D for another calibration method). It was also established that the pickup was linear to within several per cent through the strain range employed in the present experiments. These measurements were made at room temperature. Pittenger established (42) by a similar piezoelectric technique that the same pickup as was used in these experiments was linear, again to within several per cent, at temperatures up to 260°C. He also concluded that the calibration was essentially unaffected to within several per cent up to 260°C.

B. APPARATUS DETAIL

Fig. 6 shows the apparatus used in making most of the present measurements. The pickup magnet has been pulled out of position to show the placement of the specimen in the apparatus. The exciting unit or drive magnet is opposite the pickup. Both magnets are held by stainless steel supports which slide in stainless steel channels parallel to the specimen axis. Motion of the supports is controlled by backlash-free micrometer screws. Both support channels in turn are constrained to move on the opposite ends of an aluminum base rail. Removable pins can lock both of the steel support channels at desired positions along the rail. There exists a unique pinning position on the rail for each specimen such that a given magnet-specimen gap width can be maintained which is relatively independent of temperature. The correct location of the channel pins was determined in two steps for each specimen: The first was made by calculation using available coefficients of expansion for aluminum, stainless steel, and specimen material; the second involved setting the gap width near zero and using the resistance indicator as described later in

Section D to determine zero gap as the temperature increases. This method, of course, assumes that the first approximation is in error such that the gap closes with increase in temperature.

The use of the adjustable mounting on a central aluminum rail proved to be quite effective in solving the gap-width temperature dependence problem. As long as gap widths not less than 15 mils were used, it is believed that errors introduced in the strain amplitude calibration constant from changing gap width with change of temperature did not exceed five per cent.

Since it was necessary to eliminate air damping, provisions were made for enclosing the specimen in a vacuum while measurements were made at elevated temperatures. Earlier measurements were made by introducing the entire magnet-rail assembly into a vacuum chamber during a measurement run; the pressure obtainable was of the order of several microns - good enough to reduce air damping to a value not measurable. Later measurements were made in the apparatus shown in Fig. 6; the vacuum chamber enclosed only the specimen and specimen holder. Much better vacua were obtainable (10^{-3} to 10^{-4} microns); and hence, there was better control of the gaseous atmosphere surrounding the specimen. This latter design was prompted by the possibility of performing controlled hydrogenation experiments on magnesium single crystal specimens with the specimen *in situ* during gas charging. Results of several preliminary experiments in this direction will be discussed later in Part V.

In order to be able to control the gap width while maintaining a vacuum around the specimen, the vacuum case had to possess a certain mechanical flexibility in a direction parallel to the specimen axis. This flexibility was achieved by two large metal diaphragms which were hard

soldered to the stainless steel "O"-ring plates. Metal O-rings were used to provide a high-temperature seal. The most satisfactory metal was found to be either copper or commercially pure aluminum. The rings were fabricated by welding a stack of square metal plates together, turning out the inside, then mounting on a mandrel, clamping, and turning off the outside to the required dimension. The metal O-rings were coated with silicone varnish and baked at 400°C. This coating allowed a very good vacuum to be maintained even when the apparatus was cycled through a large temperature range.

Since temperatures in excess of 400°C were encountered, all joints had to be hard soldered; furthermore, since emphasis was placed on low contamination of the specimen, zinc- and cadmium-free solders were used. Most of the vacuum case was constructed of 1/8"-wall copper tubing. The ends of the tube that fit against the drive and pickup magnets were covered with 6-mil hipernik alloy sheet and hard soldered. It was found that this material was vacuum tight and gave very little eddy current loss - an important consideration when working with frequencies in the ten's of kilocycles range.

Details of the specimen support can be seen in Fig. 7. The arms and base of the support are made of a single 20-mil tantalum sheet drilled and bent into position. Tantalum wire of 6-mil diameter was threaded through the drilled holes and around a slightly undersized mandrel; then the two ends of the wire were twisted together. By slightly pinching together the support arms, the loop was enlarged; the specimen was then slipped through the loop and at the specimen's midpoint, the support arms were released; the loop shrinks, holding the specimen. Numerous experiments

show that the placement of the loop was not critical to within 1/16" on either side of the geometrical midpoint for reasonably uniform cylindrical bars. The support also functions to stabilize any imbalance between the opposing DC horizontal thrusts of the drive and pickup magnets.

The support is screwed into a fixture suspended from the top of the vacuum case through an insulating Stupakoff seal which is hard soldered to the case. The electrical insulation thus achieved was essential to the location of the zero-gap setting as was mentioned previously.

Both drive and pickup magnets were the same magnets as were used by Pittenger (12,13) in his work on the temperature dependence of kilocycle damping in aluminum and magnesium. Their construction details will be stated here; for further details, the reader is referred to Pittenger's thesis. The magnet cores are made of 40 five-mil hipernik (high-permeability, 50 per cent iron, 50 per cent nickel alloy) sheets; a silicone high-temperature varnish was used to insulate the laminations. Laminated construction was essential to reduce eddy current losses; and hipernik, when properly annealed in hydrogen, possesses a very low hysteresis. The cores are in the shape of a squared "C" with DC and AC coils on each arm of the "C." The separation distance of the tips of the arms is 1/16". The coils are wound on pyrex spools with No. 24 double silotex-covered magnet wire. In operation the DC coils carry 0.10 amps supplied by a 12-volt automobile battery. The voltage applied to the AC exciting coils varies from approximately 1/10 of a volt to 10 volts depending on the response of the specimen. The impedence of the coils is about 2000 ohms at 15,000 CPS. The geometry of both drive and pickup magnets and the coils is the same.

The horizontal thrust on the specimen due to the DC biasing field was 14 gmf at the gap width used in the experiments (15 mils).

C. MEASUREMENT OF THE EFFECTIVE YOUNG'S MODULUS AND THE DECREMENT

The raw data of the present experiments appear in the form of response curves as illustrated in Fig. 9. In this figure is plotted the output voltage from the pickup, calibrated in terms of maximum strain amplitude vs. the exciting frequency for values of relative driving force. Note that the shape of the response curve changes as the driving force, and consequently, the strain amplitude increase. For small amplitudes the response is essentially symmetrical about the central maximum and is thus characteristic of the behavior of a linear oscillator. For this linear type of response, the frequency corresponding to the position of the maximum is the resonant frequency f_r. As the strain amplitude increases, the response curve leans to the left and, finally, for large enough amplitudes becomes double valued. This double valued behavior means that different maxima can be obtained by traversing the response curve in different directions since there are unstable positions on the curve. The maximum obtained by descending from higher frequencies corresponds to a frequency called f_r'.

The peculiar response behavior noted above is characteristic of a driven oscillator whose restoring force decreases as the amplitude of oscillation increases. This kind of oscillator is called a soft non-linear oscillator (57).

It can be shown (57) that the relation between f_r' as defined above and the geometrical and physical constants of a long, thin, homogeneous, quasi-non-elastic, non-linear bar oscillating in the fundamental longitudinal mode is

$$\rho(2Lf_r')^2 = Y_o - Y_1(S) - Y_2(\delta[S]) \quad , \qquad [2.1]$$

$$Y_1 \ll Y_o, \quad Y_2 \ll Y_o$$

where ρ is the density, L is the length, and Y_o is the linear Young's modulus of the bar. Y_1 is a small, strain amplitude dependent term and Y_2 is a small term dependent on the damping, δ, which in turn may be dependent on amplitude. Thus in an isothermal experiment,

$$\frac{2\Delta f_r'}{f_r} \doteq \frac{\Delta Y(S)}{Y_o} \qquad [2.2]$$

where $\Delta Y(S) = Y_1(S) + Y_2(\delta[S])$.

In the present experiments where the decrement hardly ever exceeded 5×10^{-3}, the size of Y_2 could not have been larger than 1/20 of the observed modulus decrease $\Delta Y(S)$; thus $\Delta Y(S)$ can be attributed to $Y_1(S)$, the non-linear modulus term with only a slight contribution from the damping term. It is also qualitatively reasonable that most of the frequency shift with amplitude is due to an increase in the size of the non-linear modulus term because of the large jump effect; a shift in the frequency caused by an increase in damping is not accompanied by a jump effect.

Since the response curve at low strain amplitudes approximates the characteristics of a driven linear oscillator, the low amplitude decrement may be measured by observing A) the damping coefficient for free vibrations, B) the frequency width of the half power points on the resonance curve, and C) the ratio of the driving force to the amplitude at resonance (2).

As the response curve becomes asymmetrical and shows signs of the jump effect, methods A and B cannot be used; only method C is applicable (57) as long as the modulus shift does not exceed several per cent. Method C, however, presents the difficulty that if used by itself, the absolute value of the maximum driving force and the maximum strain amplitude must be determined.

Method B and C were used together in measuring the decrement. In method C, the driving current and output voltage were observed, the latter

being calibrated in terms of maximum strain amplitude by the method described in Section D. By measuring the decrement at low amplitudes by both methods B and C, the proportionality constant between the driving force and the driving current was determined. Method C was then used to obtain the decrement in the non-linear region.

The resonant bar technique necessarily yields values for the decrement and modulus change that have been integrated over a range of amplitudes from nearly zero at the ends of the bar to a maximum at the strain anti-nodes. It can be shown by the application of perturbation theory (58) that the integration over the bar gives for the integrated fractional frequency change $\overline{\Delta f/f}$ as a function of the maximum strain amplitude S_{max} the following:

$$\overline{\frac{\Delta f}{f}}(S_{max}) = \frac{1}{L}\int_0^L \frac{\Delta Y}{Y}\left[S(x)\right]\sin^2(\pi x/L)\,dx \qquad [2.3]$$

$$S(x) = S_{max}\sin(\pi x/L)$$

where x is measured along the length of the bar, S(x) is the strain amplitude along the bar, L is the length of the bar, Δf is the change in f associated with the change ΔY in Y, and f is the resonant frequency of a homogeneous bar of modulus Y.

Also, it can be shown (3) that:

$$\overline{\delta}(S_{max}) = \frac{2}{L}\int_0^L \delta\left[S(x)\right]\sin^2(\pi x/L)\,dx \qquad [2.4]$$

$$S(x) = S_{max}\sin(\pi x/L)$$

where $\overline{\delta}$ is the integrated decrement as a function of maximum strain amplitude.

In comparing theory with experiment, $\overline{\Delta f/f}$ and $\overline{\delta}$ give essentially the same numbers as $\Delta f/f$ and δ measured at the maximum amplitude S_{max} because

the theoretical expressions for these quantities (see Fig. 4) give an exponential dependence on the strain amplitude; and thus the maximum amplitude dominates the integration.

D. PICKUP CALIBRATION BY QUARTZ DUMMY SPECIMEN ASSEMBLY

The following discussion gives the details of the amplitude calibration and the establishment of linearity of the pickup output. Since it was impractical to obtain a quartz piezoelectric resonator the same length as the specimen (~17 cm), an assembly was constructed which consisted of a polycrystalline extruded aluminum rod the same dimension as the specimen; the center of the rod, two centimeters in length, was replaced by a piezoelectric x-cut quartz crystal of matching area by cementing together the quartz and aluminum with sauereisen cement. Because quartz and polycrystalline aluminum have about the same Young's modulus and density, the acoustical matching between the two materials was good. This assembly was supported in the same manner as the specimen, the wires acting in the dual capacity of mechanical support and electrical leads to the silver-painted electrodes of the piezoelectric oscillator. The Q of the dummy was, in general, lower than that of the specimen because the cement joints did not coincide with strain nodes; but this was of little consequence.

It was important to be certain that the gap distance between the magnetic discs and the pickup magnet was the same when the dummy was interchanged with the specimen. Good control over the gap distance was maintained throughout the experiments at room temperature by means of a spring-loaded backlash-free micrometer screw adjustment that permitted setting of the gap reproducibly to within 1/2 mil in 15 mils. Gap measurements and adjustments were made as follows: The specimen (or dummy) was electrically

isolated from the vacuum case through the wire support attached to the Stupakoff lead-through seal. Electrical contact was made to the magnetic disc end piece by painting a small aquadag strip bridging the cement. An ohm meter was connected between the case and the Stupakoff terminal; the micrometer screw was turned until continuity was established, thus determining the position at which gap width was zero.

The principal method that was used to obtain the value of the proportionality constant K connecting the cutput voltage V of the magnetic pickup and the maximum strain amplitude S in the dummy specimen was the same as that used by Marx (43).

$$S = KV \qquad [2.5]$$

Marx (43) shows that the relation between the maximum strain amplitude in a crystal resonating in the fundamental longitudinal mode and the voltage applied to the electrodes of the piezoelectric crystal is

$$S = \sqrt{2}\,\frac{bd'_{12} \cdot RV_{(rms)}}{S'_{22} \cdot Mf^2 L\delta} \qquad [2.6]$$

where $R = \sin\pi L'/2L$; L' is the length of the adherent electrodes; L is the total length of the dummy specimen; M is the total mass of the dummy specimen; b is the breadth of the bar; f is the resonant frequency of the assembly; d'_{12} is the piezoelectric constant taken to be: $d'_{12} = -6.85 \times 10^{-8}$ statcoulomb/dyne; S'_{22} is the relevant elastic compliance of quartz: $S'_{22} = 1.445 \times 10^{-12}$ cm^2/dyne; and δ is the decrement of the bar determined by measuring the frequency width between the half power points of its resonant response curve.

Calibration measurements were made as follows: The frequency of the voltage applied to the piezoelectric crystal was varied until a maximum pickup voltage was obtained; then both the pickup voltage and the piezoelectric voltage were recorded; the δ was then measured at that amplitude

by measuring the frequency width of the response curve. The driving voltage was increased and a new pickup voltage recorded. Since the decrement of the dummy oscillator was amplitude independent over a large range in strain amplitude, only one δ and frequency measurement was necessary. By this means K was determined for a given specimen-pickup gap width. To find the magnitude of the error introduced by not having the same gap width when the dummy was substituted for the specimen, K was measured for a number of widths on either side of the standard width. It was found that as long as the gap width exceeded 10 mils, K became a slowly varying function of gap width. In this way and by estimating the uncertainties in the measurements of the constants contained in [2.6] , it is believed that the strain amplitude is known to within about 10 per cent - the largest single source of error occurring in the setting of the gap.

E. FURNACE CONSTRUCTION, TEMPERATURE MEASUREMENT AND CONTROL

Most of the experiments were performed using a drop-type furnace with an open bottom. The furnace was constructed around an aluminum rectangular frame which held transite inner-lining sheets. Chromalox strip heaters were mounted around the top and sides of the inner lining. The outer side walls were covered by 1/16" 2-S aluminum sheet. The space between the outer walls and the inner lining was insulated with Silocel powder.

The apparatus was secured to a raised transite base; the space between the supporting wooden table and the transite base was filled with glass wool. The entire furnace with insulation weighed about 25 lbs., thus was relatively convenient to lower over the apparatus onto the transite base by hand.

When the best temperature control was required, the furnace received power regulated by a Raytheon line voltage regulator and then drawn from a

Variac. Part of the current to the furnace was controlled by a Wheelco Capacitrol regulator. If measurements were made below 100°C and the controller removed from the circuit, the temperature often would not drift more than several hundredths of a degree in 10 minutes - one advantage of the large thermal inertia of the furnace.

Temperature measurement was made by using a pair of iron-constantan calibrated thermocouples which were mounted firmly to the bottom of the copper vacuum case. It was determined that the equilibrium temperature recorded by a thermocouple placed in a dummy specimen and suspended in the same fashion as the regular specimen was very close to that recorded by a thermocouple mounted below the level of the specimen and close to the aluminum rail.

There was no question as to when equilibrium was established; the specimen itself was a very sensitive thermometer since the temperature variation of Young's modulus was large enough to enable a temperature change of 1/100 of a degree to produce a frequency change of about 1/20 CPS, a frequency change which was easily detectable. Conversely, good control of the temperature was essential to enable measurement of time dependent effects involving the modulus.

Generally, the thermocouples were considered sensitive enough; and it is estimated that the absolute error in the measurement of the temperature in the range 17° to 400°C did not exceed one per cent.

F. OSCILLATOR AND FREQUENCY MEASUREMENTS

The variable frequency oscillator was a negative resistance type (44) with tank circuit thermally insulated to reduce drift. Under favorable conditions, the drift rate did not exceed several CPS in an hour at 15 KC.

The smallest trimming capacitor enabled frequency increments of 1/50 CPS at 15 KC to be obtained.

The frequency measuring system consisted of a Millen standard oscillator, a multivibrator and mixer, and a Conn Chromatic Stroboscope (see Fig. 5). For construction details of the multivibrator and mixer, see (42). The 10 KC standard oscillator synchronized the output of the multivibrator which put out a one KC signal with higher harmonics. The one KC signal was mixed with the signal from the variable frequency oscillator; the resultant beat frequencies were amplified and put through a 500 to 1000 CPS band filter from which emerged only three frequencies: the one KC signal and two beat frequencies: f-1000n and (n + 1)1000-f where f is the signal frequency and n is an integer. The stroboscope was capable of measuring the beat frequency to five figures. A rough calibration of the audio oscillator was enough to determine n, and the behavior of the beat frequency when f was increased indicated which of the above-mentioned frequencies was observed.

Part III

PREPARATION AND NON-ACOUSTICAL OBSERVATIONS OF CRYSTALS

A. THE MAGNESIUM CRYSTALS

All the single crystals used in these experiments were grown by the Bridgman method in graphite crucibles. Six of the magnesium crystals were donated by the Dow Chemical Company; these crystals were grown in a Jilson-type variable resistance furnace. As received, the crystals were 13" long and 1" in diameter. To reduce the diameter of these crystals so that they could be held easily by the small wire support, each crystal was suspended vertically in a large graduate and chemically etched with 10 per cent nitric acid solution until final diameter was approximately 5 mm. Final cross sections of these crystals after etching were slightly eliptical depending on the angle with which the basal plane met the specimen axis. The crystals were then cast inside a glass cylinder with paraffin and the ends squared to the proper length with an acid-etch cut-off wheel. The orientation of each crystal (Tables I, II) and its perfection were studied by taking Laue back-reflection x-ray shots. Pictures were taken in directions perpendicular to both end faces of each specimen and the two photographs compared. Both ends of each crystal, D-1 through D-4, have the same orientation to within the limit of resolution of the back-reflection technique ($1/10^{\circ}$) and thus are considered to be single crystals in an extended sense. Crystals D-1 and D-2 were examined down their length by the same technique and again were found to be coherent crystals. Examination of the individual Laue spots indicated very little asterism in D-1, D-2, and D-3 and some slight spreading of spots on one face of D-4. The magnitude

of the asterism in the first three specimens was small enough to indicate that the local perfection was good (perhaps can be accounted for by assuming a random dislocation density of from 5×10^6 to 5×10^7 cm/cm3).

The spectroscopic analysis of the original unetched crystals supplied by Dow is as follows:

Atomic % Impurity

Al:	0.0004	Ni:	<0.0005
Ca:	<0.01	Pb:	<0.0005
Cu:	<0.0005	Si:	<0.001
Fe:	0.0033	Sn:	<0.001
Mn:	<0.0006	Zn:	<0.020

Also from other work with magnesium (45,46), the crystals used in the present work probably contain, in addition to the above, about 0.01 atomic per cent of hydrogen.

B. THE ALUMINUM CRYSTALS

The 4-9 aluminum specimens were 1 cm in diameter and about 18 cm long; 40 per cent aqua regia - 20 per cent HF acid etch - was used for the final finishing. Laue orientation pictures were taken and gave little evidence of asterism. After one of the crystals (4-9 Al-1) was acoustically measured rather extensively, it was machine cut in a manner described below to a smaller cross section to provide a better comparison with the machine-cut specimen ZR-Al-1. This machine-cut version of 4-9 Al-1 is called 4-9 Al-1C. The aluminum for the above specimen was donated by the Aluminum Company of America. The spectroscopic analysis for this material is as follows:

Atomic % Impurity

Si:	0.0019	Cu:	0.0004
Fe:	0.0005	Mg:	0.0008

Mn, Ca, and Na were not detected. There was also a possibility of carbon pickup from crucible and of gases, especially hydrogen.

The two zone-refined aluminum specimens ZR Al-1 and ZR Al-2 were made from another pure aluminum sample donated by Alcoa (sample 152461-A) with the following analysis:

Original Aluminum Stock Before Zone-Refining

Atomic % Impurity

Cu:	0.000	Si:	0.001
Fe:	0.001	Zn:	0.003

This sample was given about 40 zone passes in a carbon boat by W. A. Tiller of Westinghouse Research Laboratories. After refining, large portions of the ingot exhibited uniform optical flash planes indicative of single crystal structure. To reduce the possibility of contamination, square cross-sectioned bars were milled from the single crystal portions of the ingot using a 1/16" slitting saw. In an attempt to reduce the amount of mechanical distortion, light 20-mil cuts were made with the bed of the milling machine set at its lowest feed speed. Throughout the milling, copious quantities of oil-water coolant were used. Two 4.7 mm square bars about 18 cm long were obtained from this operation. Sections 1 cm long were removed from each end of both of these bars leaving each bar slightly over the desired specimen size.

The 1 cm long end sections were subjected to an intensive x-ray crystal perfection analysis by observing the width and fine structure of Bragg reflection spots with the Lambot technique (modified double crystal spectrometry) (47,48). This x-ray work was undertaken by L. Vassamillet at Carnegie Institute of Technology. The results of this analysis of the extent of the lattice distortion sustained by the crystal due to the milling operation are summarized in Fig. 8 where the index of lattice distortion used is the effective random dislocation density ρ. Some idea of the inhomogeneity

of the deformation was obtained by etching successive layers from the crystal sections and observing the change in the width of the x-ray patterns as etching proceeded; these observations are recorded in Fig. 8 as dislocation density ρ vs. effective specimen radius R. X-ray observation began only after a thin ($\sim$ 0.3 mm) heavily worked and recrystallized layer was etched away revealing the even flash planes of a single crystal below. It is believed that immediately under the recrystallized region, the dislocation density was as high as 10^9 cm/cm^3. As Fig. 8 illustrates, the density quickly drops to the order of 5×10^7 cm/cm^3 at R = 0.2 cm and appears to level out in the interior to a value of about 10^7 cm/cm^3. Both specimen bars were further etched so that their cross section was slightly less than 4 mm square. The etchant used to reduce the dimensions of the zone-refined specimens was an aqueous solution of 400 cc/lit HCl plus 5 gm/lit of NiCl. Other etchants including aqua regia and HF were virtually inactive. The average dislocation density of the finished bars was taken to be not more than 4×10^7 cm/cm^3.

A temperature study was undertaken, again using the Lambot x-ray technique, to discover whether the distortion configuration was stable at elevated temperatures. One of the four 1-cm sections mentioned above was studied. Ten hour anneals were made at increasing temperatures up to 550°C. No detectible change in the structure of the Bragg spot was noted until temperatures exceeding 200°C were reached. Annealing at 300°C showed strong breakup of the spot into many small lines indicating that the continuous nature of the distortion was changing into a block-like structure (polygonization). The final anneal at 550°C resulted in a sharply polygonal pattern.

With regard to the purity of the zone-refined specimens, ZR Al-1 and ZR Al-2, an estimate can be made as to what impurity species are probably not

present. The following is a list of available values of the ratio of the solubility of the given element in the solid aluminum phase to the solubility of it in the liquid aluminum phase (K values):

K	Value
Fe:	0.1
Si:	0.1
Cu:	0.3
Zn:	0.5

Since the end of the refined ingot that was used for preparing specimens was the "clean" end for K values < 1, and 40 zone passes is considered to be effectively infinite (56), one would expect to find Cu, Fe, Si, in concentrations less than 10^{-7} for the size ingot used. Very little can be said about such impurities as Mn which has $K > 1$ and hence should be concentrated in the specimen. Also little can be said about carbon or gaseous contamination; especially suspect would be hydrogen. There is some evidence (49) that hydrogen may exist in Al to as much as 10^{-5}.

C. ATTACHING MAGNETIC DISCS

The magnetic discs were attached to the aluminum specimens by cementing with a mixture of sodium silicate and aluminum oxide or sodium silicate and silicon dioxide (sauereisen cement). This cement did not crack with temperature changes if air dried for several days. Measurements by Pittenger (42) made by comparing both the eddy current drive and the magnetic drive at different temperatures showed that strains from the cement caused no observable change in the decrement. This result is reasonable since the discs are attached at strain nodes.

A two-step process proved necessary in attaching the magnetic discs to the magnesium specimens. First a thin layer of sprayed molybdenum was deposited by the Metco Spray-Bond Process; then the discs were cemented to this surface using sauereisen-type cement.

Part IV

DATA

A. AMPLITUDE DEPENDENCE OF DECREMENT AND YOUNG'S MODULUS AT ROOM TEMPERATURE

Both the decrement and Young's modulus of the aluminum and magnesium crystals described in Part III were measured as a function of strain amplitude and also as a function of temperature and time. In this section, data will be presented to describe the strain amplitude dependence of the decrement and modulus of these crystals at room temperature and for short measurement intervals (<5 seconds per measurement). The stipulation on the length of time to make a measurement anticipates the "time effect" which will be discussed in Section D.

Figs. 9 and 10 are typical examples of the highly non-linear behavior exhibited by all the high-purity and relatively undeformed single crystals studied. At low amplitudes a region exists that is relatively independent of strain amplitude; the decrement and modulus corresponding to this region will be called the zero amplitude or amplitude independent decrement and modulus - δ_o and Y_o respectively. That amplitude where the decrement and modulus show a 5 per cent change in their zero amplitude values will be called the breakaway amplitude, S_B. The quantity $\delta - \delta_o \equiv \Delta\delta$ will be called the amplitude dependent decrement, and $Y - Y_o \equiv \Delta Y$ will be called the amplitude dependent modulus or modulus change.

It will be noticed that beyond S_B both the modulus and the decrement change rapidly with increasing strain amplitudes. At still higher amplitudes both the modulus and decrement tend to decrease their rate of change

with increasing amplitude; i.e., the amplitude dependence saturates. Better examples of saturation can be seen in Figs. 9, 15, 16, 25, 28 - 31.

The decrease in the modulus with increase in strain amplitude is large enough at high strain amplitudes in all the crystals examined to exhibit the "jump effect" in the response curve (see Part II, Section C). Fig. 9 shows a good example of this effect in a zone-refined specimen of aluminum.

Fig. 11 is a plot of the amplitude dependent decrement vs. the fractional decrease in the Young's modulus $-\Delta Y/Y$, the fractional modulus change, for the aluminum crystals. It has been noted frequently (2,6 - 8, 10 - 12, 14,16,19) that this kind of plot generally gives a good linear relation over a considerable range of amplitudes. The slope r in this plot defined by

$$r = \frac{\delta - \delta_o}{-\Delta Y/Y}$$

ranges from about 0.35 in aluminum to between 1 and 3 in magnesium.

The Granato-Lücke model predicts that the quantities $\Delta\delta$ and $\Delta Y/Y$ depend on a homogeneously distributed oscillating strain amplitude S as shown in Fig. 4. To compare data obtained by the resonant bar technique with predictions from the Granato-Lücke (G-L) model, the integrated quantities $\overline{\Delta\delta}$ and $\overline{\Delta Y/Y}$ (Part II, Section C, p. 24) should of course be used. For reasons given on page 24, however, it is believed that little error results from using the unintegrated relations of Fig. 4 to fit the data.

Fig. 12 is a G-L plot : the reciprocal of the maximum strain amplitude vs. the product of the maximum strain amplitude and the amplitude dependent decrement. (In all the G-L plots, the term "decrement" stands for "amplitude dependent decrement," and "strain amplitude" means "maximum strain amplitude.")

It can be seen that the data satisfy the G-L relation moderately well. At low amplitudes, there does appear to be a definite departure from the G-L relation: In all low-amplitude cases examined there existed a "tail" with the data lying above the predicted line. The size of the deviation depends to some extent on the length of the anneal and the mechanical history of the specimen: the longer the anneal, the smaller the deviation.

Certain time effects which are evident while making room temperature measurements will be discussed here. These effects have a time constant of the order of days at room temperature and are called slow time effects. In contrast, those effects which are considered in Section D have a time constant of the order of hours and are called fast time effects.

Fig. 10 shows a good example of the slow time effect in the magnesium specimen Mg D-2 measured at 27°C. In a period of three days δ_o has dropped from 4×10^{-4} to 0.7×10^{-4}, and S_B has increased from 0.8×10^{-6} to 6.5×10^{-6}. Analogous behavior has been observed in zinc crystals (8) and has been called room temperature annealing. Similar changes in δ_o and S_B were observed in all magnesium specimens and in the 4-9 Al specimens. Along with these changes, room temperature annealing produced only a very slight increase in Y_o ($<0.1\%$).

In contrast, the room temperature annealing of ZR Al-1 and ZR Al-2 showed very little change in δ_o over a period of one week ($\delta_o = 12 \times 10^{-4}$ to 11×10^{-4}). The breakaway amplitude S_B and Y_o also showed effectively no change during this time.

In Fig. 13 is plotted the fractional increase $\Delta Y/Y_o$ in the Young's modulus measured at $S = 10^{-7}$ and 29°C vs. the time held at 150°C. This annealing has produced a large modulus increase ($\sim 1.3\%$); comparable

anneals of 4-9 aluminum and magnesium crystals produced modulus increases less than 1/10 of the above figure.

Fig. 14 shows another aspect of annealing above room temperature in the zone-refined specimens: δ_o decreases and the slope A in the G-L plot remains constant while the intercept B with the $1/S = 0$ axis decreases.

A summary of room temperature data for the aluminum specimens is contained in Table I, Page 40. Table II, page 41, gives a corresponding summary for the magnesium specimens. These summaries contain the following:

1). The gross purity and principal impurity

2). The perfection rating

3). Orientation

4). The mechanical history - annealing and handling history of the specimens

5). The slope A in the G-L plot and the quantity B/A^2 where B is the intercept with the $1/S = 0$ axis

6). The zero amplitude decrement δ_o

7). The slope r of the curve of amplitude dependent decrement vs. amplitude dependent modulus

The first three items of the above list were determined by the methods discussed in Part III. All of the above measurements were made in the fundamental mode at approximately 15,000 CPS.

The key on the following page gives the orientation values and the perfection ratings for the data listed in Tables I and II.

KEY TO TABLE I

ORIENTATION

4-9 Al-2	4-9 Al-1 4-9 Al-1C	ZR Al-1 ZR Al-2
$\alpha_1 = 73^\circ$	$\alpha_2 = 84^\circ$	$\alpha_3 = 125^\circ$
$\beta_1 = 56^\circ$	$\beta_2 = 35^\circ$	$\beta_3 = 36^\circ$
$\gamma_1 = 39^\circ$	$\gamma_2 = 123^\circ$	$\gamma_3 = 77^\circ$

where α, β, γ are the angles between the normals to the cube faces and the specimen axis

KEY TO TABLE II

The angle indicated under orientation in Table II is the angle between the normal to the basal plane and the specimen axis.

KEY TO TABLES I AND II

PERFECTION

	Dislocation Density
A	less than 10^7
B	greater than 10^7 but less than 10^8
C	probably greater than 10^8

ALUMINUM CRYSTALS MEASURED AT ~ 27°C, f~15,000 CPS.

SPECIMEN	GROSS PURITY ATM.%	PRINCIPLE IMPURITY (Al)	PERFECTION	ORIENTATION	MECH. HISTORY	ANNEALING TIME	ANNEALING TEMP.	$A \times 10^5$	B/A^2	$\delta_s \times 10^4$	r
2-9 AL-1								No observable amplitude dep.			
	99.0	Cu	C	POLYXAL	Drawn	100 hr	28°C	>10.0	---	4.0	---
4-9 AL-2	99.996	Si, Fe, Mg	A	α_1 β_1 γ_1	un-annealed	----	----	1.5	500	0.80	0.4
4-9 AL-1	99.996	Si, Fe, Mg	A	α_2 β_2 γ_2	un-annealed	----	----	1.5	800	1.0	---
		"	A	"	annealed	1000 hr	28°C	3.0	400	0.10	0.33
		"	A	"	annealed	30 hr	400°C	5.1	300	0.08	0.38
4-9 AL-1C		"	B	"	un-annealed	----	----	1.20	700	1.2	0.35
		"	B	"	annealed	30 hr	200°C	3.75	400	0.7	0.33
ZR AL-1	99.999?	C, N, O, H	B	α_3 β_3 γ_3	un-annealed	----	----	0.95	500	12.0	0.3
		"	B	"	annealed	100 hr	150°C	0.95	320	5.	0.3
		"	B	"	shock	----	----	0.72	400	11.0	0.3
ZR AL-2	99.999?	C, N, O, H	B	α_3 β_3 γ_3	un-annealed	----	----	0.90	550	14.0	0.38
					annealed	200 hr	150°C	0.95	300	6.0	0.35

TABLE I

MAGNESIUM CRYSTALS MEASURED AT ~27°C, f ~ 15,000 CPS.

SPECIMEN	GROSS PURITY ATM. %	PRINCIPLE IMPURITY	PERFECTION	ORIENTATION θ	MECH. HISTORY	ANNEALING TIME	ANNEALING TEMP.	$A \times 10^5$	B/A^2	$\delta_g \times 10^4$	τ
Mg D-1	99.97	Ca, Zn, Fe	A	26°	un-annealed	100 hrs	30°C	8.0	350	0.20	1.2
Mg D-2	99.97	"	A	65°	un-annealed	10 min	27°C	0.64	780	4.0	---
			"	"	"	72 hrs	27°C	5.0	300	0.80	---
			"	"	"	200 hrs	27°C	6.0	300	0.10	---
Mg D-3	"	"	A	30°	un-annealed	150 hrs	~27°C	2.0	600	0.9	2.5
Mg D-4	"	"	B	28°	un-annealed	100 hrs	~26°C	5.0	350	0.2	1.0

TABLE II

B. TEMPERATURE DEPENDENCE OF THE AMPLITUDE INDEPENDENT DECREMENT AND MODULUS

As the temperature is slowly increased above room temperature, the amplitude independent decrement of well-annealed aluminum and magnesium specimens increases gradually. At about 200°C for aluminum and 150°C for magnesium the rate of rise increases rather sharply. Fig. 15 is a good example of this temperature dependence in aluminum. δ is plotted vs. $1/T$. Crystal 4-9 Al-1 had been in the apparatus at 400°C for 30 hours and at successively lower temperatures for over 100 hours before the runs plotted in Fig. 15 were made.

The data show little scatter; the same curve is found by increasing as well as decreasing the temperature. Above 200°C a good straight line dependence is obtained.

Similar curves are found for annealed magnesium specimens with the exception that the straight line break starts 50° lower, and the slope and intercept of the straight line portion are slightly different.

Transient long-time constant effects can produce an apparent minimum in such a curve at temperatures between 100°C and room temperature. By either raising or lowering the temperature too rapidly, the room temperature decrement frequently could be raised five-fold. It is believed that the minimum reported by other observers (13,20) can be attributed to similar transient non-equilibrium effects.

The slope of the straight line portion in the aluminum specimens can be characterized by an activation energy of from 14 to 15 Kcal/mole; approximately the same values were obtained for the magnesium specimens. The values of the decrement δ_i obtained by extrapolating to the $1/T = 0$ axis ranged from 500 to 1000 in the aluminum specimens and from 200 to 500 in the magnesium specimens.

The following is a discussion of the dependence of Young's modulus on temperature. Measurements were made at low strain amplitudes ($S \approx 5 \times 10^{-8}$) of the resonant frequency of several aluminum and magnesium crystals as a function of temperature. A typical example, 4-9 Al-1, is shown in Fig. 16. Since the measurement is made at resonance with a thin bar, the square of the resonant frequency should show temperature dependence through the product of the Young's modulus and the reciprocal of the length of the specimen. From room temperature to about 150° C for aluminum and to about 100° C for magnesium, a linear dependency of f^2 on temperature existed; however, above these temperatures, a monotonic drop-off from linearity was exhibited in all specimens studied. By taking the difference between the observed variation of f^2 with temperature and the extrapolated (dotted line in Fig. 16) linear variation and then plotting this difference vs. the reciprocal of the absolute temperature, Fig. 17 is obtained. Variation of specimen length with temperature is excluded from contributing to the deviation from linearity since to a first approximation, it is linear. Corrections (50) due to the second order coefficient of expansion are noted in Fig. 17; they are small. The deviation observed, therefore, must be contributed only by the Young's modulus. It is seen that the deviation of Young's modulus appears to be a simply activated process with an energy of about 5.4 Kcal/mole for specimen 4-9 Al-1.

It is of interest to note the size of this deviation at several temperatures. At 200°C $(f^2 - f_o^2)/f_o^2 \equiv \Delta Y/Y = 50 \times 10^{-4}$, and at 400°C $\Delta Y/Y \approx 350 \times 10^{-4}$ for 4-9 Al-1.

The value obtained for the fractional change in Young's modulus per degree, dY/YdT, for aluminum was 5.3×10^{-4}. The literature contains values for this quantity for aluminum which range from 4.7×10^{-4} (51) to 5.9×10^{-4} (52).

C. TEMPERATURE DEPENDENCE OF THE AMPLITUDE DEPENDENT DECREMENT AND MODULUS

As the temperature increases, not only does the zero amplitude decrement increase and the modulus decrease, but the breakaway amplitude S_B also decreases as shown in Fig. 18. In Fig. 18 is plotted the total decrement vs. the strain amplitude as measured in the specimen 4-9 Al-1. This specimen first received a 30-hour anneal *in situ* at 400°C. Then the temperature was lowered at the rate of 10° per hour until 200°C was reached. The temperature was then lowered at a rate of 2° per hour until room temperature was reached.

Fig. 15 shows the course of the zero amplitude decrement during the temperature decrease. The amplitude was never increased beyond S_B during the first temperature descent. The first amplitude dependent run was made at 18°C. Care was taken to make each measurement as rapidly as possible (see Section D). As long as the measurement time was less than 5 seconds, reproducible amplitude dependent curves could be obtained. The temperature was then increased very slowly (4°/hr.) and held at the next desired measurement temperature for a minimum of 6 hours, and another amplitude dependent curve was made. This procedure was maintained throughout the experiment until 339°C was reached.

Fig. 15 also shows the zero amplitude decrement for these experiments during the second increase in temperature. It will be noticed that almost the same curve is followed on the increase as on the preceeding decrease in temperature. Reproducible amplitude dependent as well as amplitude independent curves were obtained as long as the rate of change of temperature did not exceed those used and sufficient time was taken between successive amplitude dependent runs. It became clear in earlier measurements that transient effects had to be eliminated before reproducible data could be obtained.

The amplitude independent decrement was subtracted from the data in Fig. 18, and a G-L plot was made for each temperature. Fig. 19 is the plot.

Fig. 20 is a plot of the slopes A of the curves in Fig. 19 vs. the reciprocal of the absolute temperature at which the slope was measured. It can be seen that over the range of temperatures from 18°C to 200°C the data can be fitted to an equation of the form

$$A = A_0 e^{Q/RT}$$

The following table gives the values of Q and A_0 obtained in this manner for some of the aluminum specimens:

	Q(Kcal/mole)	$A_0 \times 10^{\pm 5}$
4-9 Al-1	2.5 - 3.0	0.06
4-9 Al-1c	2.4 - 2.6	0.05
ZR Al-1	2.3 - 2.7	0.01 - 0.02

In Fig. 21 are shown the results of the plot of the quantity B/A^2 vs. 1/T obtained from the G-L plot in Fig. 19 for 4-9 Al-1. B/A^2 appears to remain approximately constant until 200°C; then it rises rapidly, increasing over 20 times in the next 100-degree interval. The break in B/A^2 vs. temperature curve occurs in the same temperature region where the exponential temperature dependence fa ls in the curve of Fig. 20. B/A^2 remained approximately constant (within 50%) for the other aluminum specimens; however, the temperature was never increased beyond 200°C with them so that no break above that temperature could be observed.

After the above experiment with 4-9 Al-1, it was removed from the apparatus, machine cut to the same dimensions by the same technique as was used to form the ZR Al specimens, entitled 4-9 Al-1C, and returned to the apparatus.

The unannealed amplitude dependent curve measured at 20° C appears in Fig. 22. This first run was made after the usual long time-constant effect had saturated (3 days). The value for δ_o was 1.2×10^{-4}. The breakaway amplitude is quite small (5×10^{-7}), and the curve levels off early only to proceed rising at higher amplitudes creating a plateau. Upon increasing the temperature to 140°C, S_B increases instead of decreasing; the plateau almost vanishes. Increasing the temperature 60° more results in the usual decrease in S_B and a regular, smooth increase after breakaway. The temperature was then slowly decreased to 26°C; the next room temperature measurements were then made. S_B had increased to about 3×10^{-6} and δ_o decreased to 0.8×10^{-4}. A slight trace of the plateau was still evident. Further room temperature annealing for 100 hours resulted in δ_o decreasing to 0.7×10^{-4} and S_B increasing to $\sim 3.5 \times 10^{-6}$. Very similar behavior was observed in the amplitude dependent modulus vs. amplitude plots with r remaining essentially constant throughout the above-mentioned changes.

Plateaus similar to that shown in Fig. 22 were observed in the other aluminum specimens before they were annealed in the apparatus. A carefully annealed specimen could be removed from the apparatus and then replaced - all the while using utmost care not to stress it - and plateaus might still appear. In all cases, S_B would decrease by almost an order of magnitude, and δ_o would rise three- or four-fold due to the handling operation. Subsequent room-temperature long time-constant effects would result in a decrease in δ_o and an increase in S_B but seldom to the same values as obtained before handling.

The handling operation could not be reproduced as far as the effects on δ_o and S_B were concerned. These observations regarding the effects of handling are consistent with the observations of others (see page 3).

Fig. 23 shows the amplitude dependent decrement vs. amplitude curves for ZR A1-1 after it had received a 100-hour anneal *in situ* at 150°C. The annealed curve for 4-9 A1-1C is included for comparison. The zero amplitude decrement vs. temperature dependence for this run is shown in Fig. 15.

In Fig. 24, a G-L plot is made of the 118°C curve obtained from the data in Fig. 23. After the run shown in Fig. 23 was completed and the temperature reduced to 27°C, the room temperature curve was again closely reproduced. Then an additional stress was applied to the crystal by increasing the DC biasing voltage by approximately a factor of 5. The points indicated by triangles show the amplitude dependence resulting from this mechanical shock.

D. TIME DEPENDENCE

Early in the investigation of the strain amplitude dependence of the decrement and modulus it became apparent, especially at elevated temperatures, that oscillations of amplitude in excess of S_B disturbed the mechanical state of both the magnesium and aluminum specimens. The disturbance was manifested by the failure of the curve of decrement and modulus vs. amplitude made by decreasing the amplitude to reproduce the curve made by increasing the amplitude. This type of behavior, analogous to the multiple valued B-H curves encountered in magnetic experiments, has been called the hysteresis effect(3,8,12). It was also noted that the size of the hysteresis effect depended upon the speed with which measurements were made. Particularly at high strain amplitudes, hysteresis effects could be induced if measurements were not completed in seconds.

In Fig. 25 an extreme case is shown in which "measurements" at several amplitudes were continued for 20 minutes and the resultant decrement vs. strain amplitude curve quickly made for lower values of amplitude. It is seen that there is considerable change from the original plot in which a measurement of the decrement at a given strain amplitude was made "instantaneously" (1 to 2 seconds per measurement). Fig. 25 also shows that the instantaneous decrement curve at amplitudes exceeding the amplitude at which the 20-minute "measurement" was made is relatively unchanged by the lower amplitude oscillation.

It is to be emphasized that only by making measurements, especially high amplitude measurements as quickly as possible, could the hysteresis behavior be avoided. If a high amplitude measurement was made too leisurely, however, and hysteresis noted, it was found that the original instantaneous

curve could be reproduced several hours later. It became evident that some sort of "excited state" which affected the amplitude dependent behavior of the crystal for amplitudes less than the highest amplitudes previously encountered was created by the oscillation and that this state was decaying and finally disappearing in the order of hours.

One crystal, 4-9 Al-2, after remaining in the apparatus for several months, was first measured instantaneously, then excited for 20 minutes at a strain amplitude of 7×10^{-6} and rested for 24 hours, measured instantaneously, excited again, etc., for a total of 15 cycles without significant changes in the instantaneous decrement vs. amplitude curve. Further investigation showed that this cycle could be reproduced apparently indefinitely.

Another effect that was noted and clearly related to the above is the following: Amplitude dependent measurements made at elevated temperatures and high amplitudes were found to be very difficult to make because both the decrement and the resonant frequency would change rapidly with time. In some cases the decrement might double in 30 seconds, which in turn would reduce the response of the crystal; the output voltage would drop necessitating an increase in the driving voltage to maintain the desired strain amplitude. Both Figs. 26a and 25 show this effect in Mg D-2 and 4-9 Al-2 respectively. This effect was evident in all the crystals measured. Fig. 26b is a plot of the variation of decrement vs. excitation time for various strain amplitudes in Mg D-2. A plot of $-\Delta Y/Y$ modulus vs. time for the same crystal shows a very similar variation, the ratio r being about unity - about the same as was observed in the instantaneous amplitude dependent measurements.

Fig. 26 a demonstrates the point mentioned above, characteristic of all specimens: No time dependence was ever noted as long as the excitation

was produced at strain amplitudes below the breakaway amplitude; also no hysteresis effects were noted if the measurements never exceeded the breakaway amplitude. Fig. 27 shows the strong temperature dependence found in the excitation experiments.

Figs. 28 through 31 represent the results of a set of time dependent experiments on the specimen ZR Al-1. The specimen was annealed in situ at 150°C for 100 hours and brought slowly to room temperature; $\delta_o = 4.5 \times 10^{-4}$ and $S_B = 1.5 \times 10^{-6}$. The temperature was increased to 45°C, and measurements were made of the decrement and resonant frequency vs. strain amplitude (Figs. 28,29). The solid triangles represent data taken "instantaneously," and the open triangles are points taken after the crystal was oscillated at $S = 2.5 \times 10^{-6}$ for 20 minutes (excitation time). The decrement at the excitation amplitude increased, and the resonant frequency dropped as indicated by the arrows. At the end of the excitation time, measurements were taken as the amplitude was lowered giving the triangle points; then the amplitude was increased and the rest of the points taken. The large increase in the zero amplitude decrement and frequency change as well as the slight depression of the decrement above the excitation amplitude should be noted.

Figs. 30 and 31 are corresponding curves taken at 115°C. The zero amplitude decrement and frequency change have become larger; the excited state is evidently decaying rapidly as can be seen by comparing the triangle points with the measurement (designated by the squares) made within several seconds after cessation of the excitation. The depression of the decrement is evident. The large change in the zero amplitude decrement and modulus following excitation was characteristic of the zone-refined material.

The following set of experiments were performed in an attempt to characterize more fully the nature of the excited state and the subsequent

decaying state. The specimen was first annealed in the apparatus at 400°C for 24 hours, then slowly (~5°/hr.) cooled to room temperature, and finally held at the desired measuring temperature until no change was detected in the zero amplitude decrement. This treatment resulted in the lowest zero amplitude decrement observed in these experiments. Next, an instantaneous decrement and modulus vs. strain amplitude curve was run. At high amplitudes where it was difficult to make a measurement fast enough or when the crystal was mistakenly oscillated for too long a period, measurement of the next higher point was delayed for several hours. Instantaneous curves taken this way were reproducible day after day. The crystal was then oscillated for a given time period (called the excitation time on some of the figures) at a high strain amplitude ($S \sim 10^{-5}$). At selected times after the end of the excitation period, instantaneous measurements were made tracing out the amplitude dependence of the decrement and modulus as the decay proceeded. These measurements were continued until the original instantaneous curve was obtained. In Fig. 32 an example of this type of measurement is shown. The specimen was 4-9 Al-1, and Fig. 32 records just three of the ten curves made at the temperatures 29° and 60°C. Very little change was observed beyond 2000 minutes in the decay sequence.

Fig. 33 is a Granato-Lücke plot of the decay sequence taken at 60°C and shown in Fig. 32. (Due to a drafting error, both scales of Fig. 33 should be divided by 3.) Only part of the decay sequence is shown, the sequence at 4 minutes and those later than 60 minutes being omitted. It is found that the slopes A of all of these curves decrease monotonically, the curve taken at 2000 minutes having the largest A.

It was also found that the quantity B/A^2 remained approximately constant during the decay sequence.

Fig. 34 represents the results of another experiment to determine both the form of the decay law and the effect of different excitation periods on that law. Crystal 4-9 A1-2 received the same annealing in situ as previously mentioned. Constant strain amplitude and temperature were maintained throughout the experiment. A short excitation period of two minutes was first made while recording the rise in decrement and decrease in resonant frequency every 30 seconds. The decrement followed the open circles starting from the zero time point indicated by a small solid circle. Following this excitation period, measurements were made instantaneously at frequent intervals. The time constant of the crystal response when the decrement was greater than 10^{-4} was such that rapid measurement could be made. The decay measurements following the two-minute excitation are recorded in Fig. 34 by solid circles. The decay was then followed until the decrement returned to the original value. Following the decay by recording the resonant frequency has been done; but since the decrement is of the order of 100 to 1000 times less sensitive to temperature changes than is the resonant frequency, the easiest measure to use was the decrement. Enough evidence has been obtained during fortunately stable thermal circumstances to show that modulus time dependence parallels that of the decrement.

By extending the excitation periods to longer times and recording the corresponding decays, the remainder of Fig. 34 was obtained. In all cases the excitation curves tend to saturate; runs to three hours and longer show very little measurable rate of change in the rise of the decrement. The reproducibility of the rise in decrement for longer excitation periods should be noted.

Fig. 35 is a plot of the quantity P defined in the figure vs. time during the decay sequence. δ_o is the initial decrement; δ_1 is the maximum decrement reached at the end of the excitation period. It is seen that such a plot shows good straight lines indicating that the decay follows the relation

$$\delta - \delta_o = (\delta_1 - \delta_o)\exp(-\beta t^n) \qquad [4.1]$$

Fig. 36 indicates that the power n of the time dependence is a function of the length of the excitation period ranging from about 1/3 for short five-minute excitations to about 2/3 for periods extending to saturation.

Figs. 37 and 38 show that β in [4.1] is inversely proportional to the strain amplitude and directly proportional to the quantity

$$(D/RT)^{1/3} \text{ where } D = D_o e^{-Q/RT}$$

for the decay following short excitation times. The Q for the decay process appears to be 8 or 9 Kcal/mole although this number is obtained from only four temperatures, three of which are included in Fig. 38.

PART V

INTERPRETATION

A. GRANATO-LÜCKE MODEL PARAMETERS

Since most of the amplitude dependent data discussed in Part IV can be satisfactorily fitted to Granato-Lücke plots, it seems that the Koehler-Granato-Lücke model would provide the best starting point for discussion of the data. The basis of this model is outlined in Part I, Section E.

From the G-L relations shown on Fig. 4, it is seen that the slope A of a G-L plot is proportional to the concentration of pinning points on the dislocation network. The intercept with the $1/S = 0$ axis gives the quantity "B." Combining these two measurements gives B/A^2 which is proportional to ΛL_N^3, a quantity which is a measure of the dimensions of the dislocation network.

It follows from the definition of the breakaway amplitude, S_B, and the G-L relations for reasonable ranges of values of δ_o, B, and S_B, that

$$A \doteq 10\, S_B;$$

so that, qualitatively at least, the concentration of pinning points is directly proportional to the breakaway amplitude.

For more quantitative information, the values of the parameters contained in the G-L model must be obtained. The following are the parameters that go into the model (compare Fig. 4):

$$R' = K\epsilon$$

$$\Omega = \frac{\sum_i f(\theta_i, \lambda_i) r(\theta_i, \lambda_i) \Lambda_i}{\sum_i \Lambda_i} \quad , \quad \sum_i \Lambda_i = \Lambda$$

ϵ is the atomic misfit parameter, $\frac{1}{a}\frac{da}{dc}$, or fractional change in the lattice constant a with the change in solute concentration C.

Λ_i is the density of dislocations active in the breakaway process on the ith slip system.

Λ is the total dislocation density active in the breakaway process.

$f(\theta_i, \lambda_i)$ is the ratio of the longitudinal component of dislocation strain to the dislocation shear strain on the i th slip system.

$r(\theta_i, \lambda_i)$ is the resolved shear stress factor on the i th slip system.

$K = [p^2 r(\theta_i, \lambda_i)]^{-1}$ where p is the cutoff parameter in Cottrell's expression for the elastic binding energy - $p \sim 2$ or 3, thus $K \sim 1/2$ to $1/5$.

The orientation factor Ω may be evaluated precisely only when the distribution of dislocations over the various slip systems is known. In lieu of strong objections to the contrary, it is assumed that all Λ_i are the same; then

$$\Omega = \overline{f(\theta_i, \lambda_i) r(\theta_i, \lambda_i)},$$

or the product $f(\theta_i, \lambda_i) r(\theta_i, \lambda_i)$ averaged over all i slip systems. Weertman (33) considers that for fcc crystals (12 slip directions on 4 slip planes)

$$\Omega \simeq 1/25.$$

The parameter K is also orientation dependent through its dependence on $r(\theta, \lambda)$.

For hcp structures (3 slip directions on the basal plane) orientation dependency should be particularly evident. Unfortunately, the four magnesium crystals used in the present experiments did not provide a good orientation spread and so were not useful in showing orientation dependence.

The appropriate values for ϵ can be estimated from x-ray studies of lattice constant change with alloying. Granato and Lücke consider $\epsilon = 0.1$ to be a representative value for some fcc systems.

From Table I, page 40, and Table II, page 41, the progress of the room temperature slow time effects and/or annealing can be followed by observing the change in the pinning point concentration C and the quantity ΛL_N^3. In the 4-9 aluminum and the magnesium specimens, the pinning point concentration increases during annealing but remains constant in the ZR aluminum specimens. The quantity ΛL_N^3 decreases in all crystals during the annealing sequence.

All the network lengths L_N are assumed to be the same size in original derivation of the G-L formulas. It is not difficult to show that if a distribution $g(L_{N_i})$ of network lengths is assumed, the quantity ΛL_N^3 is replaced by the fourth moment of L_N with respect to the distribution g: $\overline{L_N^4} = \sum_i g(L_{N_i}) L_{N_i}^4$. It is believed, then, that the most information which can reasonably be obtained from the B/A^2 measurements is that they are a measure of the distribution of network lengths with special emphasis placed on the longest lengths in the distribution. Thus in the annealing sequences, it appears that at least the longest lengths are being shortened. From x-ray studies (see Section B) it seems likely that the shortening should be attributed to the absorption of extra long lengths into the regular network.

If the G-L analysis is to hold, the amplitude dependent decrement and modulus must be associated with the long length part of the network length distribution. This relationship can be seen as follows:

Granato and Lücke point out that the mechanism of breakaway is inoperative if the excursion of a depinned loop does not exceed the local strain field of the pinning points; these considerations lead to the requirement that L_N exceed $\sim 5 \times 10^{-4}$ cm.

From the temperature studies (see Part IV, Sections B and C) in the 4-9 Al specimens, the G-L relations hold up at least to the break in the ln A vs. 1/T plot at 200°C (Figs. 20, 18). From the value of A, e.g., Fig. 20, obtained at 200°C and taking the above-mentioned estimates for K and ϵ, the concentration C of pinning points on the active dislocation lines at 200°C is 3×10^{-4}; this corresponds to an average loop length of $\sim 10^{-4}$ cm.

In the vicinity of 200°C (Fig. 16) the zero amplitude modulus deviation, $(\Delta Y/Y)_0 \sim 5 \times 10^{-3}$ (page 43). This modulus deviation is interpreted (Section B) to mean that enough pinning points have been dispersed from the entire network

by the increase in temperature to leave enough dislocation length free to decrease the modulus by ΔY.

From the relation (17,36):

$$(\Delta Y/Y)_o = 1/25 \Lambda L^2,$$

where L is the average pinned loop length at 200°C and assuming the total dislocation density Λ to be 5×10^6 cm/cm^3, L again must be $\sim 10^{-4}$ cm. But the G-L analysis breaks down for too sparce a pinning population; so L_N probably must exceed 10 times L or be $> 10^{-3}$ cm.

From room temperature values of B/A^2 and using the above-mentioned estimates for the model parameters, the quantity $\overline{L_N^4}$ is found to average 3×10^{-5}. For purposes of estimation, consider again that all L_N are equal; this leads to the product $\Lambda L_N^3 = 3 \times 10^{-5}$. If L_N is then taken to be of the order of 10^{-3} cm, $\Lambda \sim 3 \times 10^4$ cm/cm^3 where Λ is the dislocation density involved in breakaway.

The above estimates for L_N and Λ of the dislocations involved in the breakaway process should be compared with estimates of the average network length and density associated with relatively undeformed crystals. From x-ray estimates (47,48) such crystals probably have dislocation densities ranging from 10^6 to 10^7 cm/cm^3. These values for the density lead to average network lengths of $\sim$ 20 to 5×10^{-4} cm assuming once again a regular cubic-type network.

The existence of the long lengths is shown by the following strength experiments: 1) The critical resolved shear stress in pure magnesium single crystals is $\sim 35 \times 10^5$ dynes/cm^2 (71), and 2) the critical resolved shear stress in 4-9 aluminum single crystals is $\sim 10 \times 10^5$ dynes/cm^2 (68). The Frank-Read sources that produce slip at such low stresses must have a length of the order of 5×10^{-3} cm. Furthermore, Suzuki (59) points out

that dislocation lengths unattached to the dislocation network or mosaic walls have longer range stress fields than the network and, hence, gather in quantities of impurities which help to stabilize them.

Wyon and Lacombe (60) in studies on aluminum show that etch pits probably form preferentially on dislocations which have formed atmospheres of impurities. Lauriente and Pond (68) show that the etch pit density of 4-9 aluminum single crystals grown from the melt ranged from 0.7 to 2.5 x 10^5 cm/cm^3.

It seems, then, that from the above considerations relatively undeformed single crystals contain two classes of dislocations: one forming a network or mosaic and the other consisting of dislocations unattached to the network with longer effective lengths but having a total density of about 1/10 to 1/100 of the network dislocations. The unattached dislocations are surrounded by Cottrell "clouds" of the point-type imperfections; in "aged" crystals the network too is probably pinned by impurities. It is suggested that the pinned long length dislocations unattached to the network are responsible for the amplitude dependent decrement and modulus change.

B. TEMPERATURE DEPENDENCE OF THE AMPLITUDE INDEPENDENT DECREMENT AND MODULUS

Although there have been a number (30,31,19,33,36,37,38,53,54) of attempts to construct a model to explain the zero amplitude decrement in metal single crystals, only very limited success has resulted to date. In particular (31,53,54,69), it appears that an intrinsic loss based on the interaction of dislocations with a point-imperfection-free lattice yields a decrement several orders of magnitude too small at room temperature. Seeger's theory (39) of the Bordoni peaks at low temperatures appears to represent the most notable success of the intrinsic interaction theories. His mechanism involving the dislocation interaction with the Peierls stresses of the lattice is probably almost completely washed out at room temperature.

The Koehler pinned dislocation models do provide an explanation for an observed dependence of the zero amplitude decrement on the inverse fourth power of the pinning point concentration (70) but at the expense of predicting a linear frequency dependence which is not verified. The Granato-Lücke modification appears more promising in its prediction of a very slow frequency dependence in the kilocycle range.

Weertman's high temperature model (Part I, Section D) is in fair agreement with the facts, and several ways seem to exist to verify it experimentally by hunting in the right places for the peak it predicts.

At higher strain amplitudes ($S \sim 10^{-6}$) at high temperatures other effects may take place as has been pointed out by Birnbaum and Levy (18). Instead of considering that dislocation nodal intersections remain fixed as Weertman does in his treatment of the high temperature zero amplitude decrement, Birnbaum and Levy suppose that the intersections move in a non-conservative manner, i.e., producing interstitials or vacancies according to Seeger's creep theory (72).

The aluminum and magnesium zero-amplitude high temperature-dependent data obtained in the present studies are in fair agreement with Weertman's prediction (see page 42),(34).

It is interesting to note that plastic straining of the lattice increases the general level of the zero amplitude decrement but produces only slight changes in the form of its dependence on temperature (compare 4-9 Al-1C with 4-9 Al-1 in Fig. 15). Annealing is seen only to decrease the level of the decrement

If the zero amplitude decrement is the result of interactions with point-type imperfections, the increase observed in Fig. 15 as a result of the cutting operation cannot be due to an increase of impurities. Vacancies or interstitials formed during the deformation can interact with dislocations. At these temperatures they are mobile enough to be distributed quickly to low energy sites, i.e. either on the surface of the crystal, mutually annihilated, or segregated to dislocation lines. In metals like magnesium and aluminum the frequency of occurrence of jogs (61) on dislocation lines is fairly high; vacancies or interstitials can be annihilated at jogs resulting in an increase in the size of the jogged region and, on the average, contributing to the displacement of the dislocation perpendicular to its slip plane (climb). Thus in metals like magnesium and aluminum, deformation probably does not produce any additional effective point-type imperfections.

It is certain that deformation does produce an increase in total dislocation density. Thus it seems that the rise in the general level of the decrement upon deformation must be associated with an increase in the total dislocation density and the mechanism of damping be either an intrinsic interaction with the lattice or interaction at long range with the stress fields of the point-type imperfections existing before deformation.

The fact that the damping decreases with annealing probably excludes any short-range interaction mechanism such as proposed by Kessler (73).

The decrease in damping during annealing in ZR Al-2 (not shown in Fig. 15 but of the same order of magnitude as found in 4-9 Al-1C) is accompanied by a considerable increase $\sim$ 1.3 per cent in the zero amplitude modulus. X-ray studies show (page 33) that annealing of ZR aluminum at 200°C produces little observable change in either the total dislocation density or network configuration; annealing at higher temperatures (up to 550°C) showed strong evidence for the formation of a regular dislocation network pattern called polygonization but little overall change in the dislocation density.

Also the amplitude dependent data for zone-refined aluminum show little change in the pinning point concentration as a result of annealing, but $\overline{L_N^4}$ does increase.

One mechanism that would fit these observations would be the motion of dislocations which have screw orientation unattached to the general network; the damping might arise from a weak hysteretic interaction with impurities (Weertman mechanism) or an intrinsic lattice interaction.

It is very probable that in the zone-refined aluminum specimens the Weertman mechanism is not applicable since the solute concentration is probably very small (see Section C), and the dislocation density is fairly high as a result of the cutting operation. Compare the average distance λ between solute atoms with the average excursion, y, made by a dislocation at the lowest stresses ($\sigma = 5 \times 10^4$ dynes/cm^2).

$\lambda = b/C_o^{1/3}$ $\quad y = \ell^2 \sigma / 4Gb \quad$ where $\ell = 10^{-3}$ cm

$\lambda = 3 \times 10^{-6}$ cm $\quad y = 10^{-6}$ cm $\quad$ and $C_o = 10^{-6}$.

In both aluminum and magnesium the zero amplitude Young's modulus is observed to decrease linearly with increase in temperature from room temperature up to about 150°C in aluminum and about 100°C for magnesium. Above these temperatures it drops off from the linear variation in roughly exponential fashion (Figs. 16, 17). It is assumed that this departure from linearity represents an increased dislocation contribution to the strain resulting from the thermal dispersal of pinning points and perhaps freeing of dislocation nodal interactions at the highest temperatures.

It is also assumed that the Young's modulus of a perfect lattice free of phase transitions varies linearly with temperature in the temperature range investigated (63 - 66). Friedel et al. (17) have observed similar anomalies in the modulus in aluminum wires measured at low frequencies and have treated the temperature variation of the modulus in the same manner.

The apparent activation energy (5.5 Kcal/mole for aluminum) associated with this variation of the modulus is $\sim$ 2 times the pinning point binding energy (2.5 to 3.0 Kcal/mole). That this is reasonable can be seen as follows:

$$\Delta Y/Y \propto \ell^2$$

where ℓ is the average loop length, and $\ell \propto 1/C$ and $C \propto e^{Q_B/RT}$ (see Section C) so that

$$\ln \Delta Y/Y \propto -2\, Q_B/RT$$

where it is assumed that the concentration and binding energy of pinning points on the regular network is similar to the concentration and binding energy of points around the unattached dislocations, a condition probably valid only with long annealing.

C. TEMPERATURE DEPENDENCE OF THE AMPLITUDE DEPENDENT DECREMENT AND MODULUS

The basis of most of the present internal damping effects thought to be the interaction of the dislocation line with the point-type imperfections; and the Cottrell elastic binding is probably the major source of this interaction (69). Other sources of binding - "electrical" and "chemical" interaction (74,75) - have been proposed but are thought to be considerably smaller than the elastic binding (69).

Suppose a slightly deformed crystal contains solute atoms initially distributed homogeneously. Depending on the temperature and the binding energy between the solutes and dislocation, the solutes will diffuse to and condense on the dislocation lines. If the temperature is increased, a "back flow" of solutes can occur thinning out the concentration around the dislocation: At equilibrium the thinned-out concentration of solutes then forms the "Cottrell atmosphere." Cottrell et al. (76,77) developed an expression for the net flux of solutes through any volume element. By setting this net flux to zero it can be shown that the local concentration C' in an element of volume with interaction energy Q is

$$C' = C_o \, e^{Q/RT} \qquad [5.1]$$

where C_o is the concentration of solutes that would exist at very high temperatures when there is no segregation to dislocation lines and R is the gas constant.

Expression [5.1] is applicable when $C' < 1$, i.e., at a temperature $T > T_c$ where

$$T_c = Q_{max}/R \, \ln(1/C_o).$$

T_c for the measurements considered here may be estimated as follows: Q_{max} is taken to be Q_B, the Cottrell binding energy (69), estimated from the values of ϵ and p believed to be appropriate for solutes in aluminum and

magnesium (see page 55). Take Q_B = 3 Kcal/mole and $C_o = 10^{-4}$, then

$$T_c = 130^oK.$$

Thus [5.1] is applicable in the present experiments.

Pinning, therefore, must result from the acquisition of solutes from the Cottrell atmosphere and must be of a statistical nature: solutes coming from the atmosphere, sticking on the line for a time, and then moving back into the atmosphere. The "sticking" time must be longer than the period of the applied stress for pinning, in the Granato-Lücke sense, to apply.

From Fig. 4,

$$A = R'C$$

where C is the pinning point concentration, i.e., $C = C'_{max}$ where C'_{max} is the concentration of the atmosphere near the core of the dislocation. At this point the concentration is a maximum corresponding to the maximum binding energy Q_B.

If it is assumed that R' is a slowly varying function of the temperature, the variation of A with temperature may be given from [5.1] by:

$$A = A_o e^{Q_B/RT} \qquad [5.2]$$

where

$$A_o = K \epsilon C_o. \qquad [5.3]$$

Fig. 20 shows in aluminum that A does depend on temperature as [5.2] predicts up to about 200°C. A similar dependence was indicated in the magnesium specimens, but only limited data was taken and hence not reported in detail.

Although the aluminum data is fairly scattered, it seems that Q_B can be bracketed by the values 2.5 to 3.0 Kcal/mole (see table, page 45). Such values for the binding energy are not out of line with estimates made using the modified Cottrell relation (69); furthermore, from [5.3] and

the values assumed for K and ϵ on page 55

$$C_o \sim \begin{cases} 1 \times 10^{-4} & \text{for 4-9 Al-1} \\ 2 \times 10^{-5} & \text{for ZR Al-1} \end{cases}$$

These values for C_o are high, but not unreasonably so, since little is know about impurities such as the gas content not contained in the usual analysis. It is questionable whether dissolved gas can interact strongly enough to give a misfit parameter of the order of 0.1.

Throughout the above experiments the ratio r remained constant as shown by Fig. 11. Thus the same information concerning Q_B and C_o was obtained by observing the amplitude dependence of the modulus as was obtained by measuring .

That Figs. 19 and 20 represent an approach to equilibrium measurements was demonstrated by measuring the decrement and modulus vs. amplitude curve first by going to successively higher temperatures and then by decreasing the temperature slowly. Curves obtained in this fashion were quite repeatable as long as close attention was paid to maintaining very gradual temperature changes. Apparently thermal stresses were sufficient to displace pinned dislocation lines from their atmospheres and to reduce S_B making the crystal appear to be at a higher temperature than it actually was. Also, of course, the speed with which the Cottrell atmosphere might adjust to changes in temperature was diffusion controlled and could be a limiting factor at lower temperatures.

When data was repeatable, as discussed above, $\overline{L_N^4}$ remained essentially constant up to 200°C (Fig. 21) for aluminum specimens. The magnesium crystals were so very sensitive to thermal stressing that scatter obscured any trend which might have been present.

It would seem, therefore, that the Cottrell atmosphere could be either thinned by going to higher temperatures or concentrated by decreasing the

temperature while the distribution of network lengths remained relatively unchanged.

When well-annealed aluminum or magnesium received slight handling or thermal shock, S_B decreased; and many times the form of the breakaway curve changed from its characteristic smooth rise to the plateau mentioned on page 46. Apparently these small static stresses can pull dislocations out of weak parts of the pinning atmosphere and effectively change the random exponential distribution of loop lengths to a distribution in which an excess of long loop lengths prevails. The new non-equilibrium distribution makes the early part of a G-L plot resemble a plot taken at higher temperatures. Fig. 24 shows this effect in ZR Al-1. Either diffusion of the atmosphere to the new site of the dislocation or migration of the dislocation back to the atmosphere is probably responsible for the annealing effects shown in Fig. 22.

"Weak" parts of the pinning atmosphere probably occur because the concentration should depend on the orientation of the dislocation - the G-L model applies only to dislocations in edge orientation. Since the elastic binding force between a point imperfection which creates only dilatational strain and a close pair of partials forming a total dislocation in screw orientation is about one half of the force when the total dislocation is in edge orientation, one can expect less attraction of point imperfections to sections of the network in screw orientations. As a consequence, the proportions of long loop lengths are increased over the regular distribution; this, in turn, means that the breakaway should occur earlier. An explanation is thus suggested for the occurrence of the general "tail" in the G-L plot at low strain amplitudes even in well-annealed crystals and the early rise and plateaus in slightly stressed crystals.

D. TIME DEPENDENCE

The following is a summary of the experimental conditions that characterize the occurrence of the fast time dependence:

1. If the excitation amplitude S_E is less than the breakaway amplitude S_B, there is no change observed in the instantaneous curve - this includes the case when S_B is slowly increasing in a slow time annealing sequence.
2. A. There is effectively no influence of excitation on the modulus at amplitudes greater than the excitation amplitude S_E.
   B. Above S_E there does exist a slight depression of the decrement compared with the "instantaneous" curve measured in the same amplitude region.
3. If $S_E > S_B$, the instantaneous curve below S_E is
   A. Increased.
   B. An increase is evident in both the decrement and modulus measured at $S \sim 10^{-7}$, the increase being larger in crystals with smaller C_o.
4. The ratio r remains constant during excitation.
5. Excitation at very high amplitudes($S \sim 10^{-5}$) produces instantaneous amplitude dependent curves that resemble instantaneous curves taken at a higher temperature.
6. Excitation produces reproducible instantaneous amplitude dependent curves.
7. There is little or no time dependence in freshly strained crystals. Time dependence begins to occur as the crystal ages; return of time dependence is accelerated by high temperature anneal.
8. If there is no time dependence, there is no hysteresis effect; and if there is no hysteresis effect, there is no time dependence.

9. The decay following excitation at high amplitudes can be characterized by a sequence of G-L plots which show that:

   A. The pinning point concentration increases monotonically with time.

   B. The distribution of network lengths remains constant in time.

10. The dependence of the pinning point concentration on time during the decay following short excitation follows a $t^{1/3}$ law and following long excitation, approaches a $t^{2/3}$ law.

11. Limited observations indicate that the decay following short excitations is governed by a diffusion activation energy in the range 7 to 10 Kcal/mole.

From the summary 1 - 11 and the previous Sections A, B, and C, the use of the G-L model to interpret the amplitude data results in the following:

(a) Breakaway is necessary to produce time dependence - item 1.

(b) The disturbance produced by breakaway is such that it increases the number of long loop lengths - items 2, 5.

(c) From the nature of the loop length problem, the number of long loop lengths can be increased by 1) decreasing the number of pinning points on the line or 2) redistributing those present on the line, or both.

(d) The original distribution of loop lengths is recovered when the breakaway process is stopped - items 6, 9A - and during excitation and decay the network lengths are unchanged - items 6, 9B.

(e) Items 2 and 3A follow from (a) because network lengths either with a "strong" distribution of pinning points or larger concentration of pinning points will not have experienced breakaway and thus show no change in their response to instantaneous increases in S, while network lengths with either "weaker" distribution of pinning

points or smaller concentration of pinning points will have experienced breakaway and hence become weaker (b).

(f) Item 2B follows from 9B and (b) as well as the G-L relation.

(g) From the arguments used in Section C, it appears that pinning is statistical in nature; and therefore, it seems more reasonable to assume that the loop length distribution on each network length is randomized. Thus (e) must be interpreted in terms of different network lengths having different concentrations of atmospheres instead of different distributions of pinning points. Thus the orientation consideration mentioned in Section C isuseful here. Also only (c)-1 is permissible for the same reasons.

From these considerations, then, the excitation time dependence seems to be due to the thinning of the Cottrell atmosphere surrounding the long network lengths; the thinning is directly related to the phenomenon of breakaway. The decay following excitation is considered to be the densification of the atmosphere by diffusion back to the dislocation. The occurrence of the $t^{2/3}$ law following long excitations is suggestive of the Cottrell-Bilby strain aging relation (76). This in turn suggests that the excitation for long times has produced a thinning of the atmosphere which is fairly extensive and possesses cylindrical symmetry. The occurrence of the $t^{1/3}$ law suggests a planar distribution (78) of the atmosphere following short excitation.

The very low activation energy for diffusion (item 11) suggests that the atmosphere may be composed of nitrogen, hydrogen (see Note, p. 70), carbon, or perhaps vacancies. The difficulty with the assumption of a gas atom is that a mobile imperfection probably produces little dilatation and, hence, will have a very small binding energy to a dislocation. A vacancy is in a unique position of being both mobile and able to produce a relatively strong

interaction with a dislocation. It is believed, however, as was mentioned earlier (page 60) that vacancies are readily absorbed at jogs and thus removed from the pinning population in metals like aluminum and magnesium.

From the above arguments, the cause of the fast time dependence is considered to be: a pinning atmosphere which has high diffusivity and can be dispersed easily by a dislocation segment moving through it.

From evidence like item 7, the dislocation must have, in addition, a more substantial pinning atmosphere probably composed of metallic solutes and not subject to easy dispersal.

NOTE: That hydrogen was considered important in producing internal damping effects was shown by Marx and others (12,42). Some preliminary hydrogenation experiments on magnesium were undertaken prior to the present work, but the extreme thermal stress sensitivity of magnesium made decisive experiments difficult.

CONCLUSIONS

The interpretations of the results of this study are summarized below:

1. The Granato-Lücke pinned dislocation model satisfactorily explains most of the amplitude dependent decrement and modulus data for four nines pure aluminum single crystals from room temperature to 200°C. There is less detailed agreement for zone-refined aluminum and relatively pure magnesium crystals.
2. The density of the dislocations responsible for amplitude dependent damping and modulus is probably 1/10 to 1/100 of the total dislocation density.
3. The binding energy of the pinning point responsible for the amplitude dependent damping and modulus change in aluminum is 0.11 to 0.14 eV.
4. In four nines aluminum there is as yet an unidentified pinning point which has the above-mentioned binding energy but is very mobile; it appears to be responsible for the time dependent effects observed at room temperature and above.

REFERENCES

1 Zener, C., Elasticity and Anelasticity of Metals, Chicago, 1948.

2 Nowick, A. S., "Internal Friction in Metals" in Progress in Metal Physics, Vol. 4, Interscience Publishers, 1953.

3 Read, T. A., Internal Friction of Single Metal Crystals, Phys. Rev., 58, 371 (1940).

4 Seitz, F. and Read, T. A., Theory of the Plastic Properties of Solids, I., J. Appl. Phys., 12, 100 (1941).

5 Read, T. A., Internal Friction of Single Crystals of Copper and Zinc, Trans. AIME, 143, 30 (1941).

6 Lawson, A. W., The Effect of Stress on Internal Friction in Polycrystalline Copper, Phys. Rev., 60, 330 (1941).

7 Read, T. A. and Tyndall, E. P. T., Internal Friction and Plastic Extension of Zinc Single Crystals, J. Appl. Phys., 17, 713 (1946).

8 Swift, I. H. and Richardson, J. E., Internal Friction of Zinc Single Crystals, J. Appl. Physl, 18, 417 (1947).

9 Bordoni, P. G., Nuovo Cimento, 4, 179 (1947).

10 Wert, C. A., Internal Friction of Zinc Single Crystals, J. Appl. Phys., 20, 29 (1949).

11 Nowick, A. S., Variations of Amplitude Dependent Internal Friction in Single Crystals of Copper with Frequency and Temperature, Phys. Rev., 80, 249 (1950).

12 Marx, J. W. and Koehler, J. S., "Decrement and Young's Modulus Measurements on Single Crystals of Copper and Lead" in Symposium on the Plastic Deformation of Crystalline Solids, Office of Naval Research, 1950.

13 Pittenger, J., Temperature Dependence of Internal Friction of Single Crystals, Phys. Rev., 83, 872 (1951).

14 Weertman, J. and Koehler, J. S., Internal Friction and Young's Modulus of Cold-Worked Copper Single Crystals, J. Appl. Phys., 24, 624 (1953).

15 Bordoni, P. G., Elastic and Anelastic Behavior of Some Metals at very Low Temperatures, J. Acous. Soc. Am., 26, 495 (1954).

16 Takahashi, S. and Konno, H., Jap. Phys. Soc. Annual Meeting, 1954.

17 Friedel, J., Boulanger, C., and Crussard, C., Elastic Constants and Internal Friction of Polygonized Aluminum, Acta Met., 3, 380 (1955).

18 Birnbaum, H. and Levy, M., The Internal Friction of Aluminum Single Crystals as a Function of Temperature, Acta Met., 4, 84 (1956).

19 Weertman, J. and Salkovitz, E. I., The Internal Friction of Dilute Alloys of Lead, Acta Met., 3, 1 (1955).

20 Beshers, D. N., Internal Friction of Copper and Copper Alloys, Thesis, Univ. of Illinois, 1955.

21 Kamentsky, L. A., A Study of the Internal Friction and Young's Modulus of Pure Copper Single Crystals in the Temperature Range 25°C to 750°C, Thesis, Cornell Univ., 1956.

22 Weinig, S. and Machlin, E. S., Strain Amplitude Dependent Internal Friction Studies of Dilute Alloys of Copper, J. Appl. Phys., 27, 734, 1956.

23 Chambers, R. H. and Smoluchowski, R., Bulletin Am. Phys. Soc., March 1957.

24 Taylor, G. I., The Mechanism of Plastic Deformation of Crystals I, II, Proc. Roy. Soc., A145, 362, 388, 405 (1934).

25 Polanyi, M., Zeits. f. Physik, 89, 660 (1934).

26 Orowan, E., Zeits. f. Physik, 89, 605, 614, 634 (1934).

27 Cottrell, A. H., Report on Strength of Solids, (London: Physical Society), p. 30 (1948).

28 Nowick, A. S., "A Study of Amplitude-Dependent Internal Friction Arising from the Motion of Dislocations in Single Crystals of Copper" in Symposium on Plastic Deformation of Crystalline Solids, Office of Naval Research, 1950.

29 Read, T. A., (quoted in discussion to reference 28).

30 Koehler, J. S., "The Influence of Dislocations and Impurities on the Damping and Elastic Constants of Metal Single Crystals" in Imperfections in Nearly Perfect Crystals, Wiley, 1952.

31 Eshelby, J. D., Dislocations as a Cause of Mechanical Damping in Metals, Proc. Roy. Soc. London, 197, 396 (1949).

32 Minorsky, N., Non-Linear Mechanics, Chap. 12, Edwards Bros., 1947.

33 Weertman, J., Internal Friction of Metal Single Crystals, J. Appl. Phys., 26, 202 (1955).

34 Weertman, J., Dislocation Damping at High Temperatures, J. Appl. Phys., 28, 193 (1957).

35 Marx, J. W., (quoted in reference 33).

36 Granato, A. and Lücke, K., Theory of Mechanical Damping Due to Dislocations, J. Appl. Phys., 27, 583 (1956).

37 Granato, A. and Lücke, K., Application of Dislocation Theory to Internal Friction Phenomena at High Frequencies, J. Appl. Phys., 27, 789 (1956).

38 Mason, W. P., Relaxations in the Attenuations of Single Crystal Lead at Low Temperature and Their Relation to Dislocation Theory, J. Acous. Soc. Am., 27, 643 (1955).

39 Seeger, A., On the Theory of the Low-Temperature Internal Friction Peak Observed in Metals, Phil. Mag. (Eighth Ser.) 1, No. 7, 651 (1956).

40 Wegel, R. L. and Walther, H., Physics, 6, 141 (1935).

41 Kennelly, A. E., Electric Vibration Instruments, Macmillan, 1923.

42 Pittenger, J., Thesis, Carnegie Institute of Technology, 1952.

43 Marx, J. W., Use of the Piezoelectric Gage for Internal Friction Measurements, Rev. Sci. Inst., 22, 503 (1951).

44 Cruft Electronics Staff, Electronic Circuits and Tubes, McGraw-Hill, 1947.

45 Busk, R. S. and Bobalek, E. G., Hydrogen in Magnesium Alloys, Trans. AIME, 171, 261 (1947).

46 Bobalek, E. G. and Schrader, S. A., Ind. and Eng. Chem. Anal. Ed., 17, 544 (1945).

47 Lambot, H., Vassamillet, L., and Dejace, J., Sur la Mésure des Désorientations Réticulaires dans les Monocristaux Métalliques, Acta Met., 1, 711 (1953).

48 Lambot, H., Vassamillet, L., and Dejace, J., Détermination des Sous-Structures dans les Monocristaux Métalliques à l'Aide des Rayons X, Acta Met., 3, 150 (1955).

49 Schmid and von Schweinitz, Aluminum, 21, 772 (1939).

50 Hidnert, Bureau of Standards, 1925, as quoted in Handbook of Chemistry and Physics, Chemical Rubber.

51 Sutton, P. M., The Variation of Elastic Constants of Crystalline Aluminum with Temperatures between 63°K and 773°K, Phys. Rev., 91, 816 (1953).

52 Zucker, C., Elastic Constants of Aluminum from 20° to 400°, J. Acous. Soc. Am., 27, 318 (1955).

53 Leibfried, G., Über den Einfluss thermish angeregter Schallwillen auf die plastischen Deformation, Zeit. f. Physik, 127, 344 (1950).

54 Nabarro, F. R. N., Proc. Roy. Soc. A209, 279 (1951).

55 Mott, N. F. and Nabarro, F. R. N., Report of a Conference on the Strength of Solids, Phys. Soc., London, p. 1, 1948.

56 Pfann, W. G., Private Communication.

57 Stoker, J. J., Nonlinear Vibrations, p. 93, Interscience Publishers, 1950.

58 Slater, J. S., and Frank, N. H., Introduction to Theoretical Physics, p. 156, McGraw-Hill (1933).

59 Suzuki, T. and Imura, T., "Sub-Structures and Networks of Dislocations in Face-Centered Cubic Metals," in the Report of the Conference on Defects in Crystalline Solids, University of Bristol, 1954, The Physical Society, London, 1955, p. 347.

60 Wyon, G. and Lacombe, P., "The Influence of Dislocations and Impurities on the Distribution and Size of Etch Figures on Pure Aluminum," in the Report of the Conference on Defects in Crystalline Solids, University of Bristol, 1954, The Physical Society, London, 1955, p. 187.

61 Seeger, A., "Jogs in Dislocation Lines," in the Report of the Conference on Defects in Crystalline Solids, University of Bristol, 1954, The Physical Society, London, 1955, p. 391.

62 Levy, M. and Metzger, M., Effect of Heat Treatment on the Internal Friction of Aluminum Crystals, Phil. Mag., 46, 1021 (1955).

63 Bradburn, M., Cambridge Phil. Soc. Proc., 39, 113 (1943).

64 Ludloff, H. F., J. Acous. Soc. Amer., 12, 193 (1940).

65 Born, M., J. Chem. Phys., 7, 591 (1939).

66 Fürth, R., Proc. Cambridge Phil. Soc., 37, 34 (1941).

67 Baker, G. S., Internal Friction in the Presence of a Static Stress, J. Appl. Phys., 28, 734 (1957).

68 Lauriente, M. and Pond, R. B., Effect of Growth Imperfections on the Strength of Aluminum Single Crystals, J. Appl. Phys., 27, 950 (1956).

69 Cottrell, A. H., Dislocations and Plastic Flow in Crystals, Oxford, 1953.

70 Thompson, D. O. and Holmes, D. K., Dependence of Young's Modulus and Internal Friction of Copper upon Neutron Bombardment, J. Appl. Phys., 27, 191 (1956).

71 Nash, R. R. and Sheely, W. F., "Properties of Magnesium and Magnesium Single Crystals at Room Temperature," in Rensselaer Polytechnic Institute Technical Report, 1955.

72 Seeger, A., Phil. Mag. 45, 771 (1954).

73 Kessler, J. O., Internal Friction and Defect Interaction in Germanium: Theoretical, Phys. Rev., 106, 654 (1957).

74 Cottrell, A. H., Hunter, S. C., and Nabarro, F. R. N., Electrical Interaction of a Dislocation and a Solute Atom, Phil. Mag.

75 Suzuki, H., Chemical Interaction of Solute Atoms with Dislocations, Science Reports, Research Institute Tohoku Univ., A4, 455 (1952).

76 Cottrell, A. H. and Bilby, B. A., Dislocation Theory of Yielding and Strain Aging of Iron, Proc. Phys. Soc., 62A, 49 (1949).

77 Cottrell, A. H. and Jaswon, M. A., Proc. Roy. Soc., A199, 104 (1949).

78 Lement, B. S. and Cohen, M., A Dislocation-Attraction Model for the First Stage of Tempering, Acta Met., 4, 469 (1956).

79 Turnbull, D. and Hoffman, R. E., Acta Met., 2, 419 (1954).

APPENDIX

The properties of dislocations are discussed at length in such works as:

Read, W. T. Dislocations in Crystals, McGraw-Hill, 1953.

Cottrell, A. H. Dislocations and Plastic Flow in Crystals, Oxford, 1953.

Nabarro, F. R. N. "The Mathematical Theory of Stationary Dislocations," Adv. in Phys., July 1952.

A shorter account may be found in:

Kittel, C. Introduction to Solid State Physics, 2nd ed., Wiley 1956.

For the purpose of aiding in the formation of a concept of a dislocation which will suffice for the purpose of explaining internal damping phenomena, the following partial list of their properties is given (only dislocations related to slip are considered).

1. They are internal boundaries separating slipped from unslipped atomic planes.

2. As a boundary between two areas on a surface, they are essentially one dimensional.

3. As a boundary, they possess a boundary energy or energy per unit length or line tension and hence resist bending.

4. Since the slipped region will change its extent under the influence of a shear stress, the dislocation moves in response to an applied shear stress; dislocations, unimpeded, move very easily.

5. A dislocation can interact with other dislocations in such a way as to be made relatively immobile.

6. A dislocation can interact with point-type lattice defects; the interaction can influence the motion of both dislocation and point defect.

7. At increased temperatures, point-type defects interact less strongly with dislocations.

8. At increased temperatures, dislocations can move more easily under the influence of internal stress fields - move either to certain groups of dislocations and accumulate or annihilate or move to the surface of the lattice.

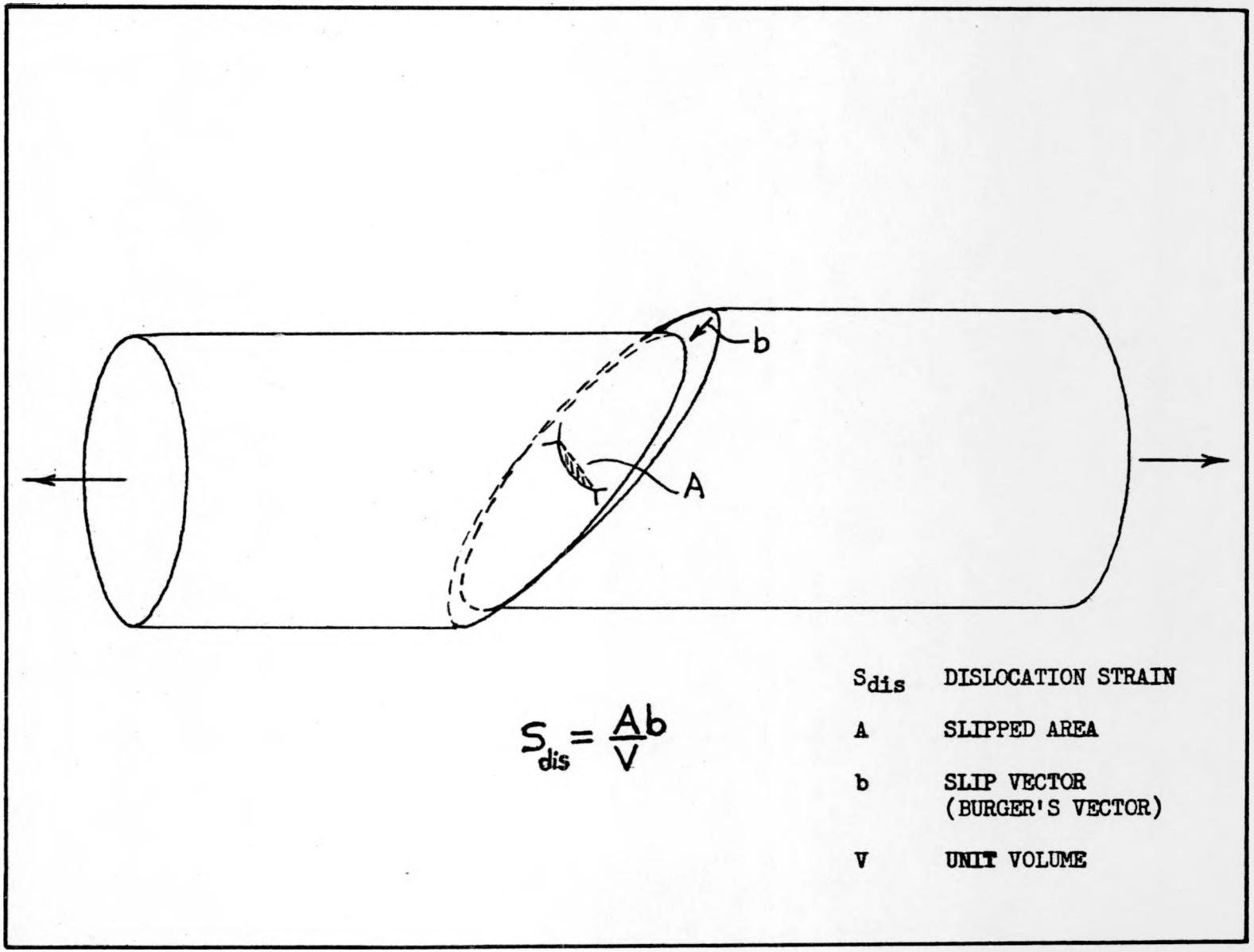
b
A
$S_{dis} = \frac{Ab}{V}$
S_{dis} DISLOCATION STRAIN
A SLIPPED AREA
b SLIP VECTOR (BURGER'S VECTOR)
V UNIT VOLUME

FIG. 1

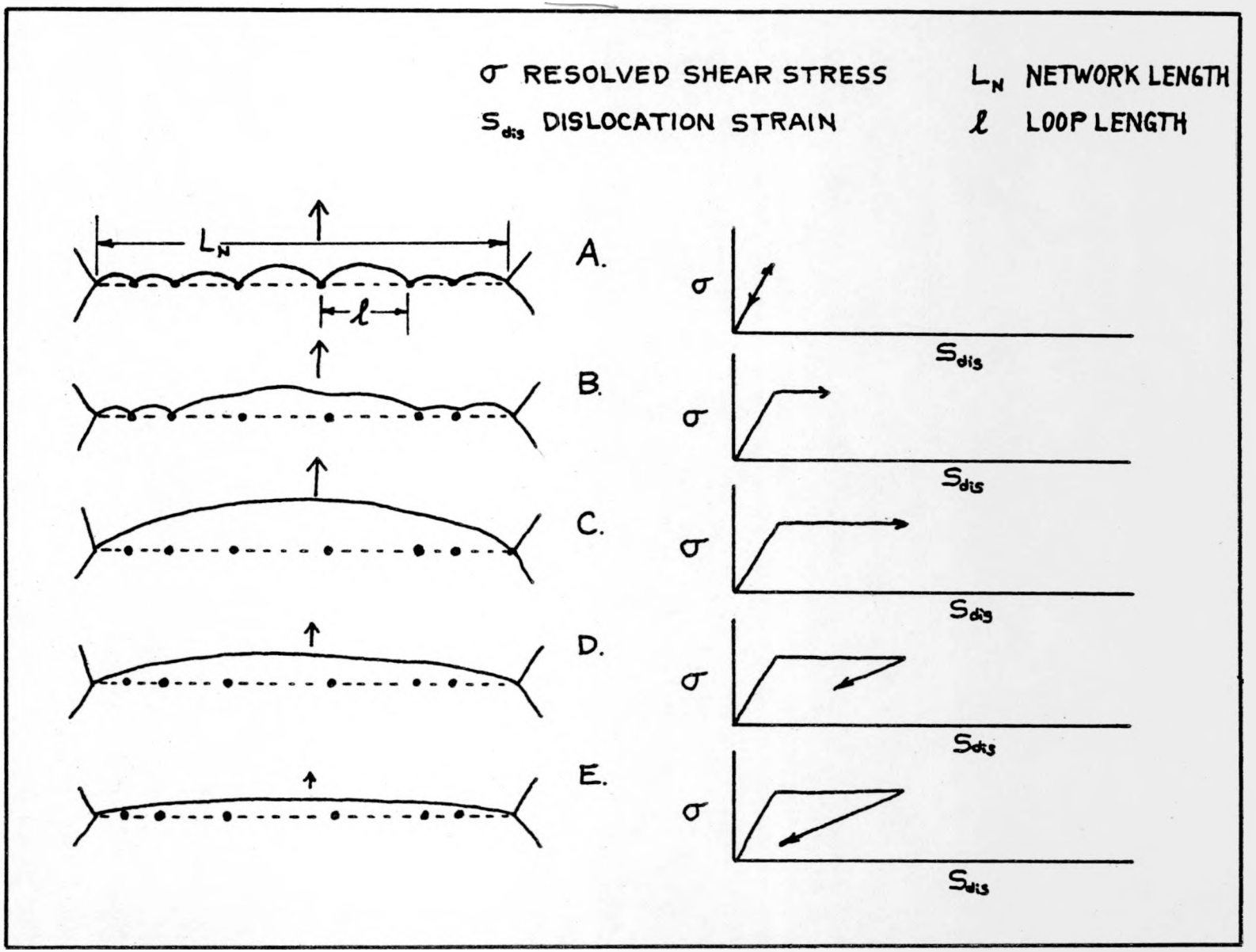
σ RESOLVED SHEAR STRESS
L_N NETWORK LENGTH
S_{dis} DISLOCATION STRAIN
ℓ LOOP LENGTH
L_N
ℓ
A.
B.
C.
D.
E.
σ
S_{dis}

FIG. 2

$\mathcal{L} \propto 1/\sigma$

$\mathcal{l}$ LOOP LENGTH

L_N AVERAGE NETWORK LENGTH

σ RESOLVED SHEAR STRESS

S_T TOTAL DISLOCATION STRAIN

$N_1(\mathcal{l})$ DISTRIBUTION FUNCTION FOR LOOP LENGTHS — 1ST 1/4 CYCLE

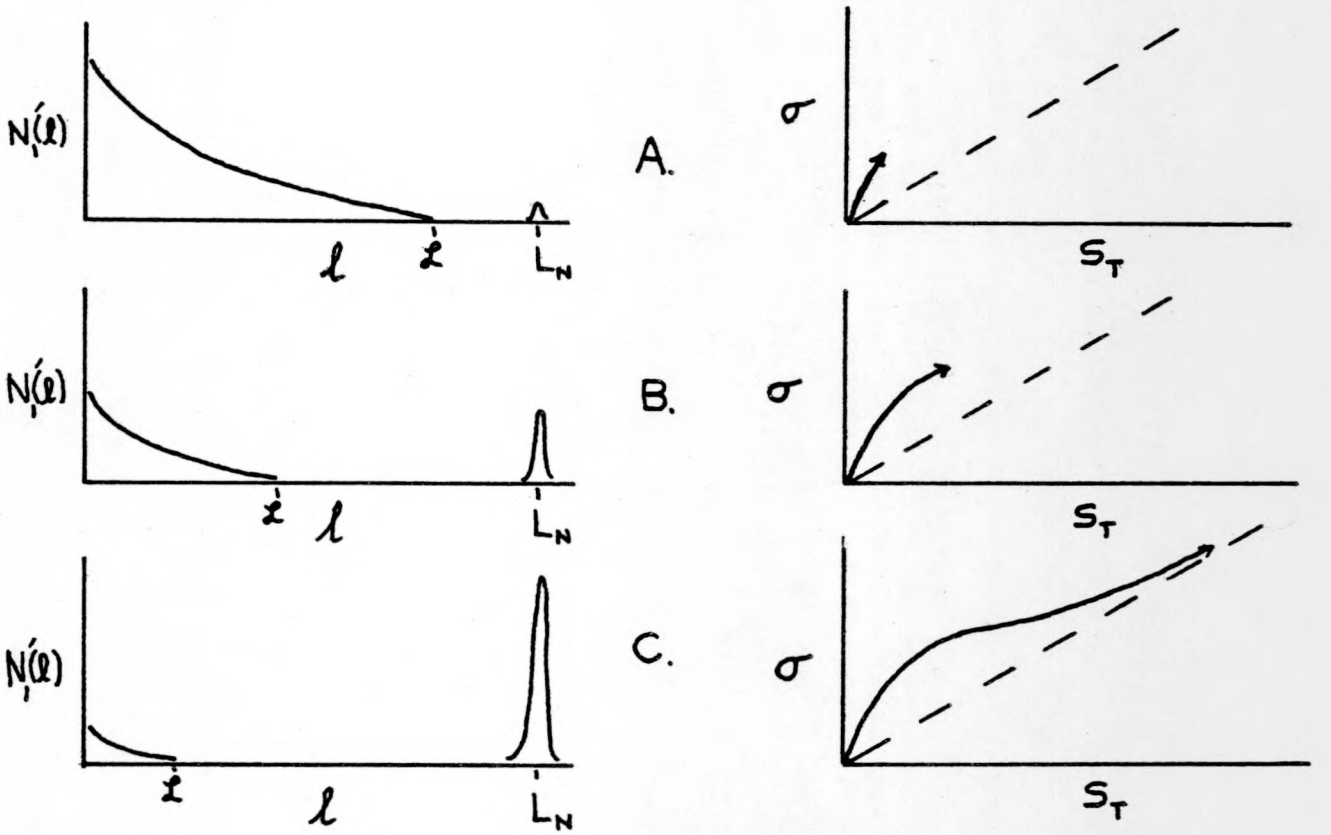

FIG. 3

$$\Delta\delta \simeq \frac{\Delta Y}{Y} = \frac{B}{S} e^{-\frac{A}{S}}$$

$$B \equiv R \Lambda L_N^3 A^2$$

$$A \equiv R' \frac{a}{L_c} = R' c$$

$$R \equiv \frac{\Omega}{2aR'}$$

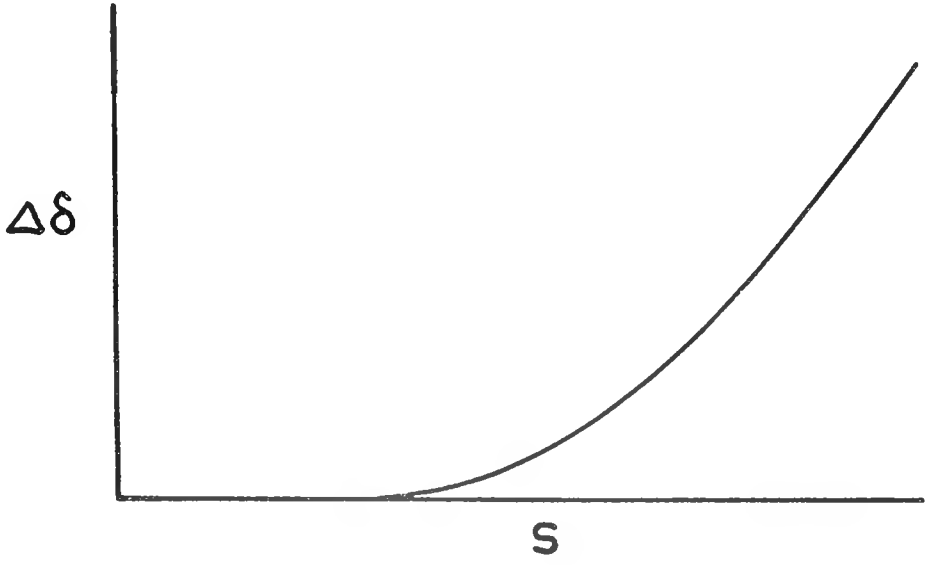

$\Delta\delta$	AMPLITUDE DEPENDENT DECREMENT
$\Delta Y/Y$	AMPLITUDE DEPENDENT FRACTIONAL CHANGE IN YOUNG'S MODULUS
S	STRAIN AMPLITUDE
R'	CONSTANT RELATED TO COTTRELL BINDING AND ORIENTATION
Ω	CONSTANT RELATED TO ORIENTATION
a	LATTICE CONSTANT
L_c	AVERAGE LOOP LENGTH
C	CONCENTRATION OF PINNING POINTS
Λ	DISLOCATION DENSITY INVOLVED IN BREAKAWAY
L_N	AVERAGE NETWORK LENGTH

FIG. 1

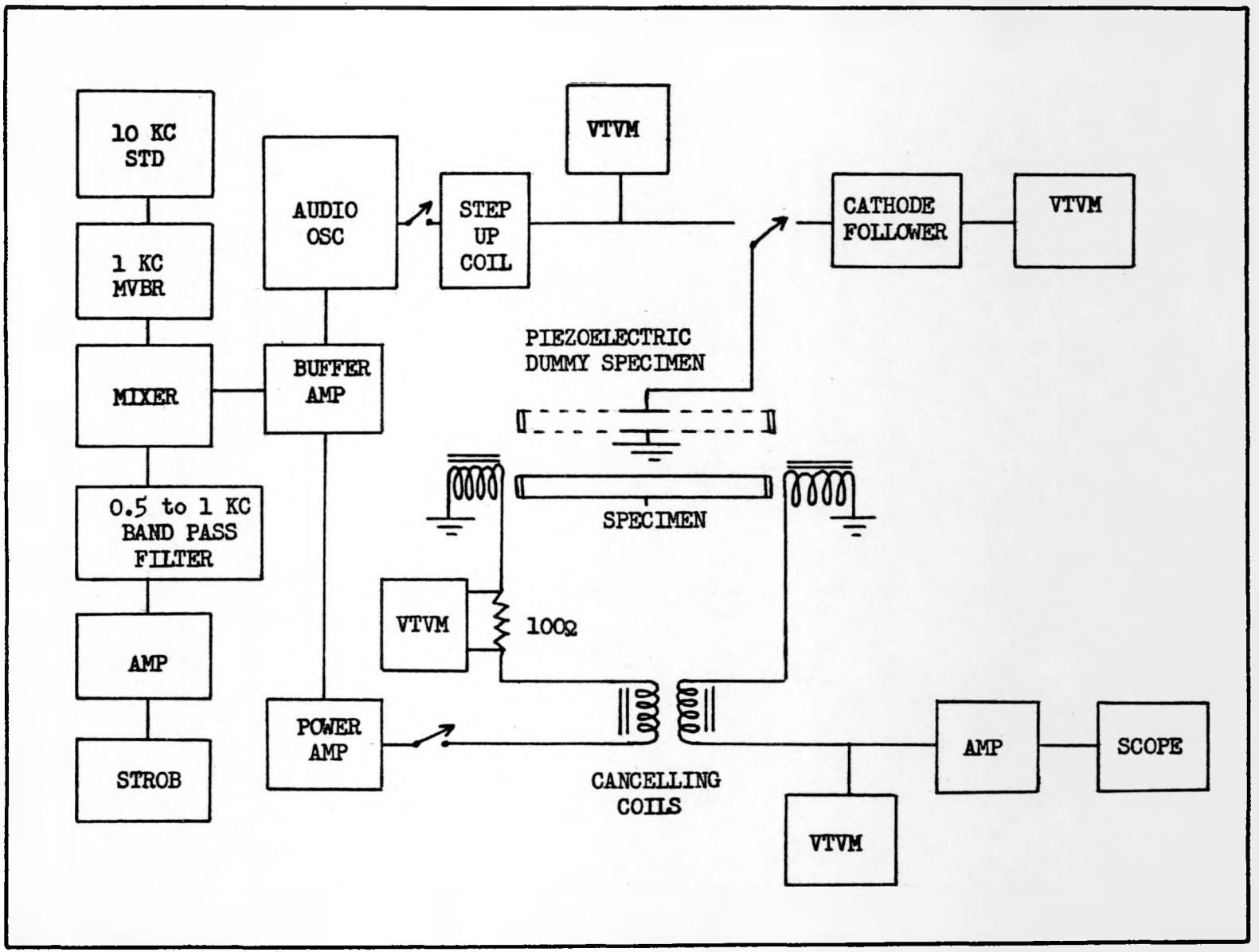
10 KC STD
1 KC MVBR
MIXER
0.5 to 1 KC BAND PASS FILTER
AMP
STROB
AUDIO OSC
BUFFER AMP
POWER AMP
VTVM
STEP UP COIL
CATHODE FOLLOWER
VTVM
PIEZOELECTRIC DUMMY SPECIMEN
SPECIMEN
VTVM
100Ω
CANCELLING COILS
AMP
SCOPE
VTVM

FIG. 5

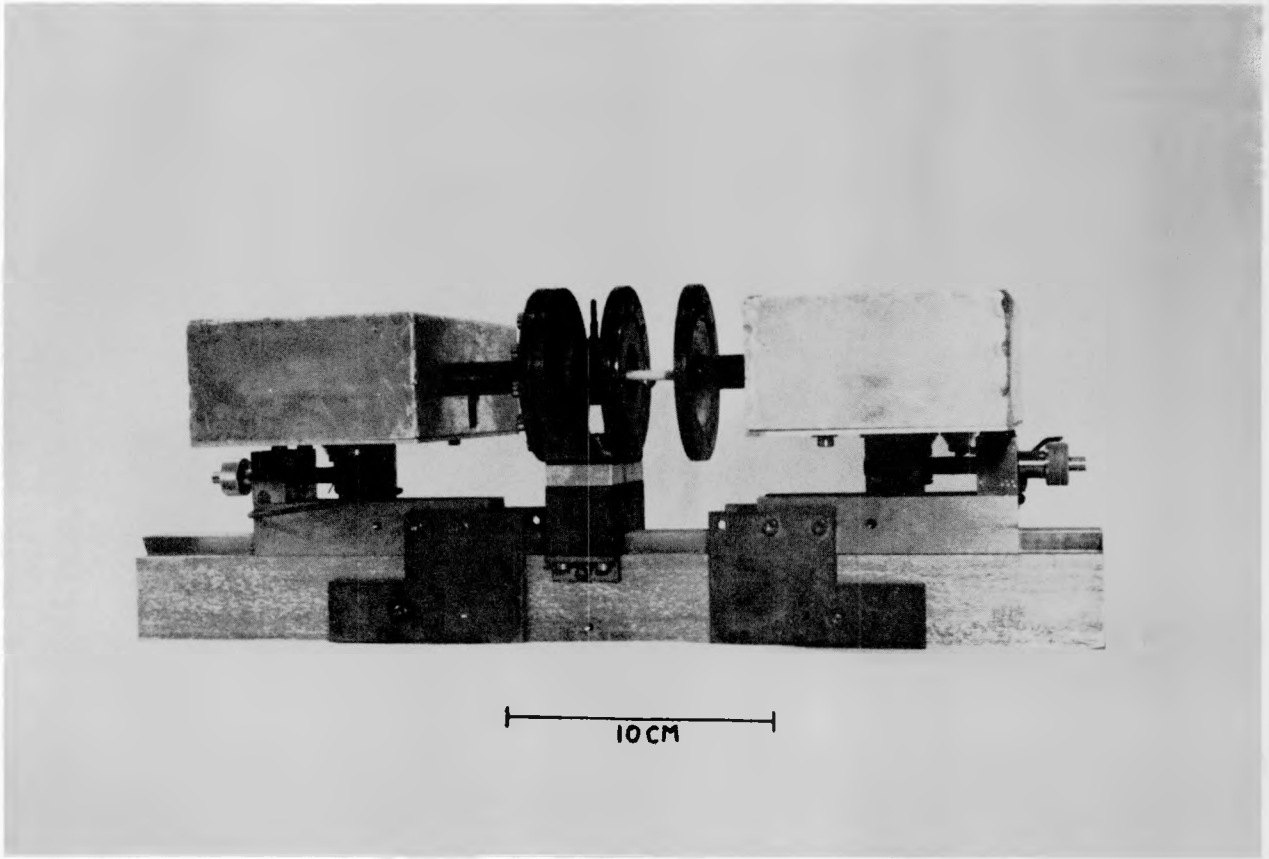

FIG. 6

FIG. 7

FIG. 8

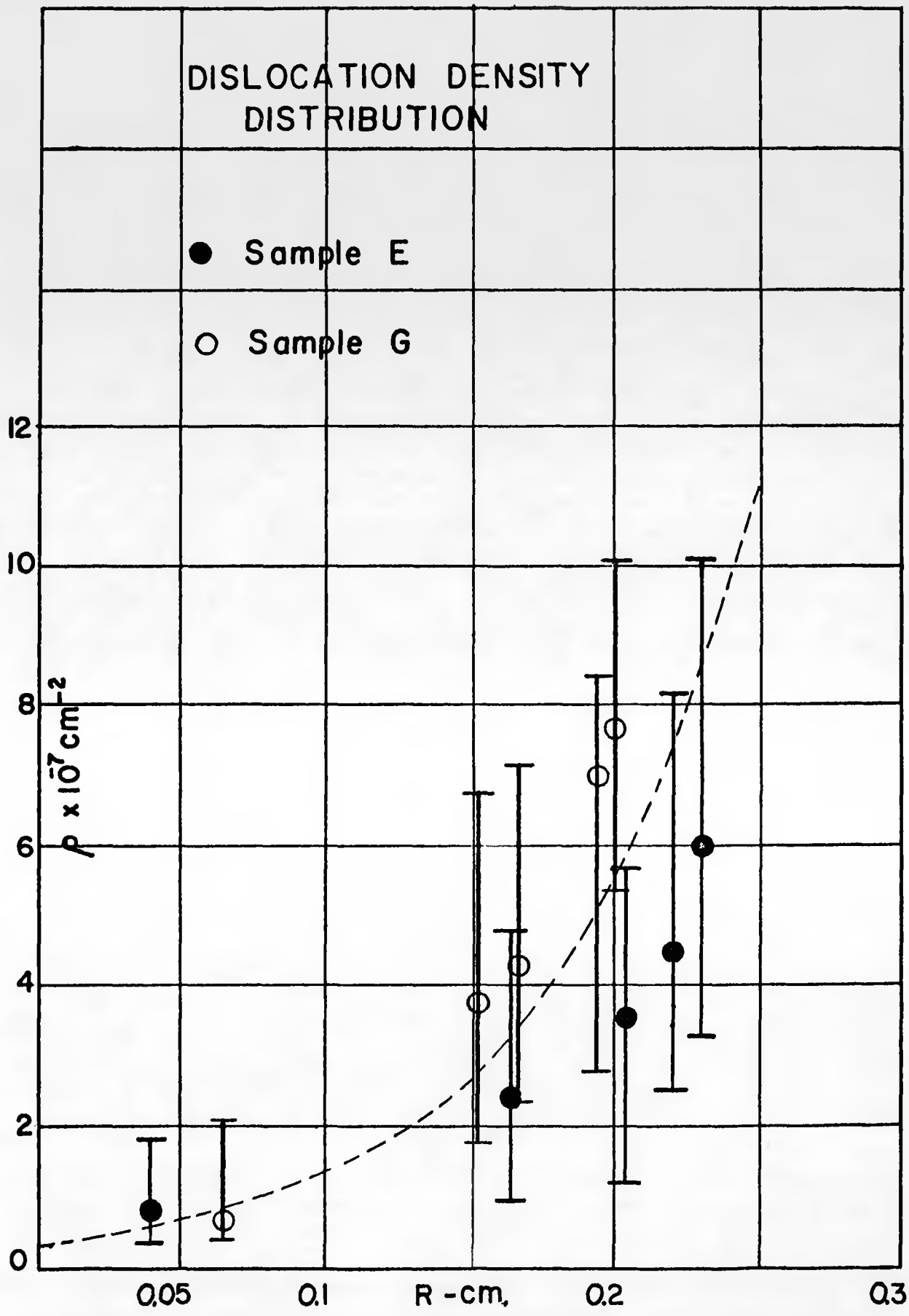
DISLOCATION DENSITY DISTRIBUTION
Sample E
Sample G
12
10
8
6
4
2
0
$\rho \times 10^{-7}$ cm^{-2}
0.05
0.1
R - cm.
0.2
0.3

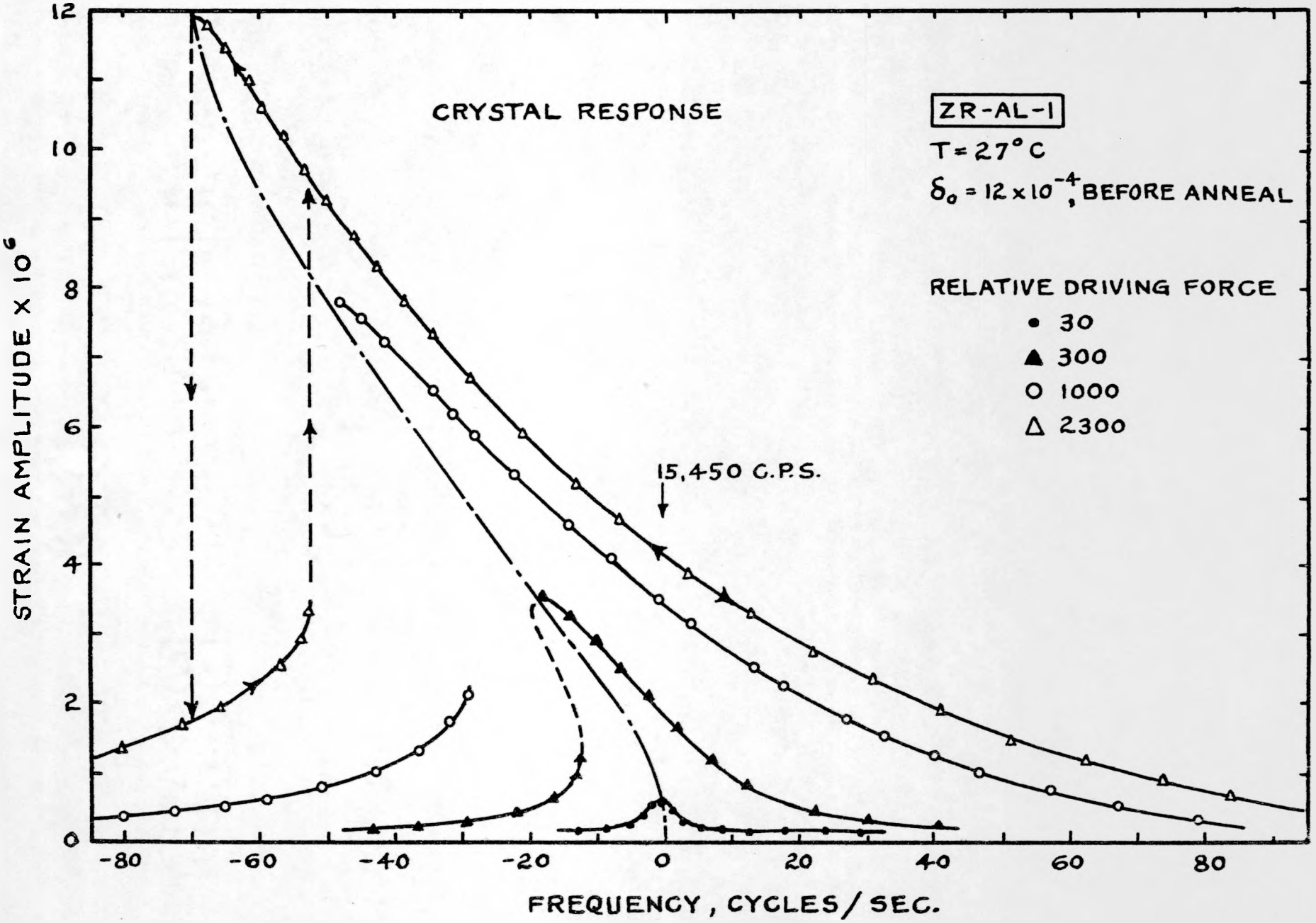
CRYSTAL RESPONSE
ZR-AL-1
T = 27° C
$\delta_o = 12 \times 10^{-4}$, BEFORE ANNEAL
RELATIVE DRIVING FORCE
• 30
▲ 300
O 1000
Δ 2300
15,450 C.P.S.
STRAIN AMPLITUDE X 10^6
FREQUENCY, CYCLES/SEC.
12
10
8
6
4
2
0
-80
-60
-40
-20
0
20
40
60
80

FIG. 9

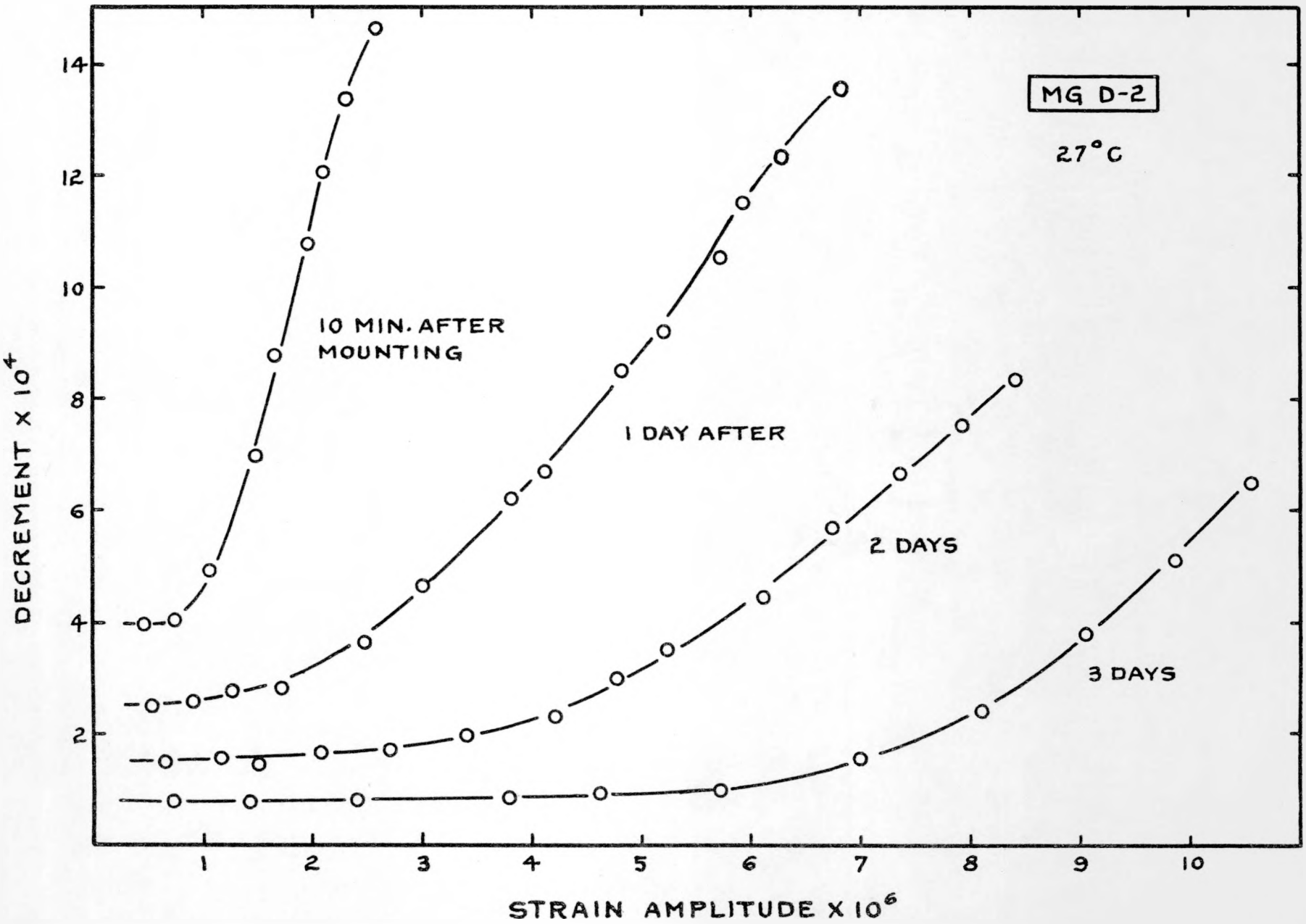
MG D-2
27°C
10 MIN. AFTER MOUNTING
1 DAY AFTER
2 DAYS
3 DAYS
DECREMENT X 10⁴
STRAIN AMPLITUDE X 10⁶
2
4
6
8
10
12
14
1
2
3
4
5
6
7
8
9
10

FIG. 10

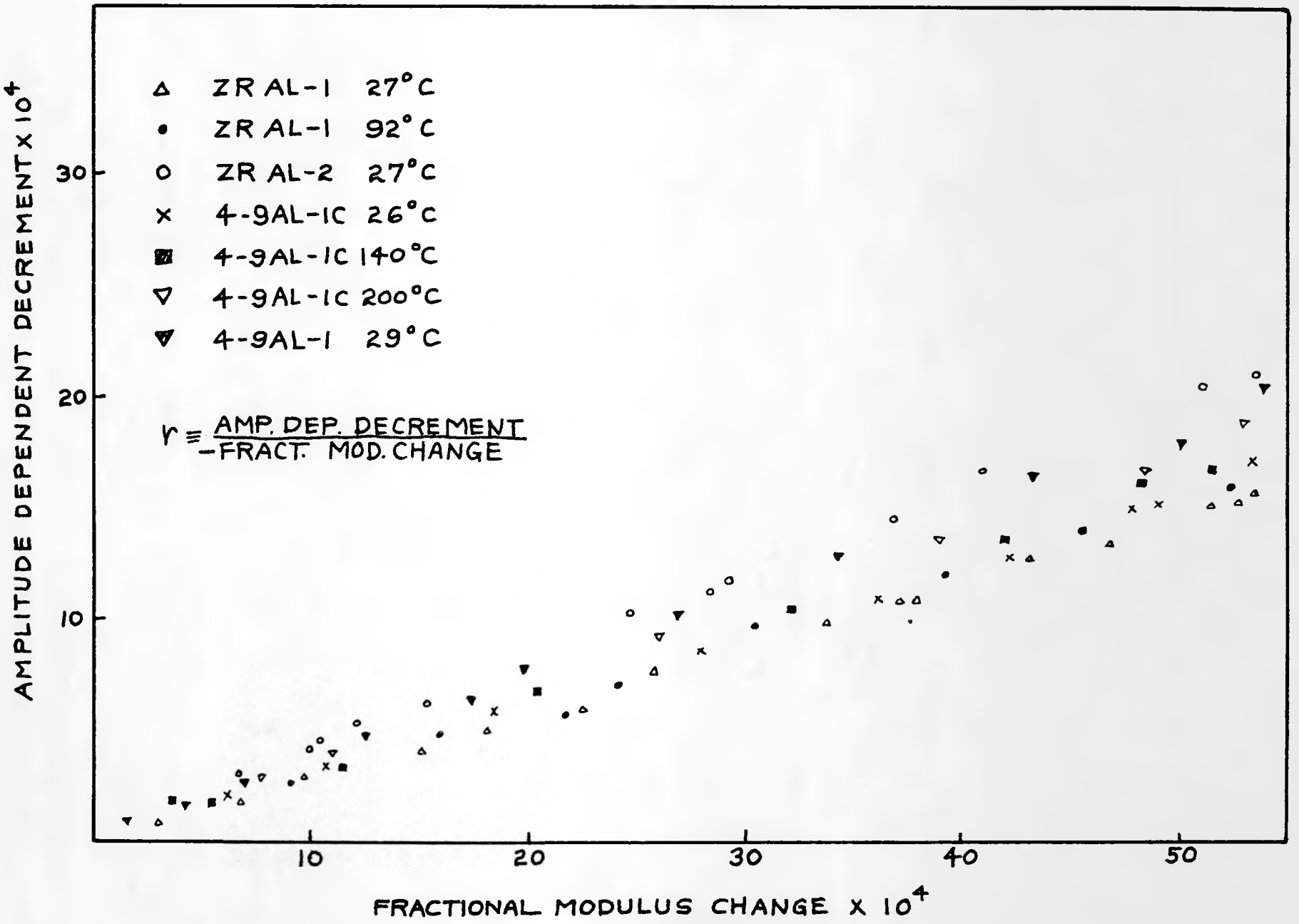
△ ZR AL-1 27°C
• ZR AL-1 92°C
○ ZR AL-2 27°C
× 4-9AL-1C 26°C
■ 4-9AL-1C 140°C
▽ 4-9AL-1C 200°C
▼ 4-9AL-1 29°C
γ ≡ AMP. DEP. DECREMENT / −FRACT. MOD. CHANGE
AMPLITUDE DEPENDENT DECREMENT X 10⁴
30
20
10
10
20
30
40
50
FRACTIONAL MODULUS CHANGE X 10⁴

FIG. 11

FIG. 12

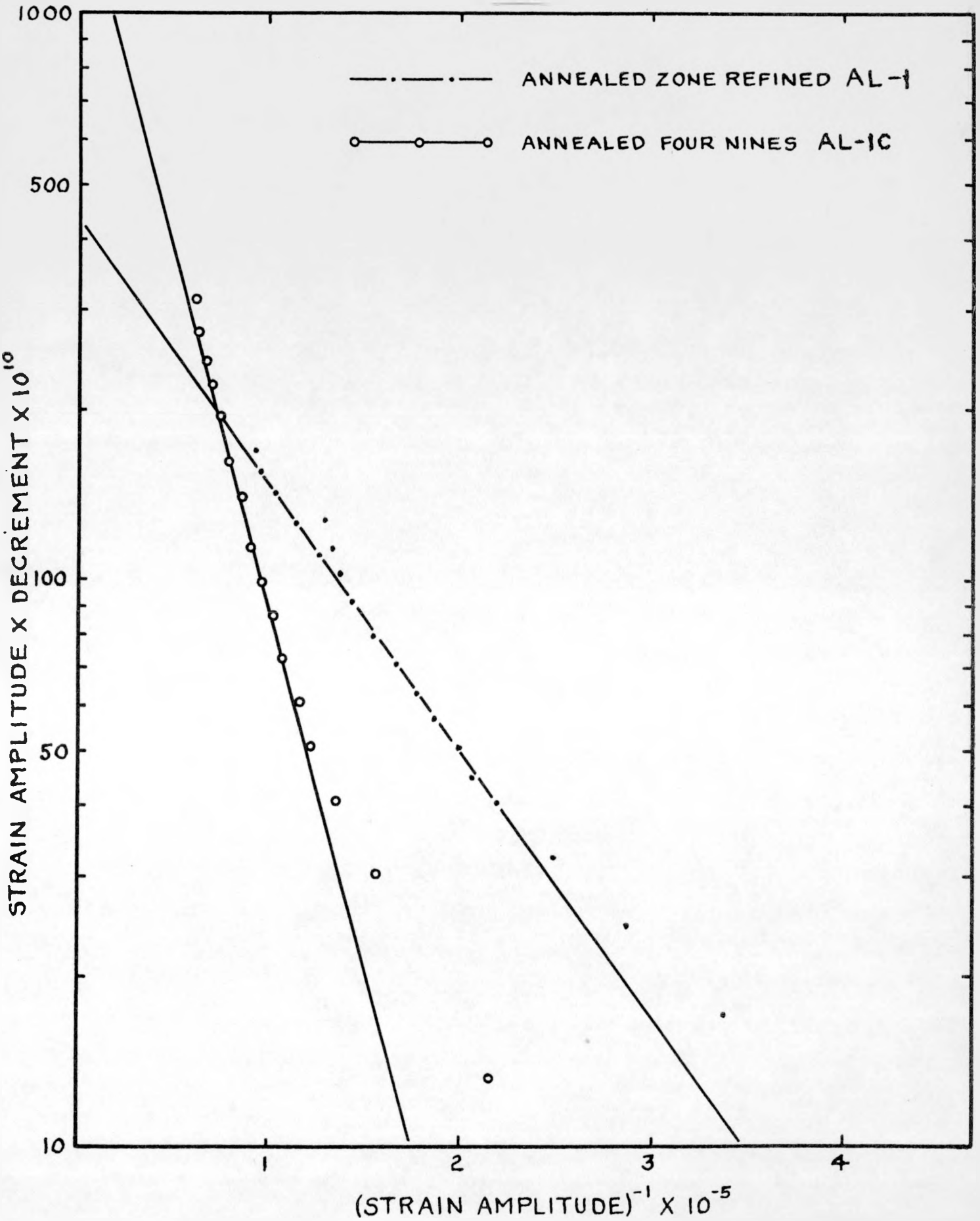
ANNEALED ZONE REFINED AL-1
ANNEALED FOUR NINES AL-1C
1000
500
100
50
10
STRAIN AMPLITUDE X DECREMENT X 10^10
1
2
3
4
(STRAIN AMPLITUDE)^-1 X 10^-5

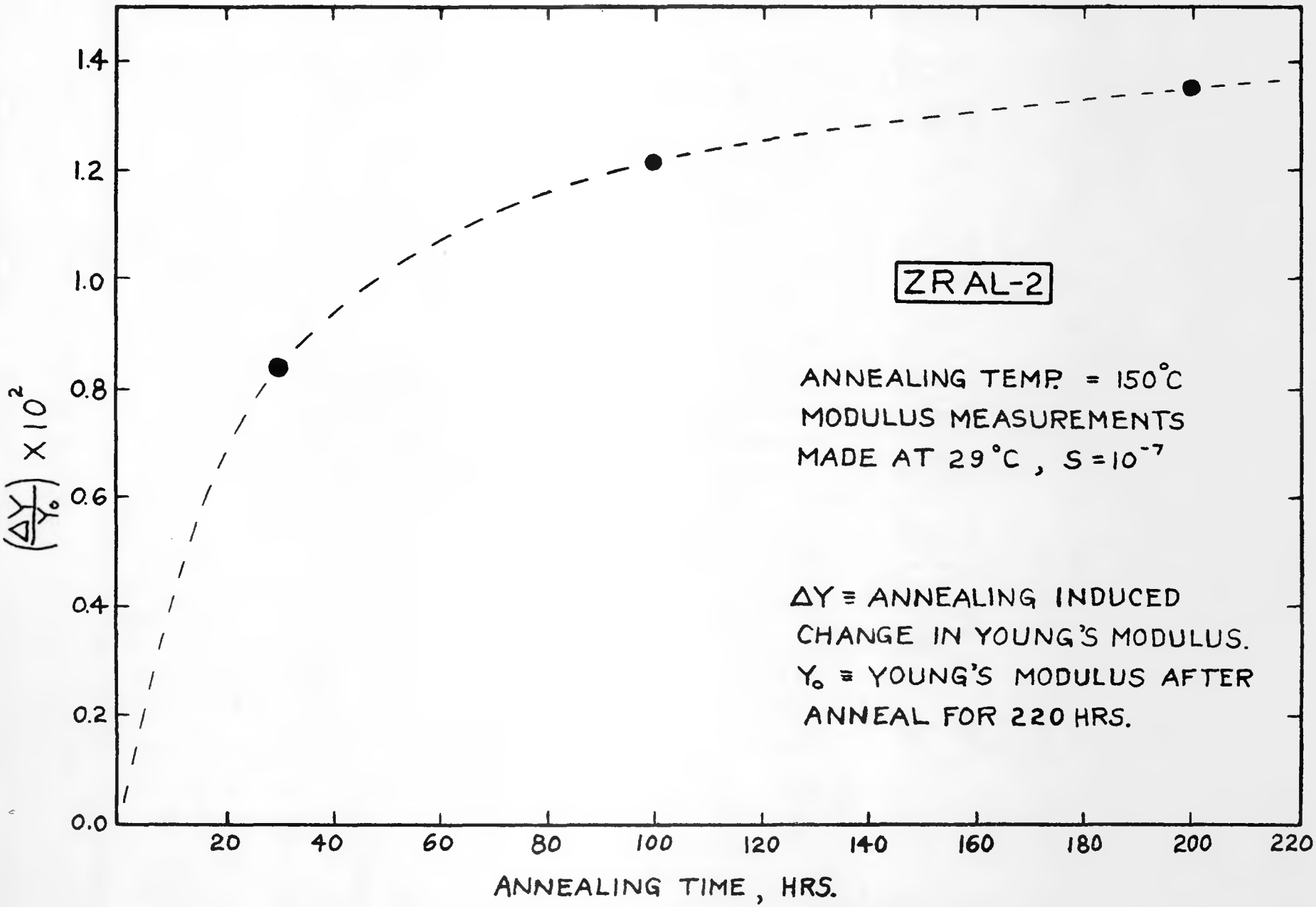
1.4
1.2
1.0
0.8
0.6
0.4
0.2
0.0
$\left(\frac{\Delta Y}{Y_0}\right) \times 10^2$
20
40
60
80
100
120
140
160
180
200
220
ANNEALING TIME, HRS.
ZR AL-2
ANNEALING TEMP. = 150°C
MODULUS MEASUREMENTS
MADE AT 29°C, S = 10^{-7}
ΔY = ANNEALING INDUCED
CHANGE IN YOUNG'S MODULUS.
Y_0 = YOUNG'S MODULUS AFTER
ANNEAL FOR 220 HRS.

FIG. 13

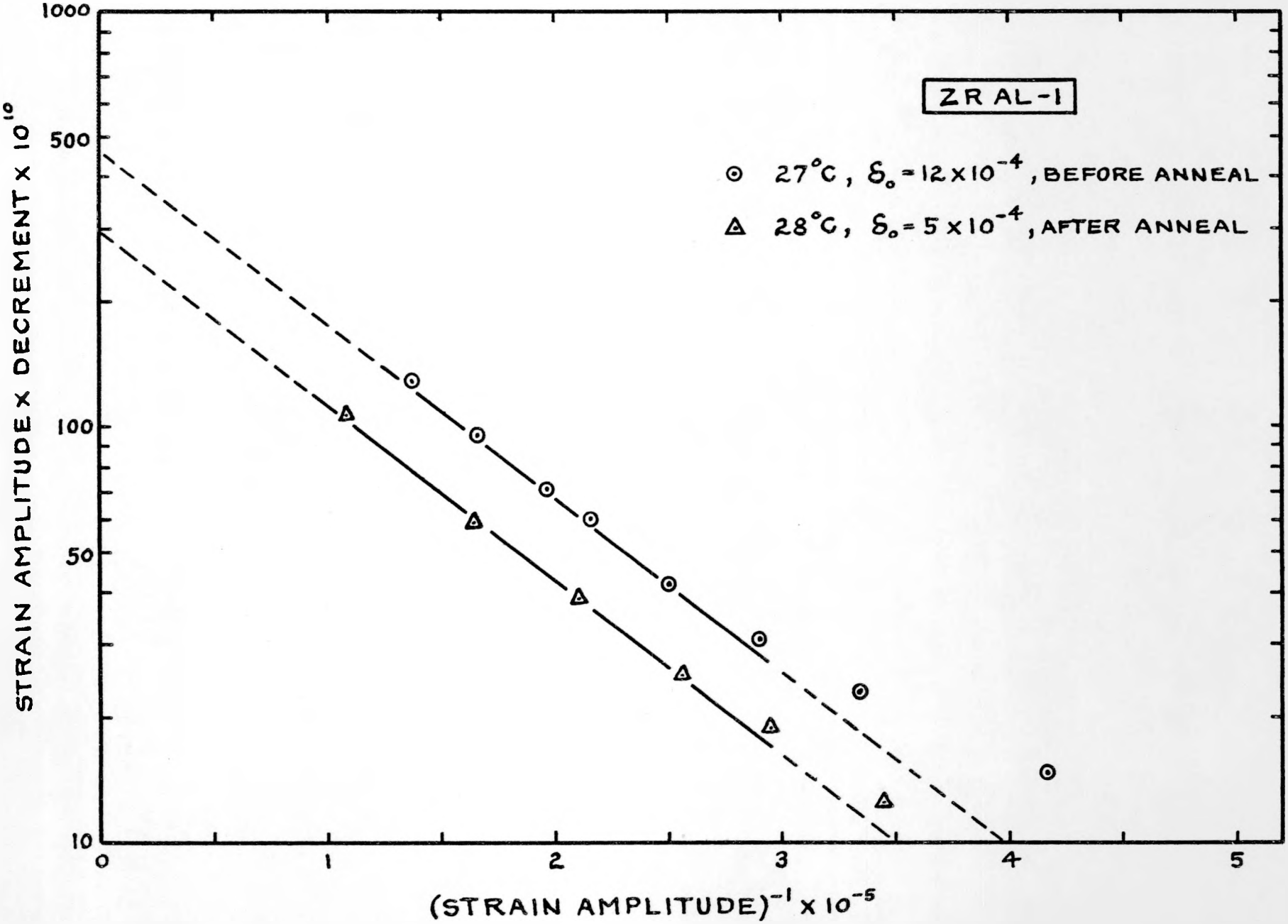
ZR AL-1
⊙ 27°C, $\delta_0 = 12 \times 10^{-4}$, BEFORE ANNEAL
△ 28°C, $\delta_0 = 5 \times 10^{-4}$, AFTER ANNEAL
STRAIN AMPLITUDE X DECREMENT X 10^{10}
1000
500
100
50
10
0
1
2
3
4
5
(STRAIN AMPLITUDE)$^{-1}$ X 10^{-5}

FIG. 14

FIG. 15

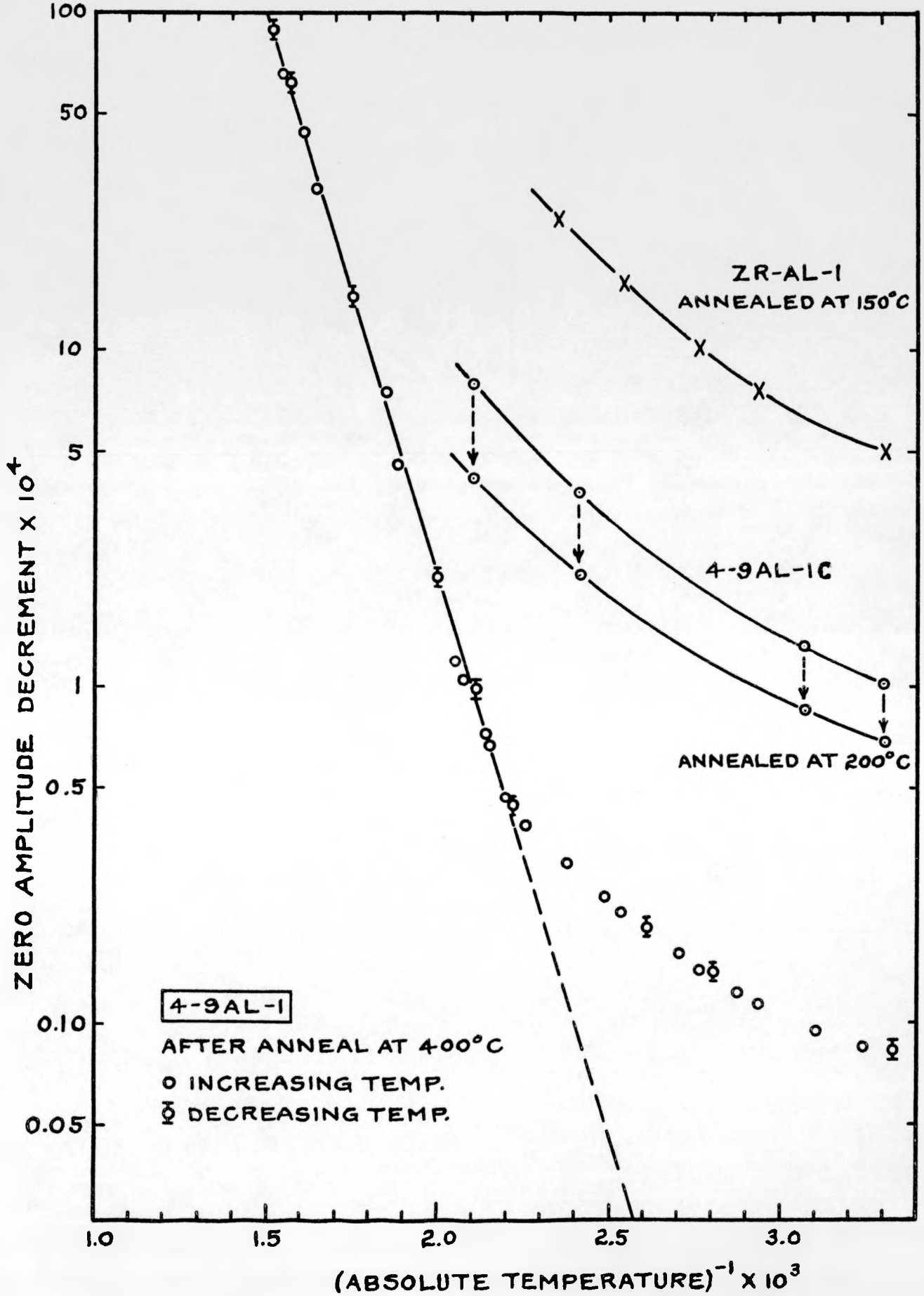
100
50
10
5
1
0.5
0.10
0.05
ZERO AMPLITUDE DECREMENT X 10^4
ZR-AL-1
ANNEALED AT 150°C
4-9AL-1C
ANNEALED AT 200°C
4-9AL-1
AFTER ANNEAL AT 400°C
o INCREASING TEMP.
Ø DECREASING TEMP.
1.0
1.5
2.0
2.5
3.0
(ABSOLUTE TEMPERATURE)$^{-1}$ X 10^3

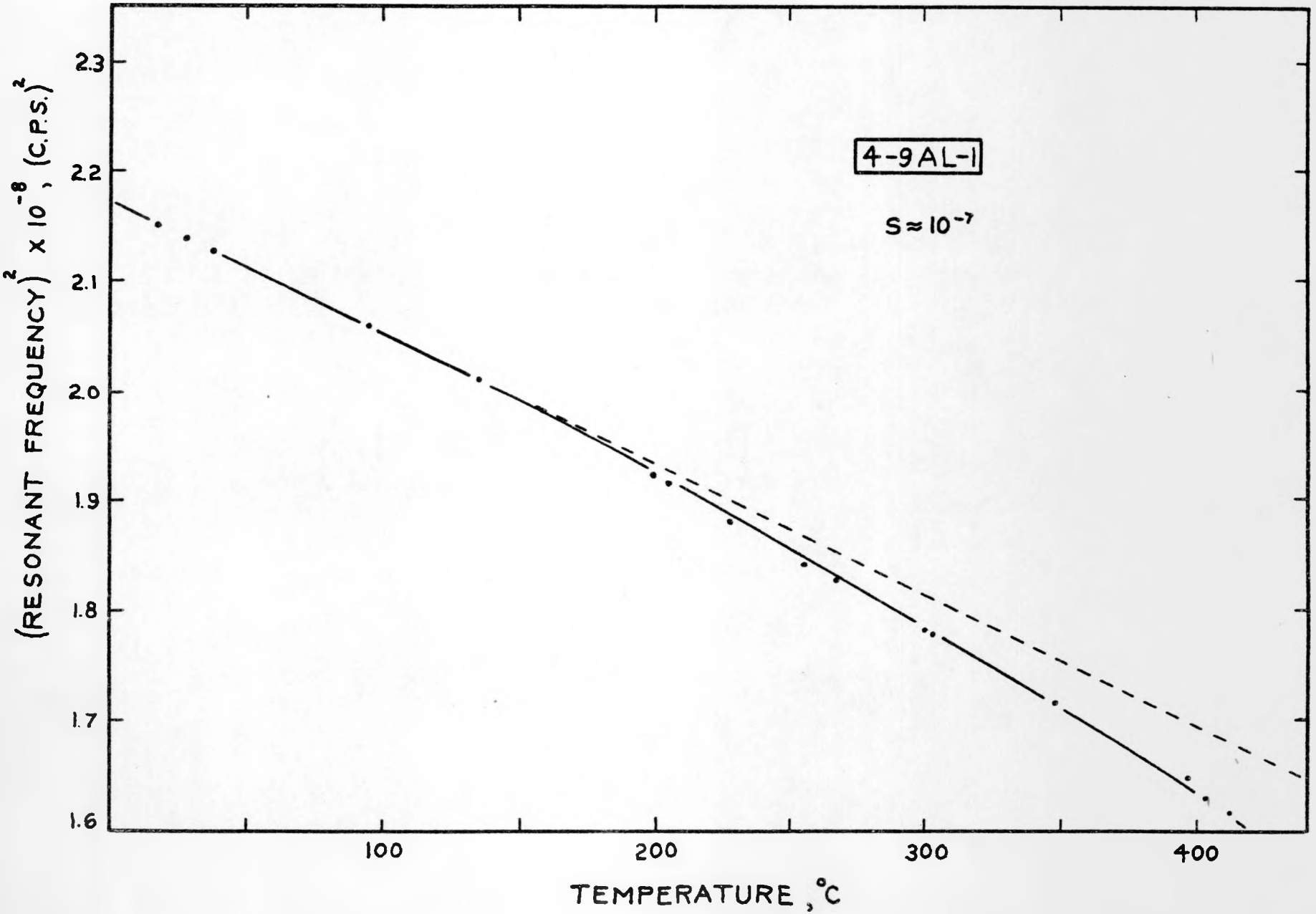
4-9AL-1
S≈10⁻⁷
(RESONANT FREQUENCY)² X 10⁻⁸, (C.P.S.)²
2.3
2.2
2.1
2.0
1.9
1.8
1.7
1.6
100
200
300
400
TEMPERATURE, °C

FIG. 16

FIG. 17

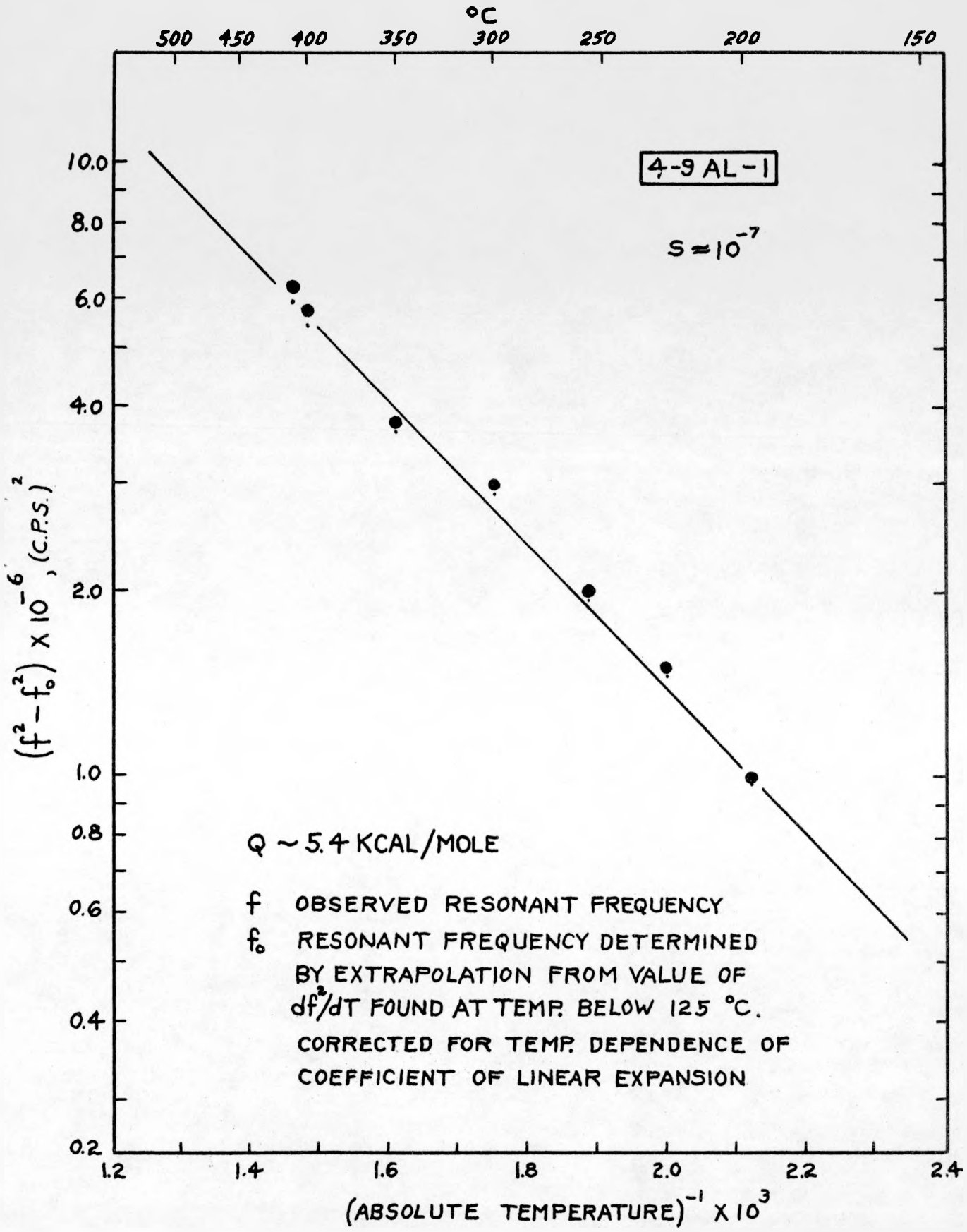
°C
500 450 400 350 300 250 200 150
4-9 AL-1
S ≈ 10^-7
10.0
8.0
6.0
4.0
2.0
1.0
0.8
0.6
0.4
0.2
(f² - f₀²) X 10^-6, (C.P.S.)²
Q ~ 5.4 KCAL/MOLE
f OBSERVED RESONANT FREQUENCY
f₀ RESONANT FREQUENCY DETERMINED BY EXTRAPOLATION FROM VALUE OF df²/dT FOUND AT TEMP. BELOW 125 °C. CORRECTED FOR TEMP. DEPENDENCE OF COEFFICIENT OF LINEAR EXPANSION
1.2 1.4 1.6 1.8 2.0 2.2 2.4
(ABSOLUTE TEMPERATURE)^-1 X 10^3

FIG. 18

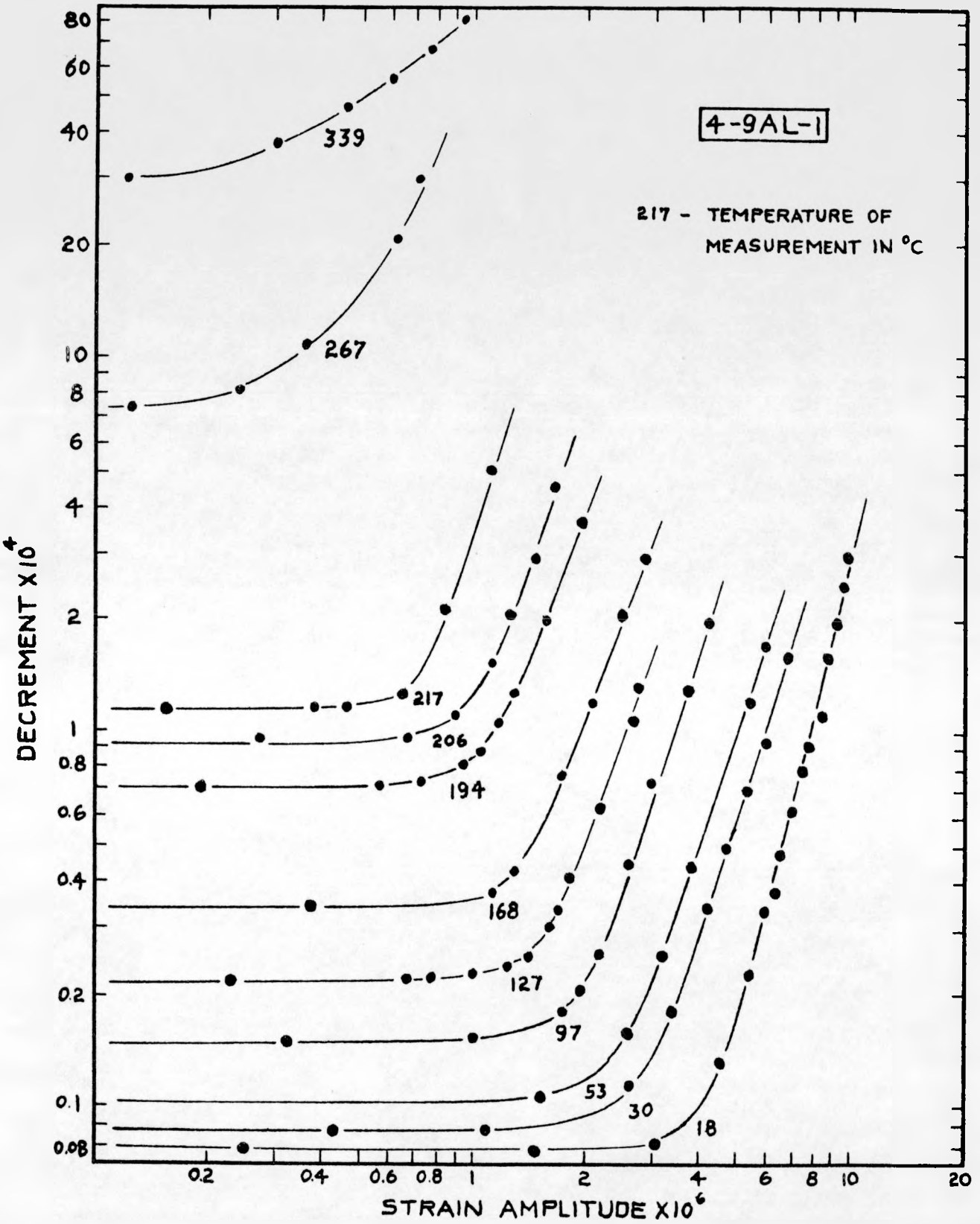
4-9AL-1
217 - TEMPERATURE OF MEASUREMENT IN °C
339
267
217
206
194
168
127
97
53
30
18
DECREMENT X10⁴
STRAIN AMPLITUDE X10⁶
80
60
40
20
10
8
6
4
2
1
0.8
0.6
0.4
0.2
0.1
0.08
0.2
0.4
0.6
0.8
1
2
4
6
8
10
20

FIG.19

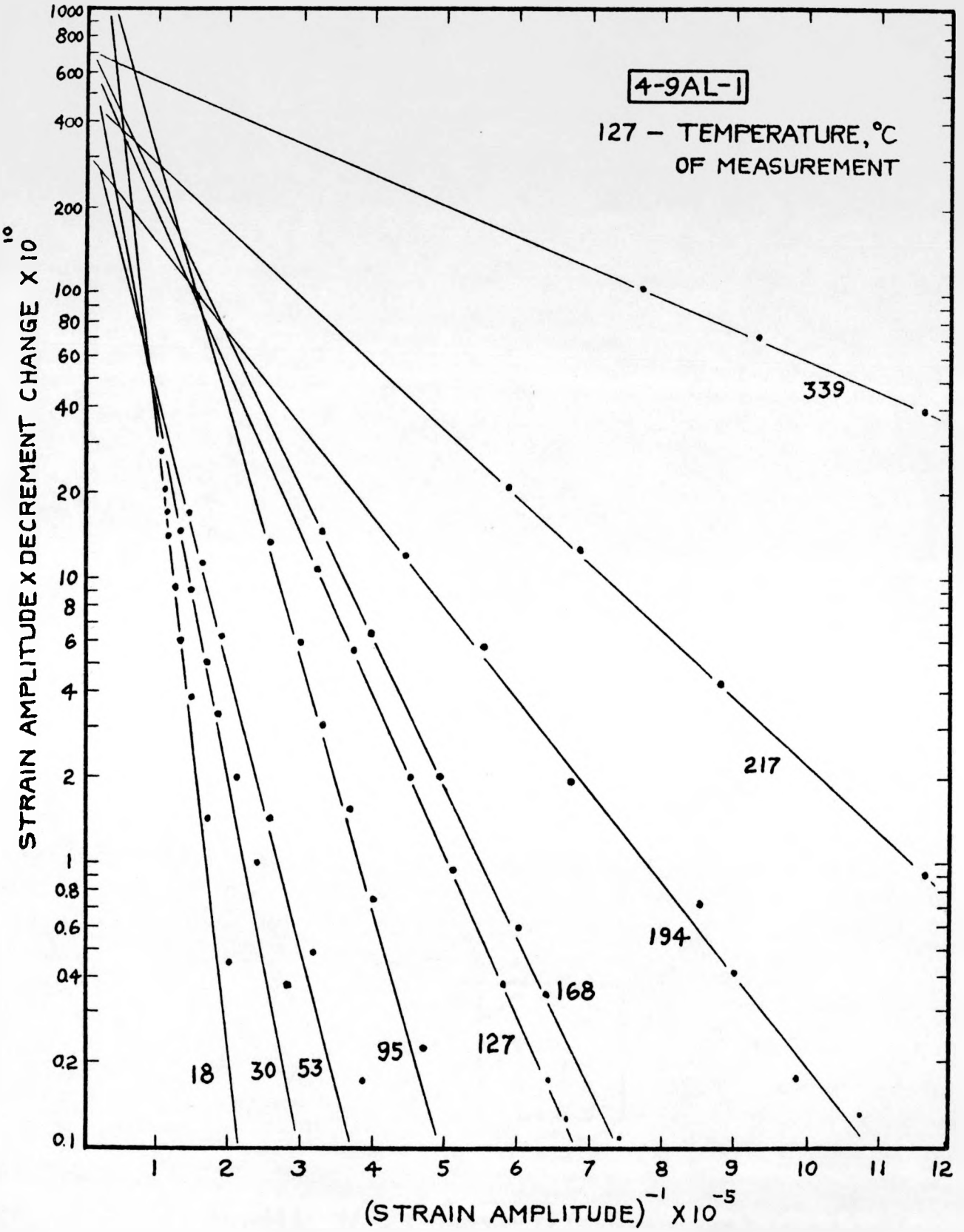
4-9AL-1
127 – TEMPERATURE, °C
OF MEASUREMENT
STRAIN AMPLITUDE X DECREMENT CHANGE X 10^0
(STRAIN AMPLITUDE)^-1 X 10^-5
1000
800
600
400
200
100
80
60
40
20
10
8
6
4
2
1
0.8
0.6
0.4
0.2
0.1
1
2
3
4
5
6
7
8
9
10
11
12
339
217
194
168
127
95
53
30
18

FIG. 20

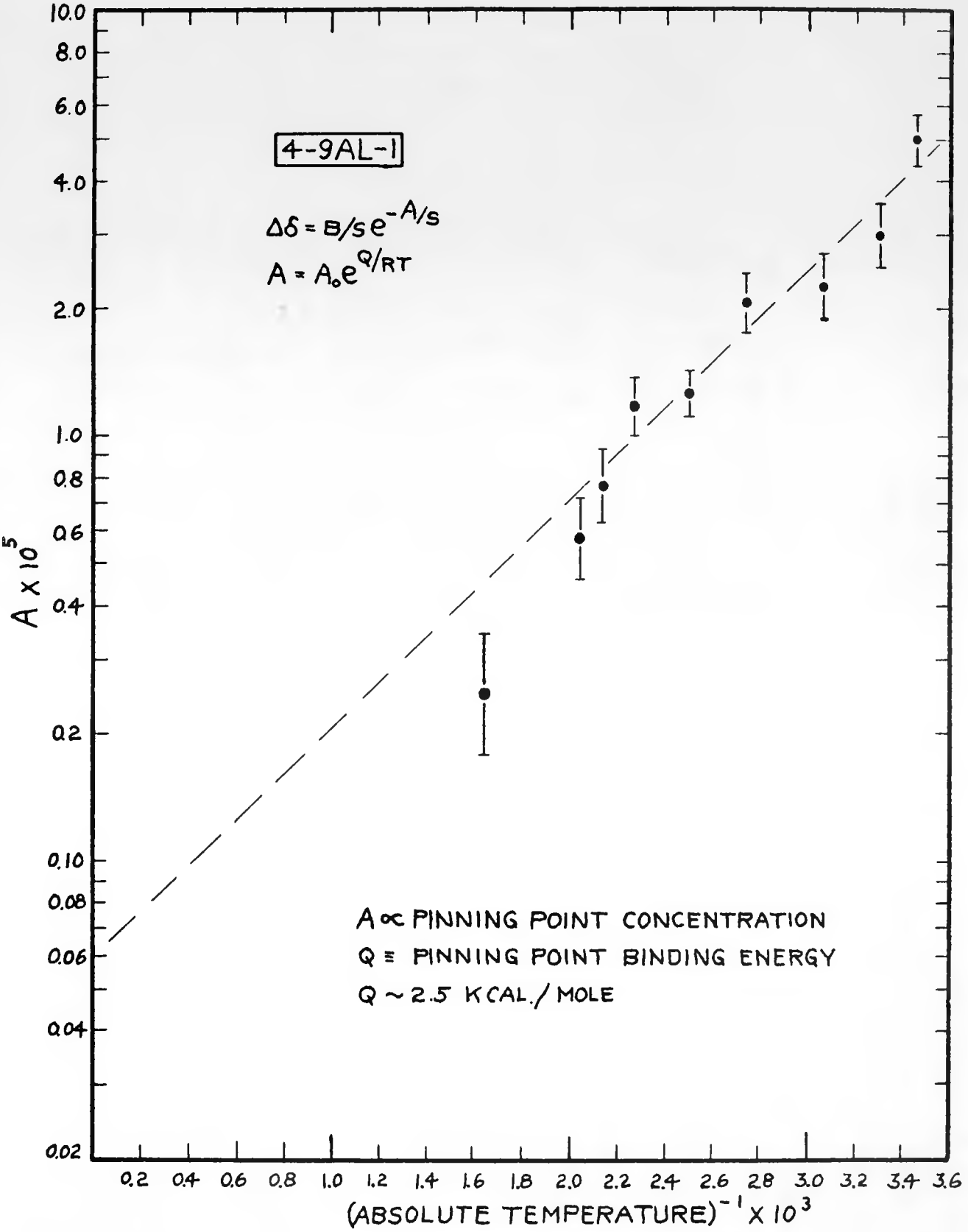
4-9AL-1
$\Delta\delta = B/s\, e^{-A/s}$
$A = A_0 e^{Q/RT}$
A ∝ PINNING POINT CONCENTRATION
Q = PINNING POINT BINDING ENERGY
Q ~ 2.5 KCAL./MOLE
A x 10^5
10.0
8.0
6.0
4.0
2.0
1.0
0.8
0.6
0.4
0.2
0.10
0.08
0.06
0.04
0.02
0.2 0.4 0.6 0.8 1.0 1.2 1.4 1.6 1.8 2.0 2.2 2.4 2.6 2.8 3.0 3.2 3.4 3.6
(ABSOLUTE TEMPERATURE)^-1 X 10^3

FIG. 21

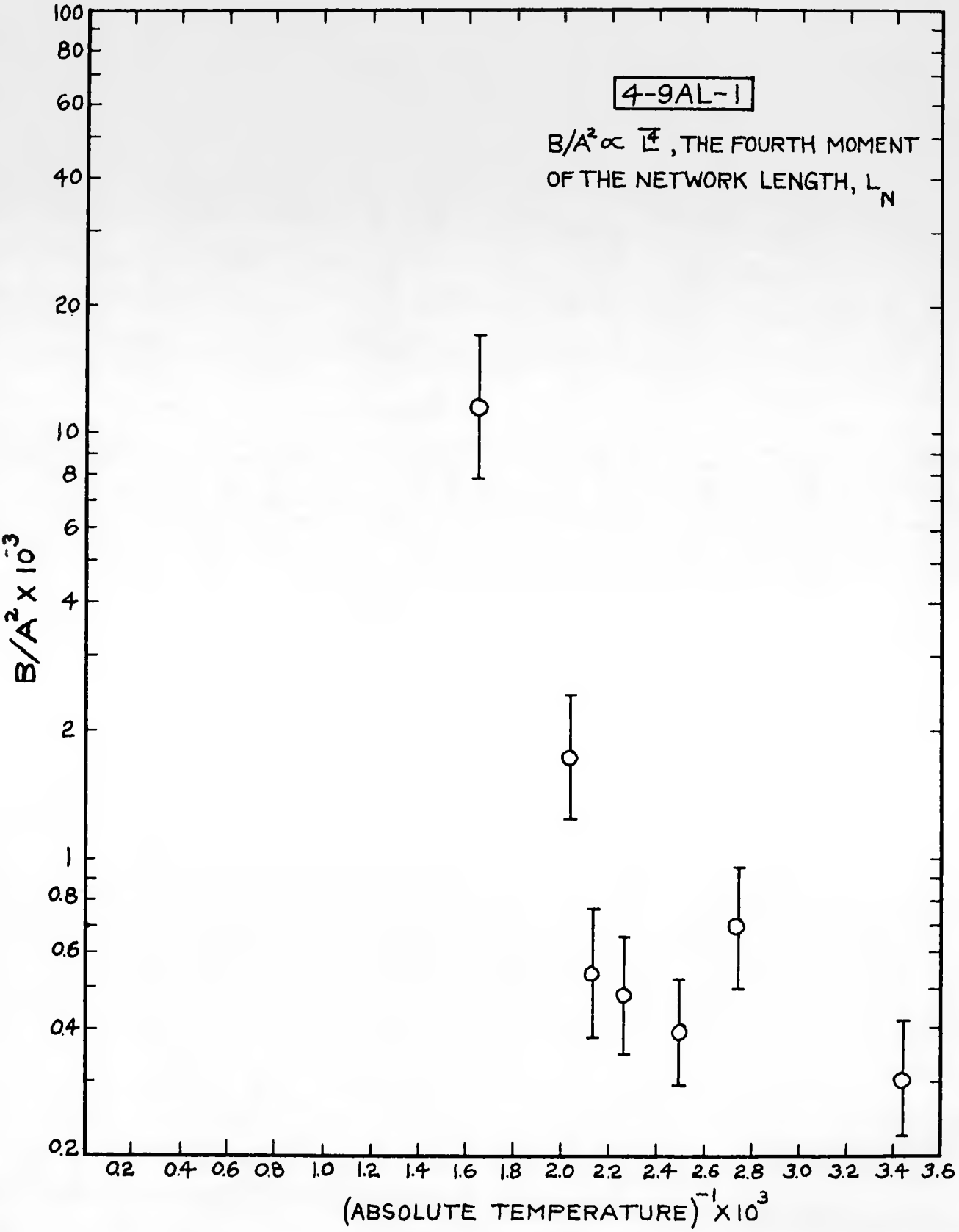
4-9AL-1
B/A² ∝ L̄⁴, THE FOURTH MOMENT OF THE NETWORK LENGTH, L_N
B/A² X 10⁻³
100
80
60
40
20
10
8
6
4
2
1
0.8
0.6
0.4
0.2
0.2 0.4 0.6 0.8 1.0 1.2 1.4 1.6 1.8 2.0 2.2 2.4 2.6 2.8 3.0 3.2 3.4 3.6
(ABSOLUTE TEMPERATURE)⁻¹ X 10³

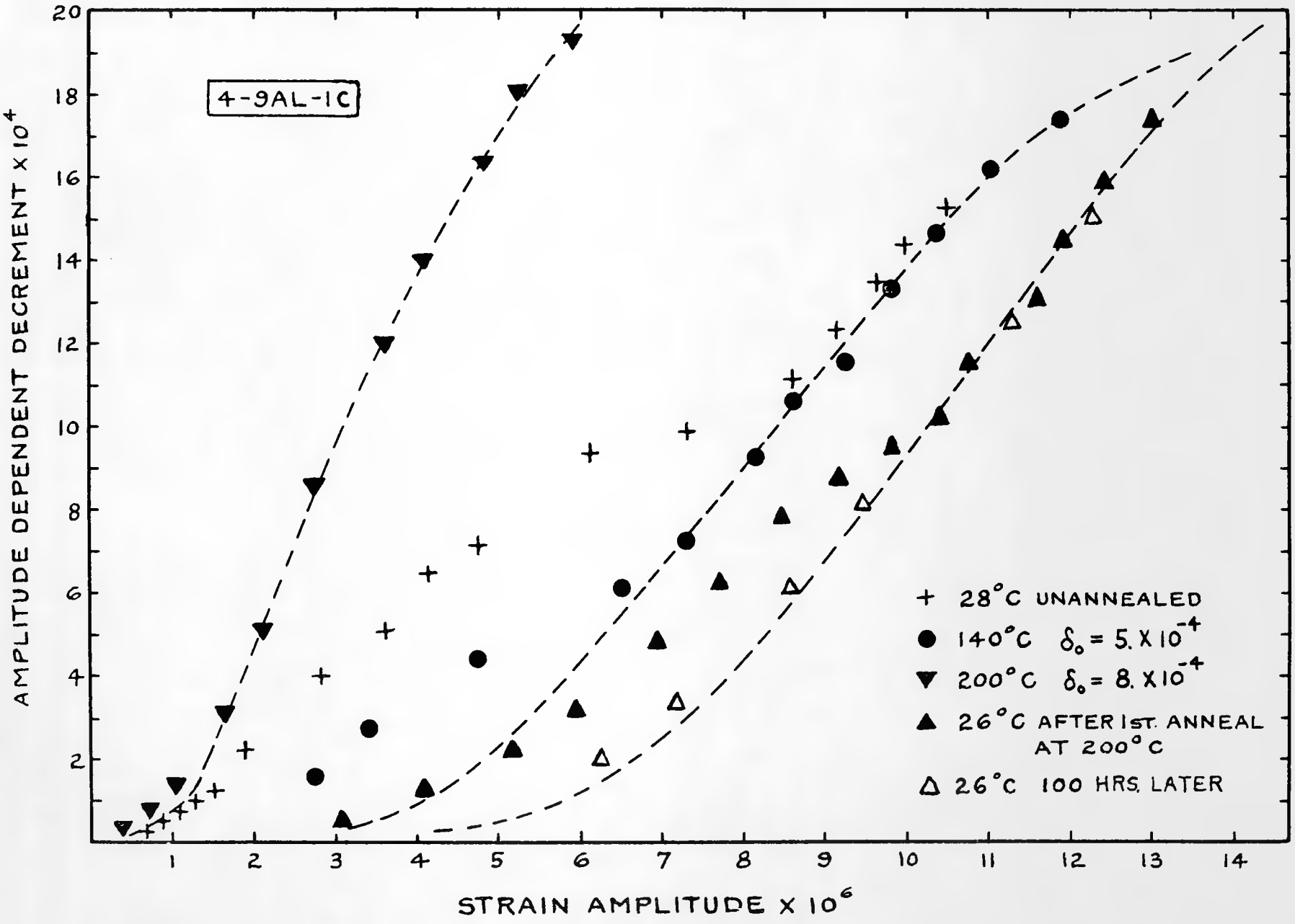
4-9AL-1C
AMPLITUDE DEPENDENT DECREMENT X 10⁴
STRAIN AMPLITUDE X 10⁶
+ 28°C UNANNEALED
● 140°C δ₀ = 5. X 10⁻⁴
▼ 200°C δ₀ = 8. X 10⁻⁴
▲ 26°C AFTER 1st. ANNEAL AT 200°C
△ 26°C 100 HRS. LATER

FIG. 22

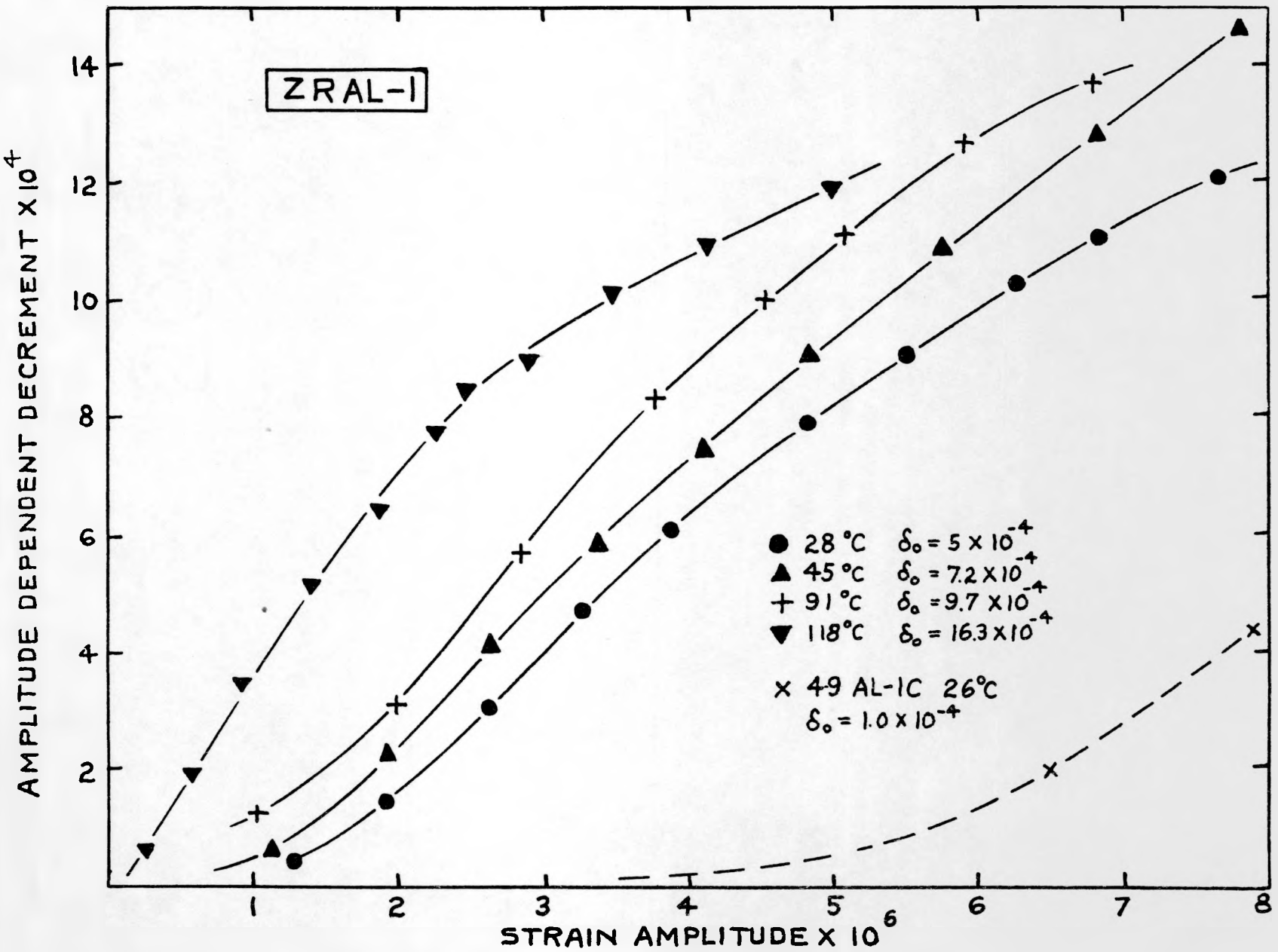
ZRAL-1
AMPLITUDE DEPENDENT DECREMENT X 10^4
STRAIN AMPLITUDE X 10^6
14
12
10
8
6
4
2
1
2
3
4
5
6
7
8
● 28 °C δ₀ = 5 X 10^-4
▲ 45 °C δ₀ = 7.2 X 10^-4
+ 91 °C δ₀ = 9.7 X 10^-4
▼ 118°C δ₀ = 16.3 X 10^-4
× 49 AL-1C 26°C
δ₀ = 1.0 X 10^-4

FIG. 23

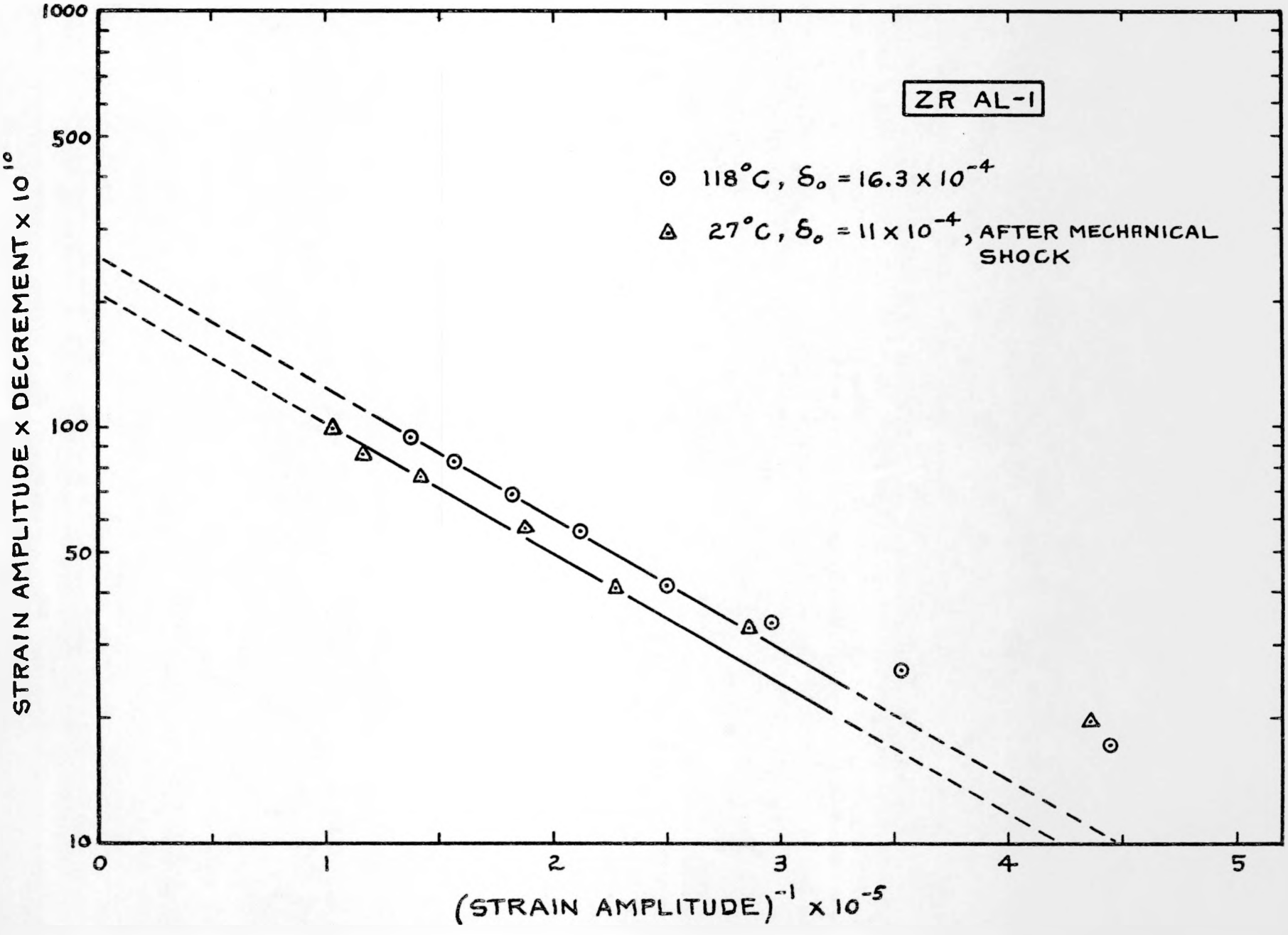
ZR AL-1
⊙ 118°C, $\delta_o = 16.3 \times 10^{-4}$
△ 27°C, $\delta_o = 11 \times 10^{-4}$, AFTER MECHANICAL SHOCK
STRAIN AMPLITUDE x DECREMENT x 10^{10}
1000
500
100
50
10
0
1
2
3
4
5
(STRAIN AMPLITUDE)$^{-1}$ x 10^{-5}

FIG. 24

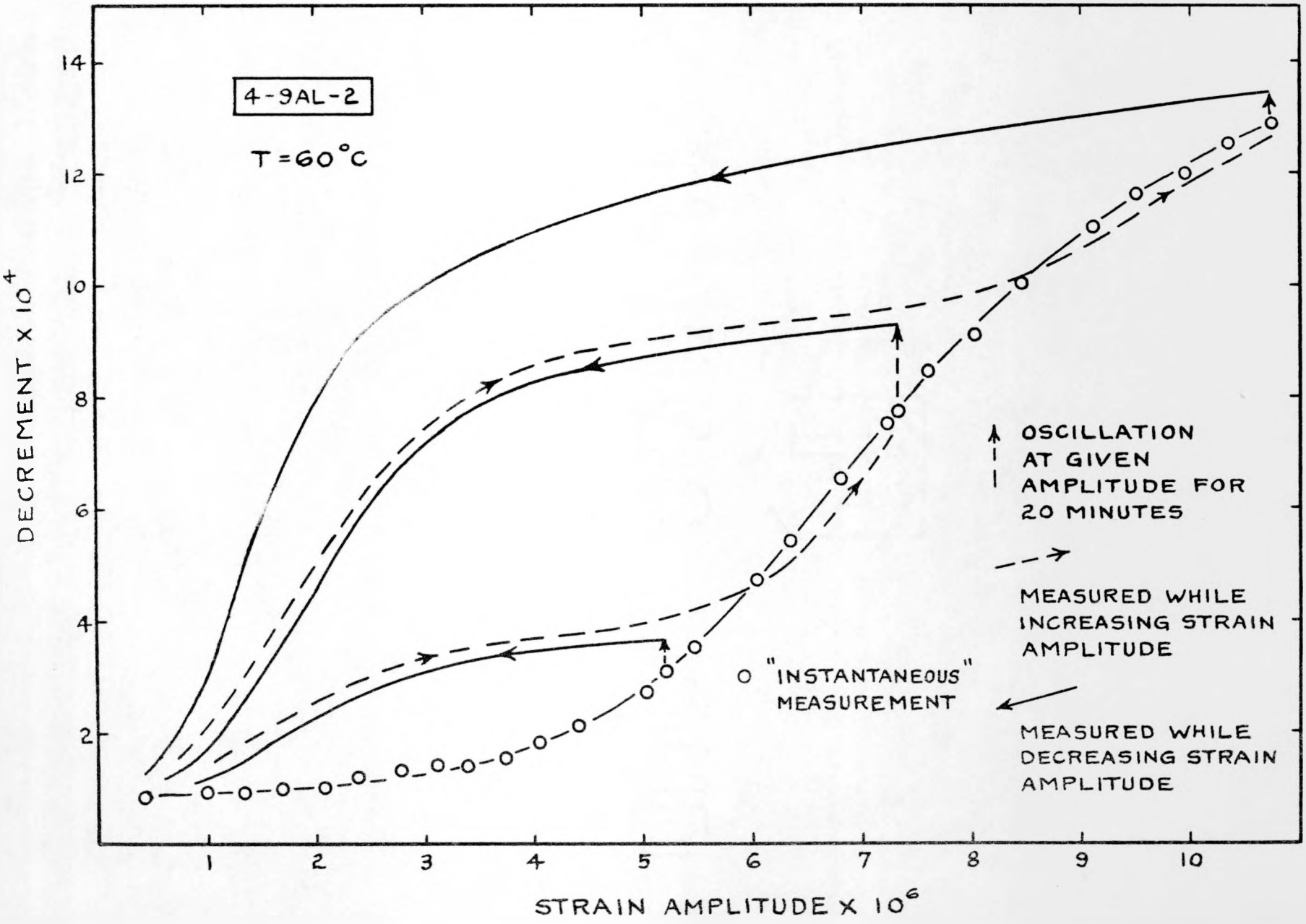
4-9AL-2
T=60°C
DECREMENT X 10⁴
STRAIN AMPLITUDE X 10⁶
OSCILLATION AT GIVEN AMPLITUDE FOR 20 MINUTES
MEASURED WHILE INCREASING STRAIN AMPLITUDE
"INSTANTANEOUS" MEASUREMENT
MEASURED WHILE DECREASING STRAIN AMPLITUDE

FIG. 25

FIG. 26a

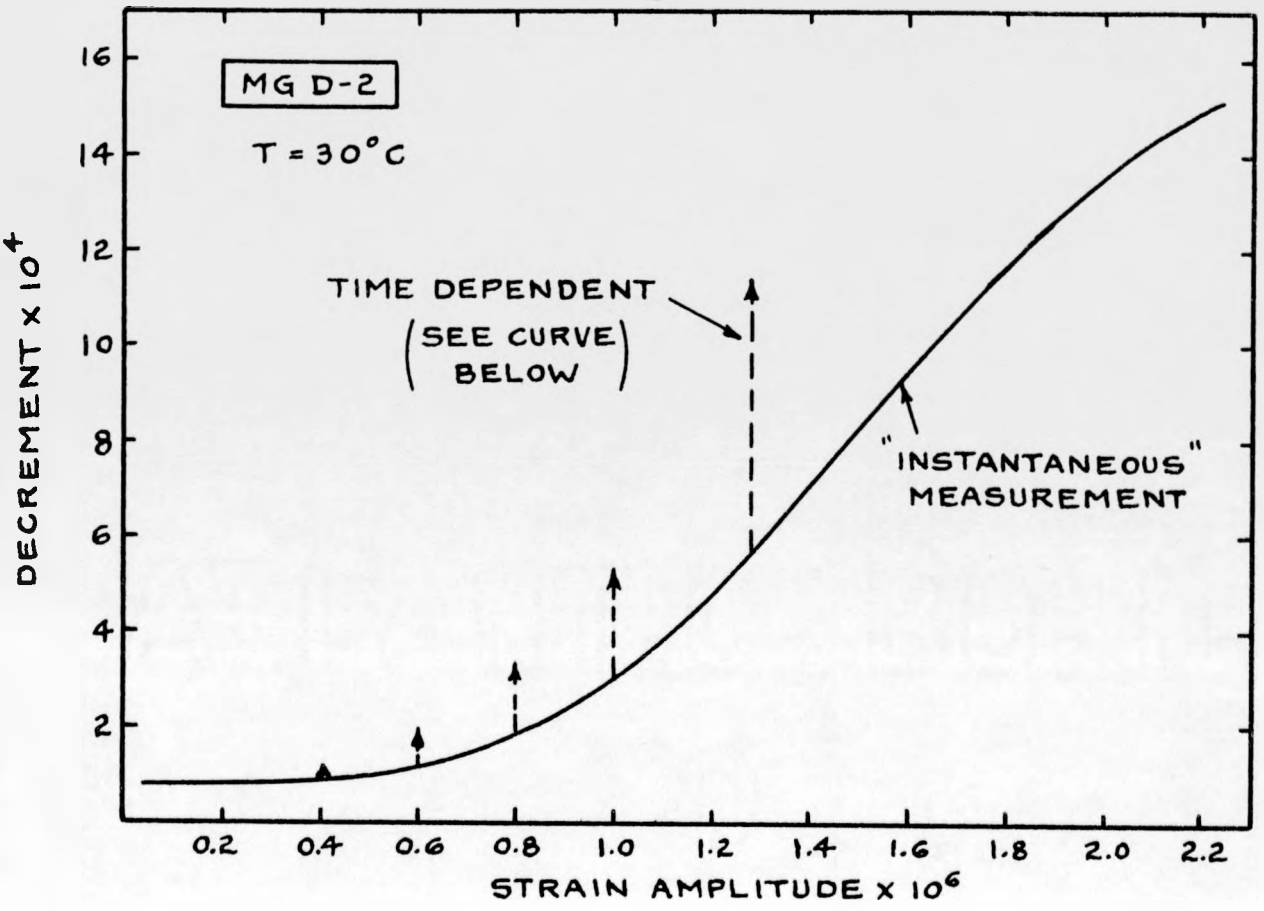

FIG. 26b

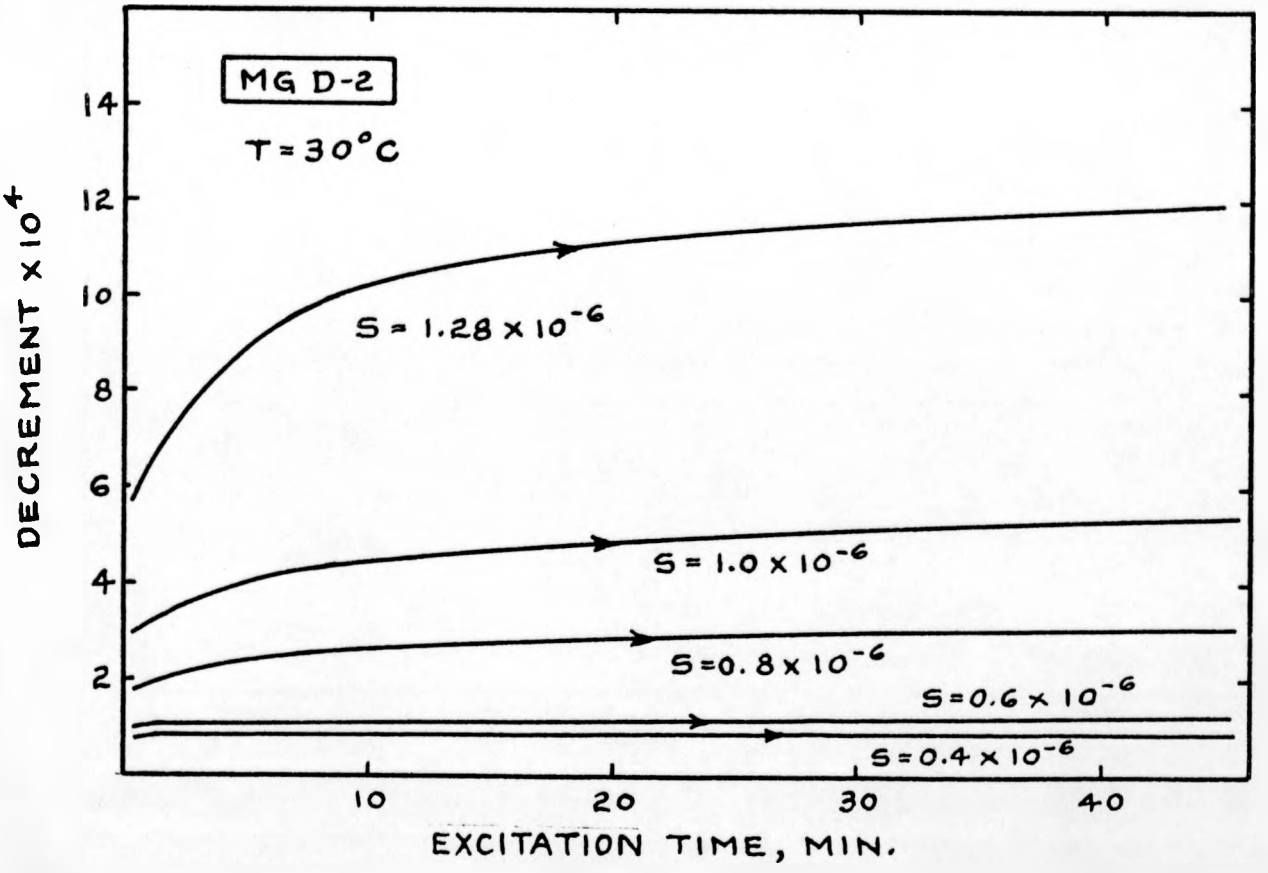

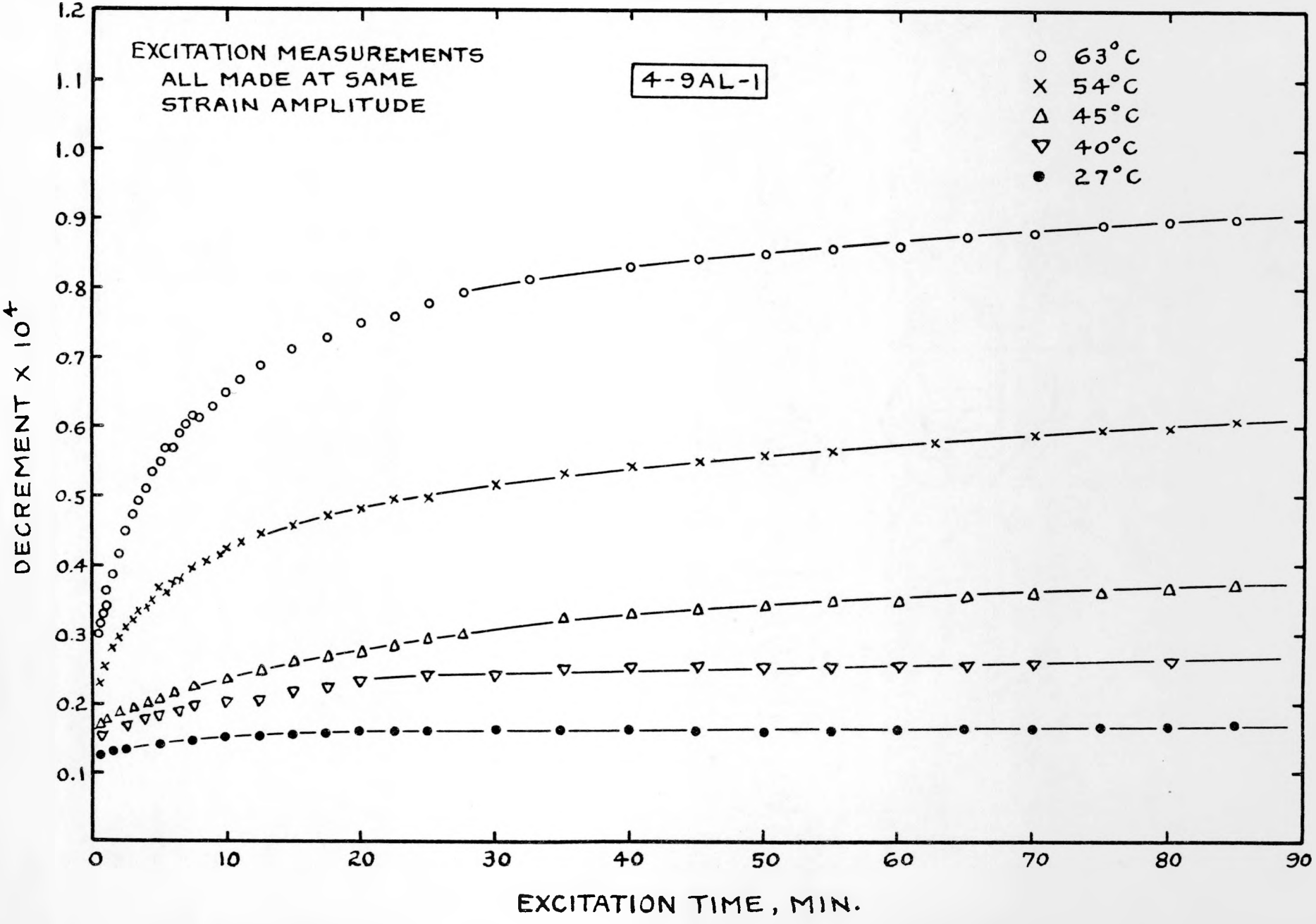
EXCITATION MEASUREMENTS
ALL MADE AT SAME
STRAIN AMPLITUDE
4-9AL-1
63°C
54°C
45°C
40°C
27°C
DECREMENT X 10⁴
EXCITATION TIME, MIN.
1.2
1.1
1.0
0.9
0.8
0.7
0.6
0.5
0.4
0.3
0.2
0.1
0
10
20
30
40
50
60
70
80
90

FIG. 27

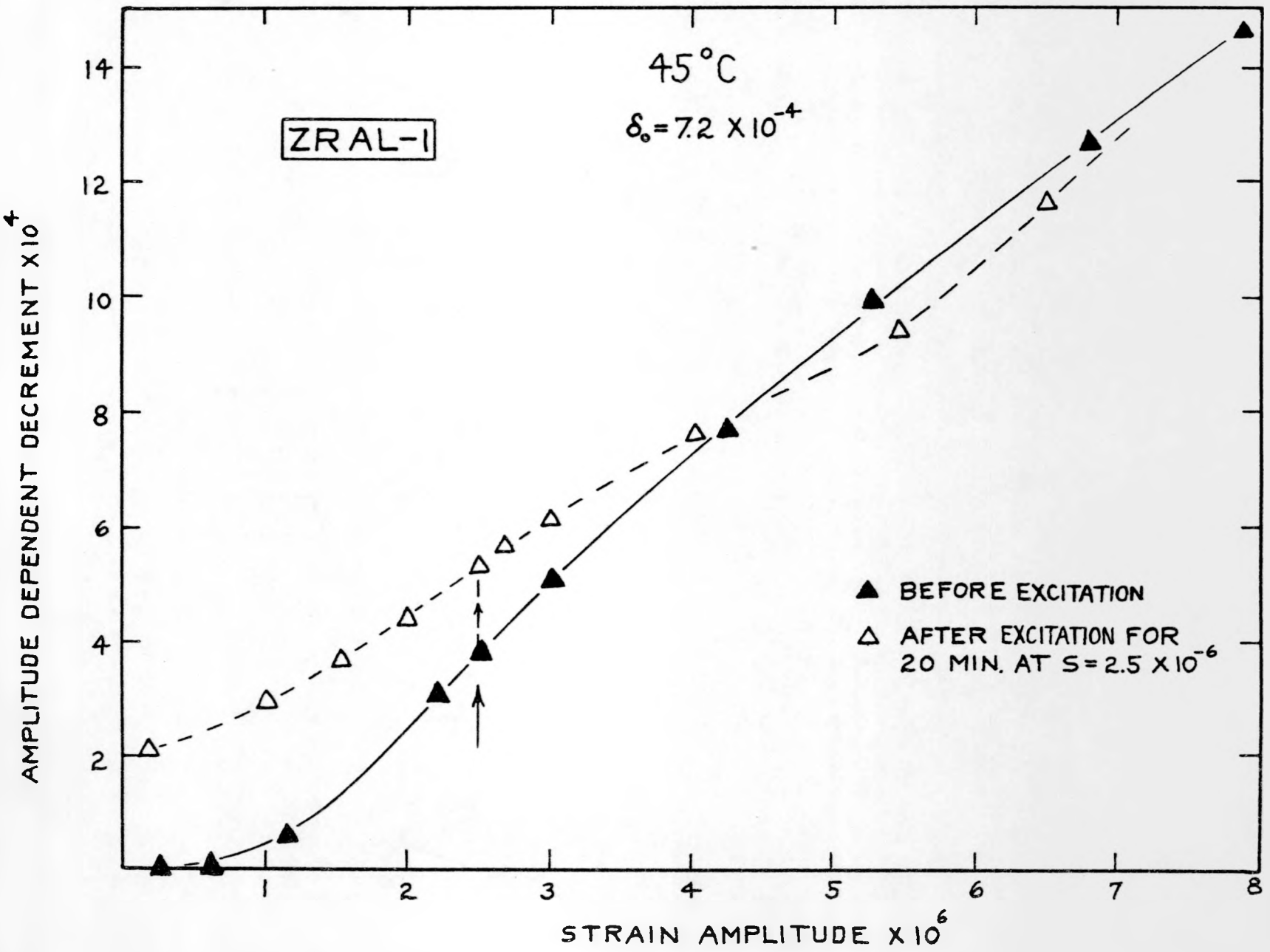
45°C
$\delta_0 = 7.2 \times 10^{-4}$
ZR AL-1
BEFORE EXCITATION
AFTER EXCITATION FOR 20 MIN. AT S = 2.5 X 10^{-6}
AMPLITUDE DEPENDENT DECREMENT X 10^{4}
STRAIN AMPLITUDE X 10^{6}
2
4
6
8
10
12
14
1
2
3
4
5
6
7
8

FIG. 28

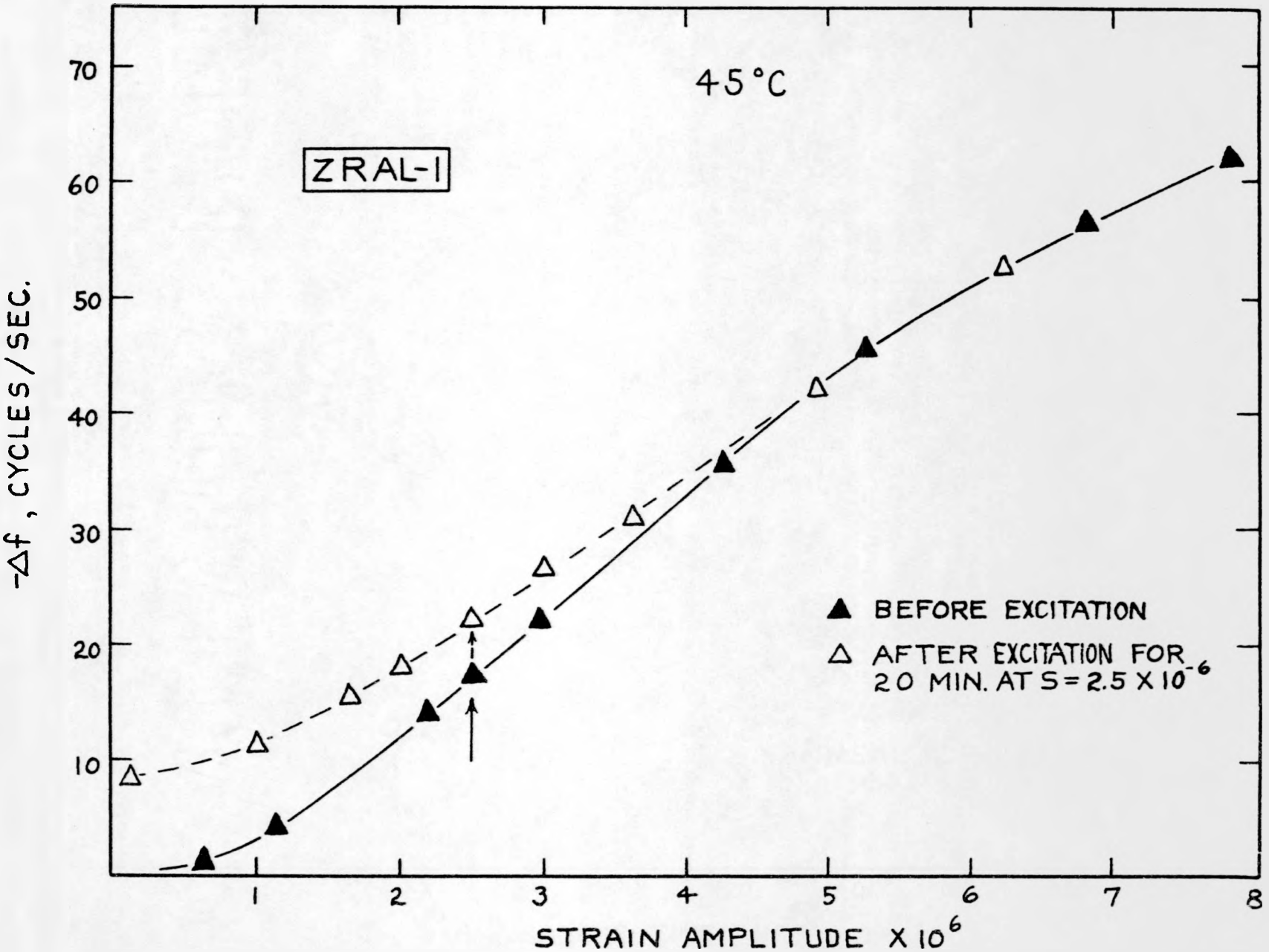
45°C
ZRAL-1
-Δf, CYCLES/SEC.
70
60
50
40
30
20
10
1
2
3
4
5
6
7
8
STRAIN AMPLITUDE X 10^6
BEFORE EXCITATION
AFTER EXCITATION FOR 20 MIN. AT S = 2.5 X 10^-6

FIG. 29

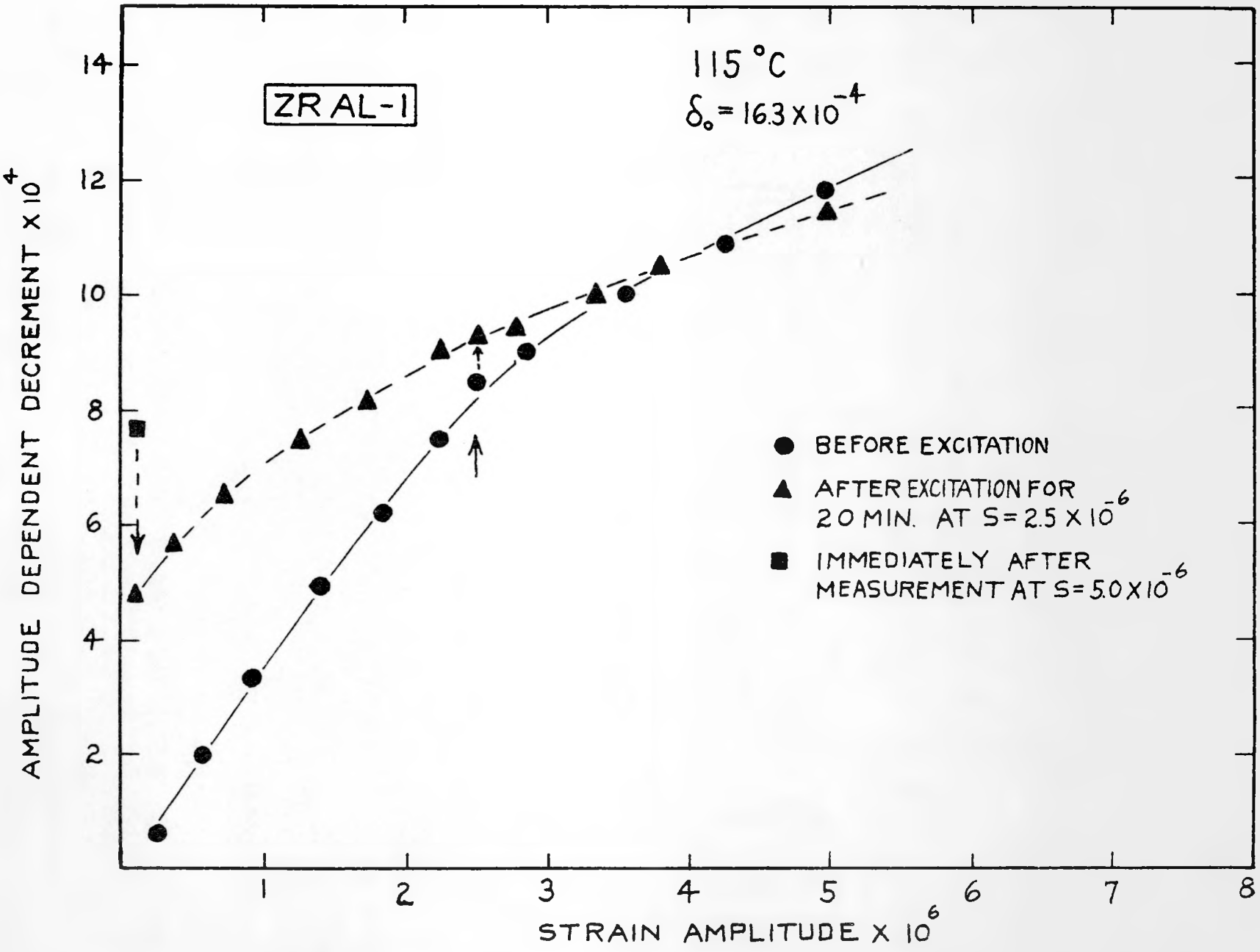
ZR AL-1
115 °C
$\delta_o = 16.3 \times 10^{-4}$
BEFORE EXCITATION
AFTER EXCITATION FOR 20 MIN. AT $S = 2.5 \times 10^{-6}$
IMMEDIATELY AFTER MEASUREMENT AT $S = 5.0 \times 10^{-6}$
AMPLITUDE DEPENDENT DECREMENT X 10^{4}
STRAIN AMPLITUDE X 10^{6}
2
4
6
8
10
12
14
1
2
3
4
5
6
7
8

FIG. 30

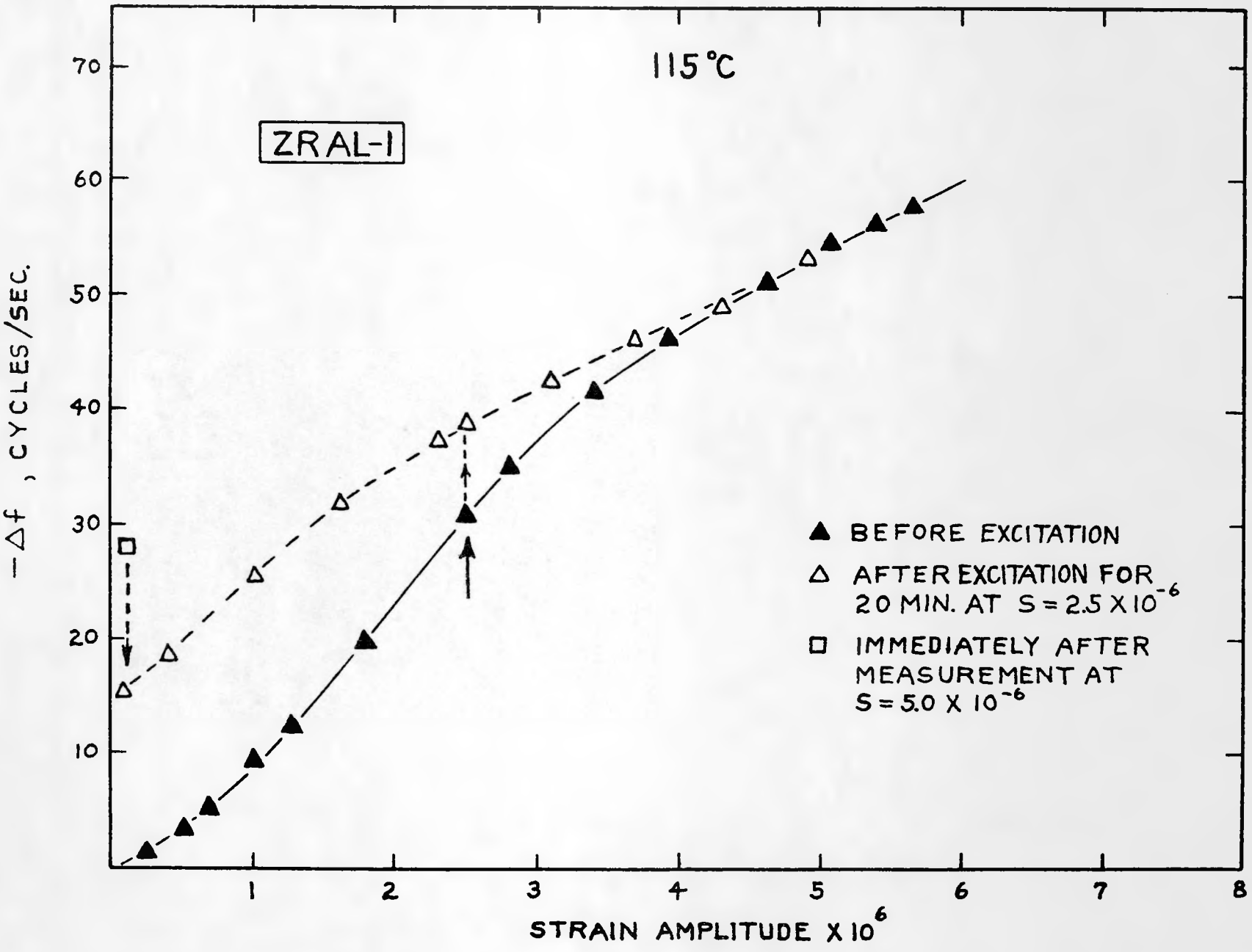
115 °C
ZRAL-1
70
60
50
40
30
20
10
$-\Delta f$, CYCLES/SEC.
1
2
3
4
5
6
7
8
STRAIN AMPLITUDE X 10^6
▲ BEFORE EXCITATION
△ AFTER EXCITATION FOR 20 MIN. AT $S = 2.5 \times 10^{-6}$
□ IMMEDIATELY AFTER MEASUREMENT AT $S = 5.0 \times 10^{-6}$

FIG. 31

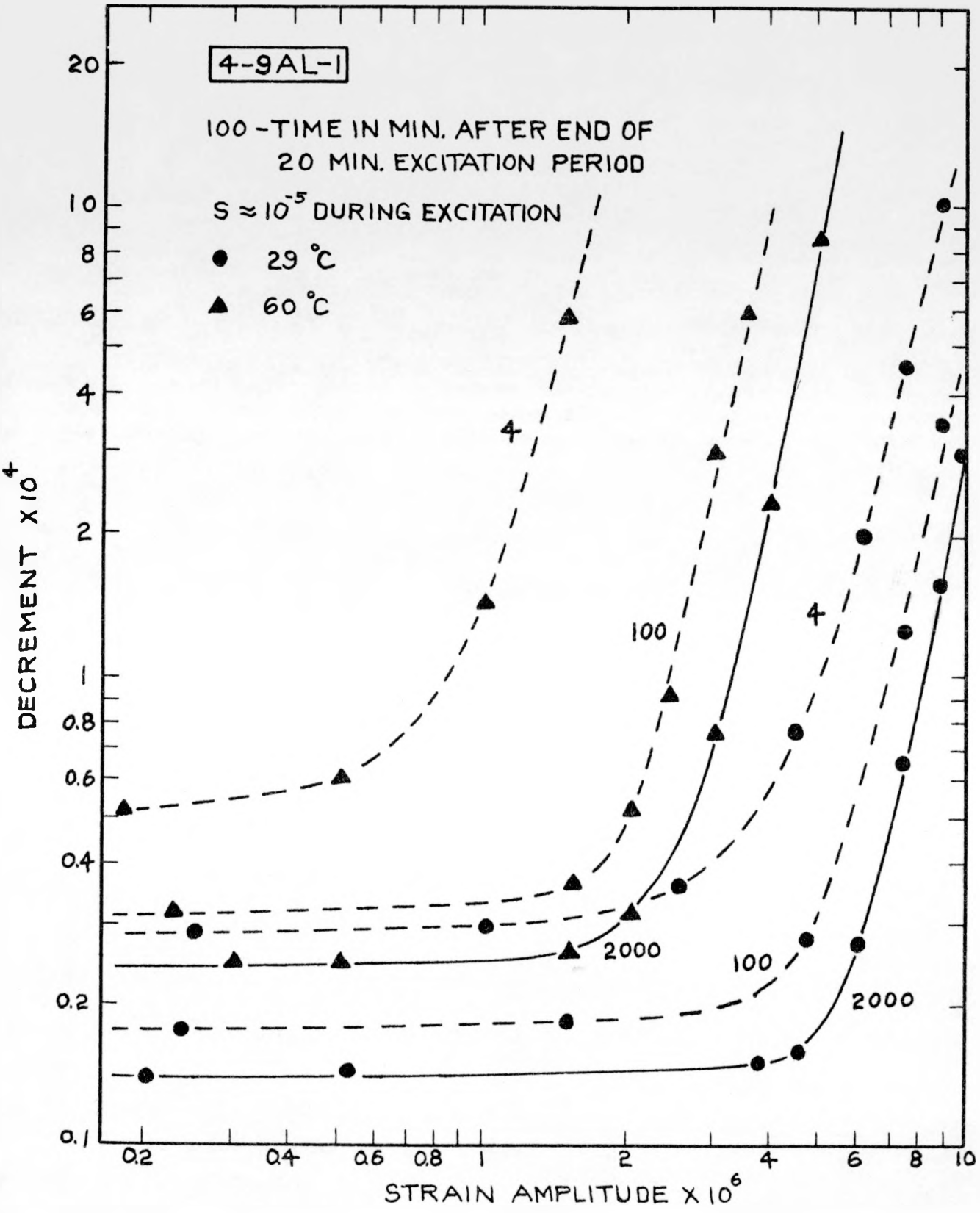
4-9AL-1
100 - TIME IN MIN. AFTER END OF 20 MIN. EXCITATION PERIOD
S ≈ 10⁻⁵ DURING EXCITATION
29 °C
60 °C
DECREMENT X 10⁴
STRAIN AMPLITUDE X 10⁶
4
100
2000
4
100
2000
20
10
8
6
4
2
1
0.8
0.6
0.4
0.2
0.1
0.2
0.4
0.6
0.8
1
2
4
6
8
10

FIG. 33

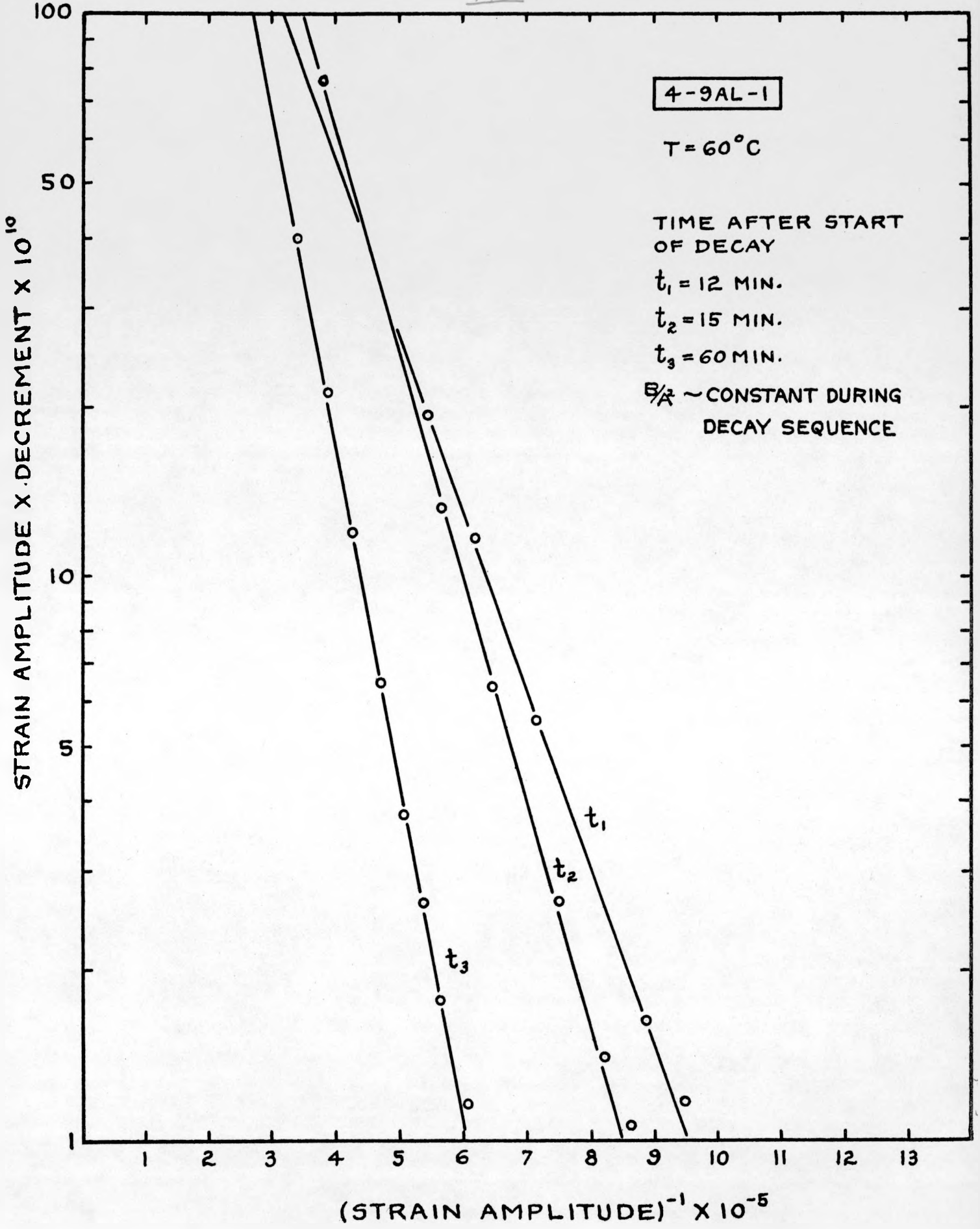
4-9AL-1
T = 60°C
TIME AFTER START OF DECAY
t_1 = 12 MIN.
t_2 = 15 MIN.
t_3 = 60 MIN.
B/A ~ CONSTANT DURING DECAY SEQUENCE
STRAIN AMPLITUDE X DECREMENT X 10^{10}
100
50
10
5
1
1 2 3 4 5 6 7 8 9 10 11 12 13
(STRAIN AMPLITUDE)$^{-1}$ X 10^{-5}
t_1
t_2
t_3

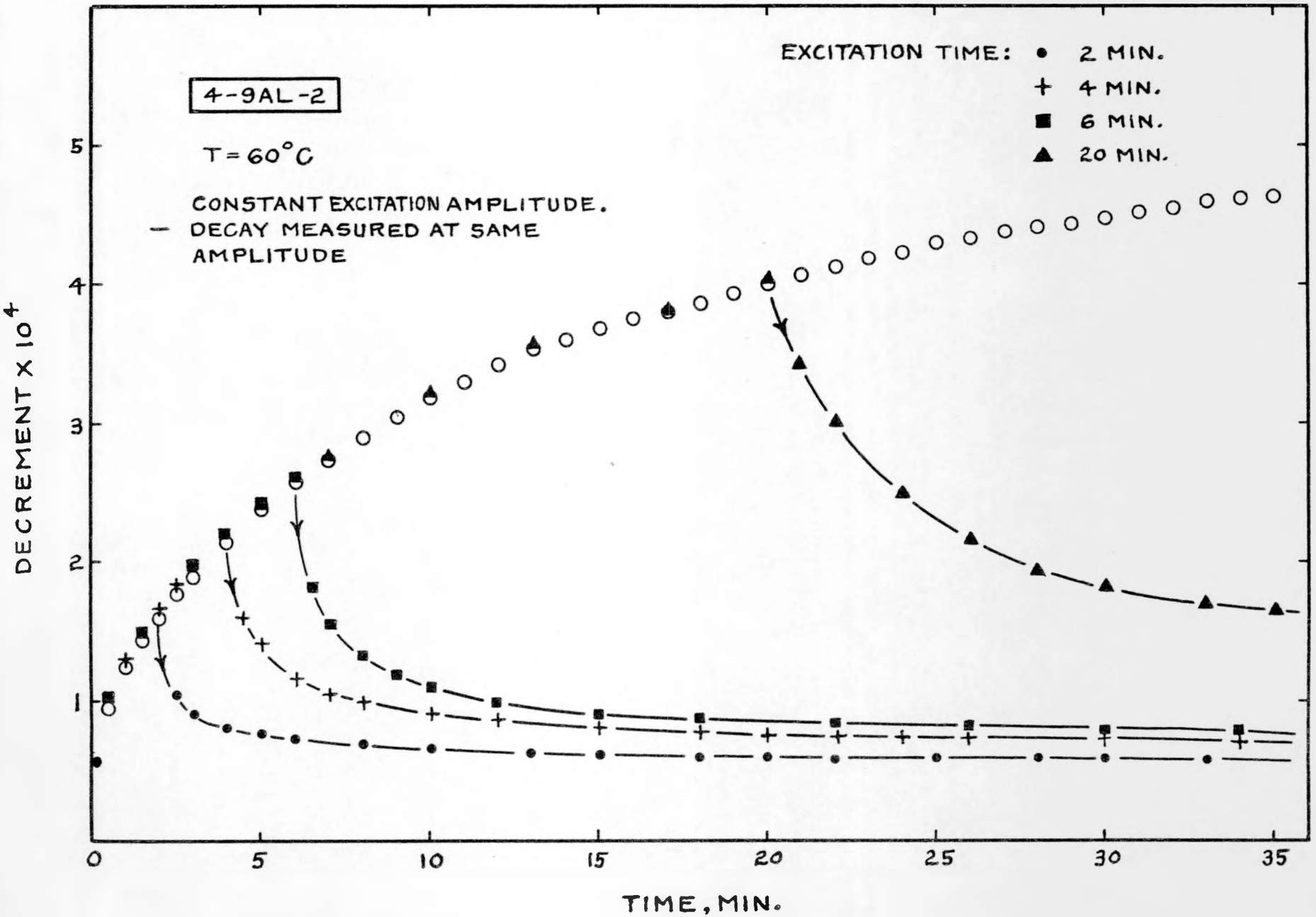
4-9AL-2
T = 60°C
CONSTANT EXCITATION AMPLITUDE.
— DECAY MEASURED AT SAME AMPLITUDE
EXCITATION TIME:
2 MIN.
4 MIN.
6 MIN.
20 MIN.
DECREMENT X 10⁴
TIME, MIN.
0
5
10
15
20
25
30
35
1
2
3
4
5

FIG. 34

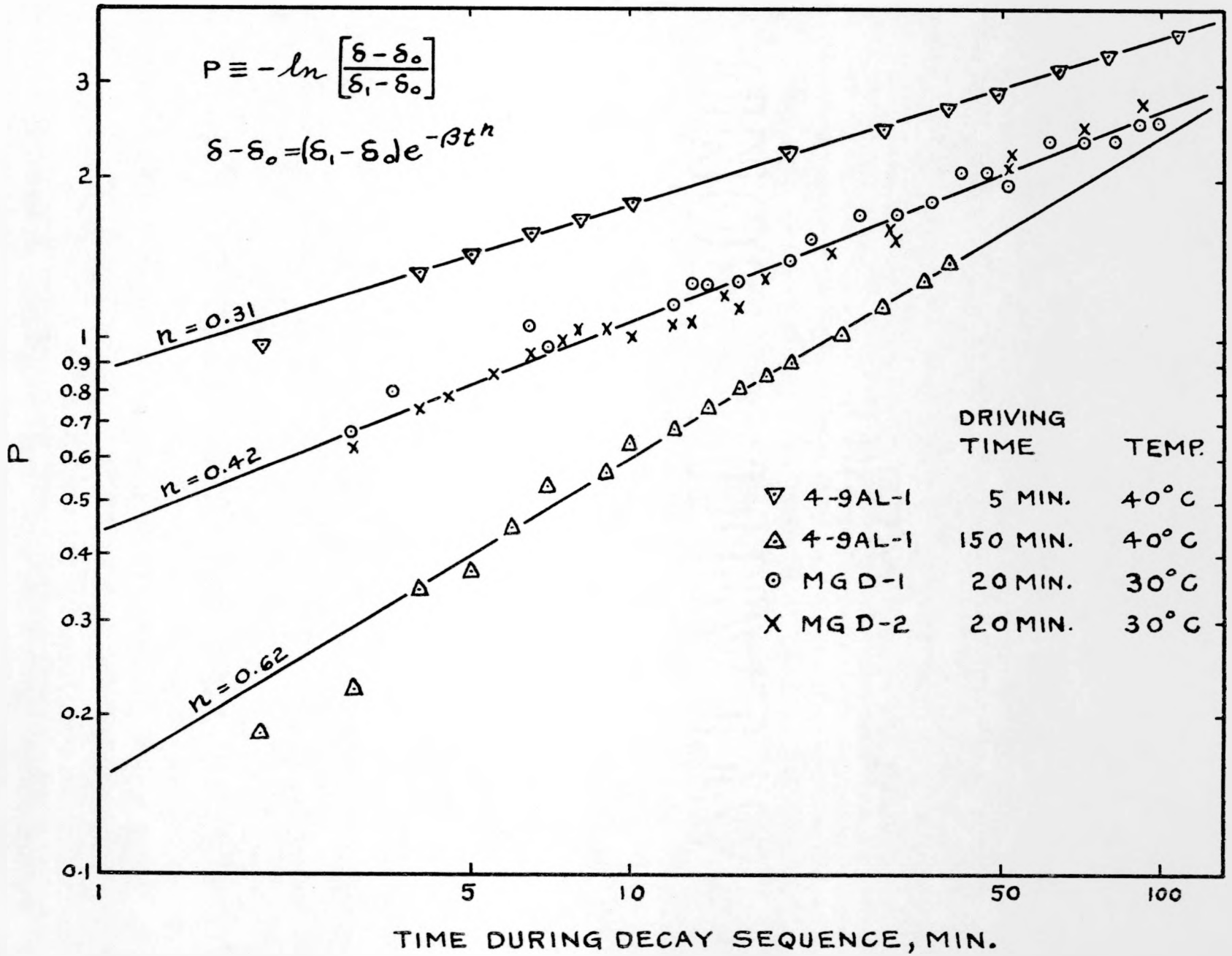
$P \equiv -\ln\left[\frac{\delta-\delta_0}{\delta_1-\delta_0}\right]$
$\delta-\delta_0=(\delta_1-\delta_0)e^{-\beta t^n}$
n = 0.31
n = 0.42
n = 0.62
P
3
2
1
0.9
0.8
0.7
0.6
0.5
0.4
0.3
0.2
0.1
1
5
10
50
100
TIME DURING DECAY SEQUENCE, MIN.
DRIVING TIME
TEMP.
4-9AL-1 5 MIN. 40°C
4-9AL-1 150 MIN. 40°C
MG D-1 20 MIN. 30°C
MG D-2 20 MIN. 30°C

FIG. 35

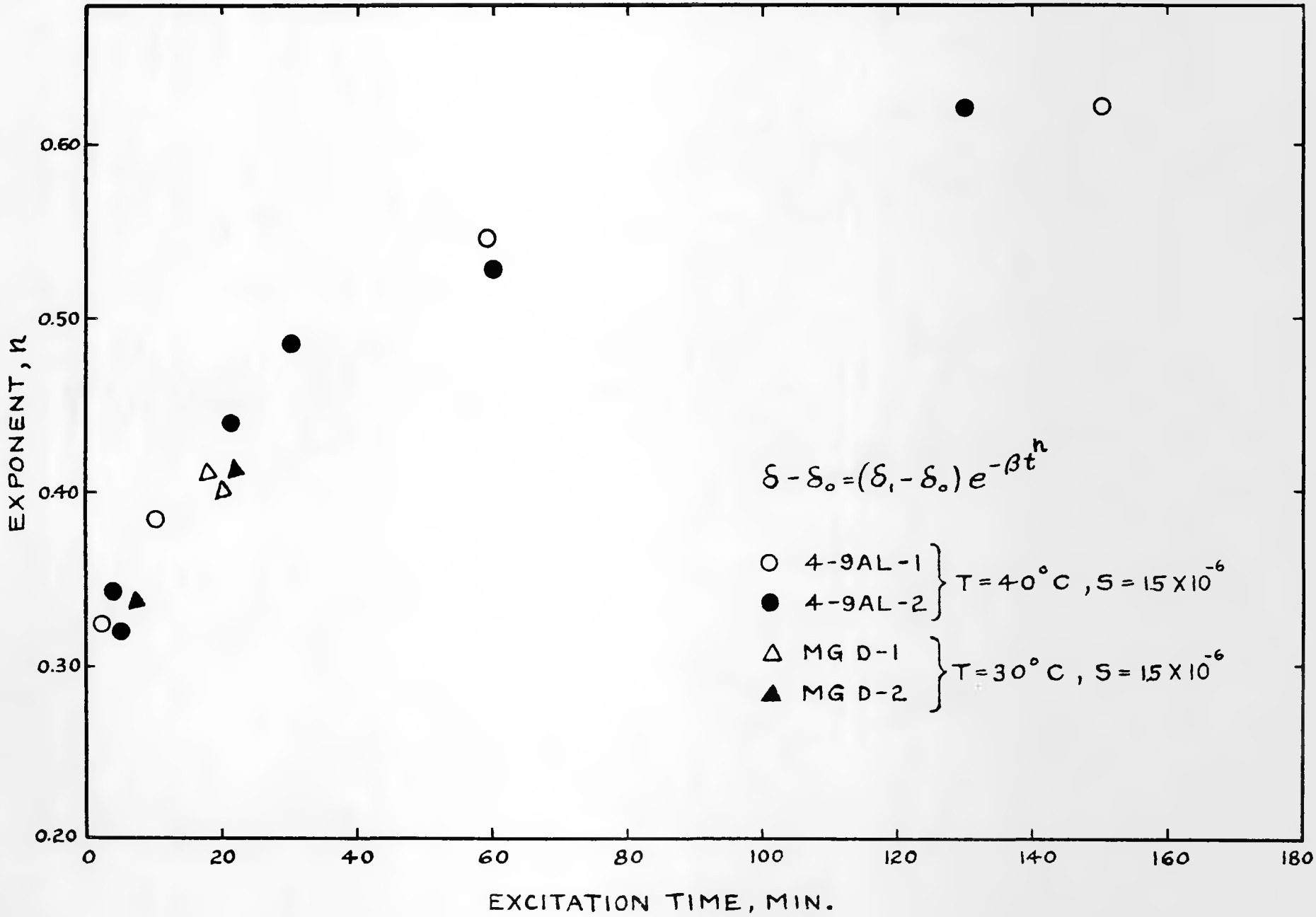
EXPONENT, n
0.60
0.50
0.40
0.30
0.20
0
20
40
60
80
100
120
140
160
180
EXCITATION TIME, MIN.
$\delta - \delta_o = (\delta_1 - \delta_o) e^{-\beta t^n}$
○ 4-9AL-1
● 4-9AL-2
T = 40°C, S = 1.5 X 10⁻⁶
△ MG D-1
▲ MG D-2
T = 30°C, S = 1.5 X 10⁻⁶

FIG. 36

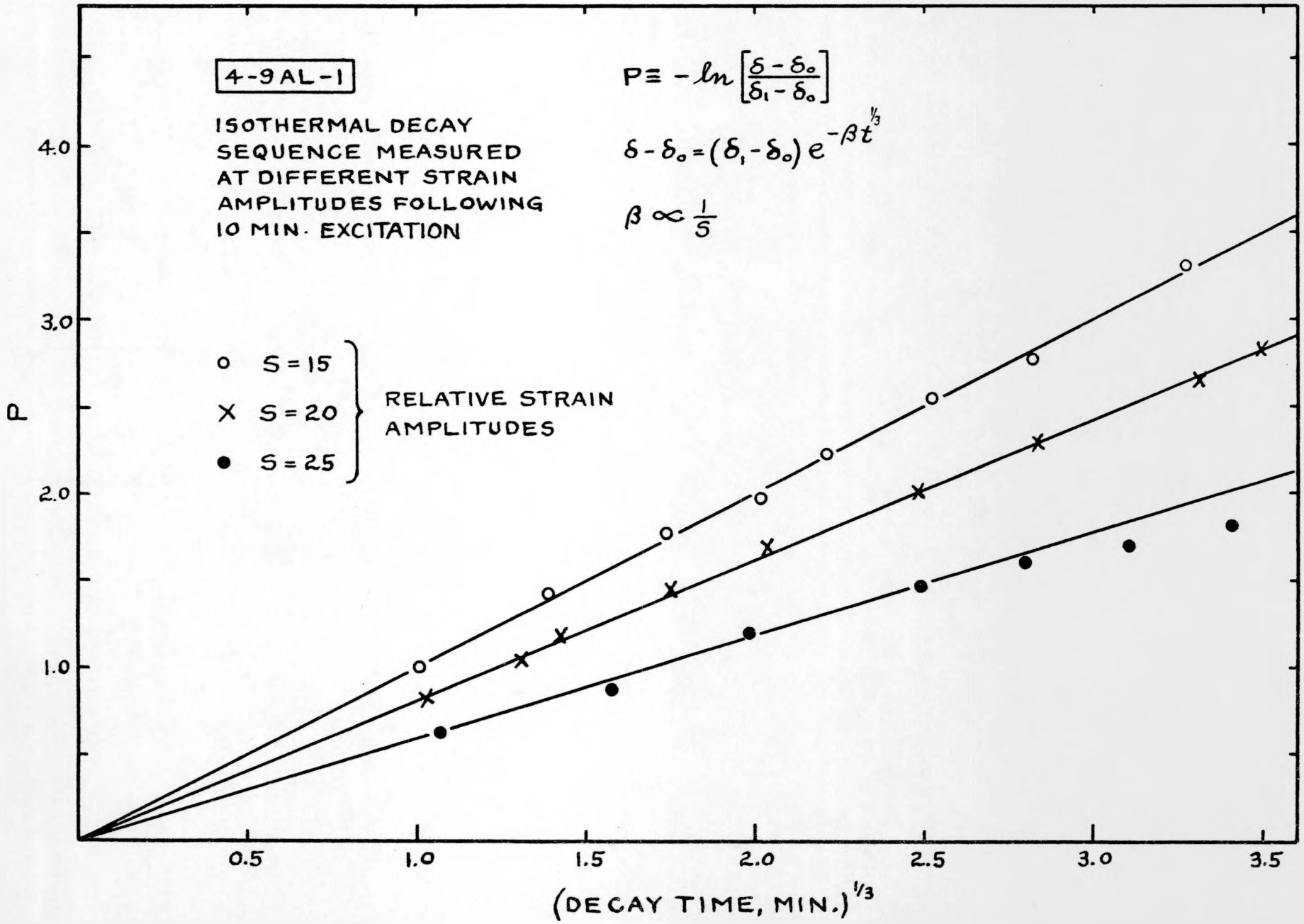
4-9AL-1
ISOTHERMAL DECAY SEQUENCE MEASURED AT DIFFERENT STRAIN AMPLITUDES FOLLOWING 10 MIN. EXCITATION
$P \equiv -\ln\left[\frac{\delta-\delta_o}{\delta_1-\delta_o}\right]$
$\delta-\delta_o=(\delta_1-\delta_o)\,e^{-\beta t^{1/3}}$
$\beta \propto \frac{1}{S}$
o S = 15
X S = 20
● S = 25
RELATIVE STRAIN AMPLITUDES
P
4.0
3.0
2.0
1.0
0.5
1.0
1.5
2.0
2.5
3.0
3.5
(DECAY TIME, MIN.)$^{1/3}$

FIG. 37

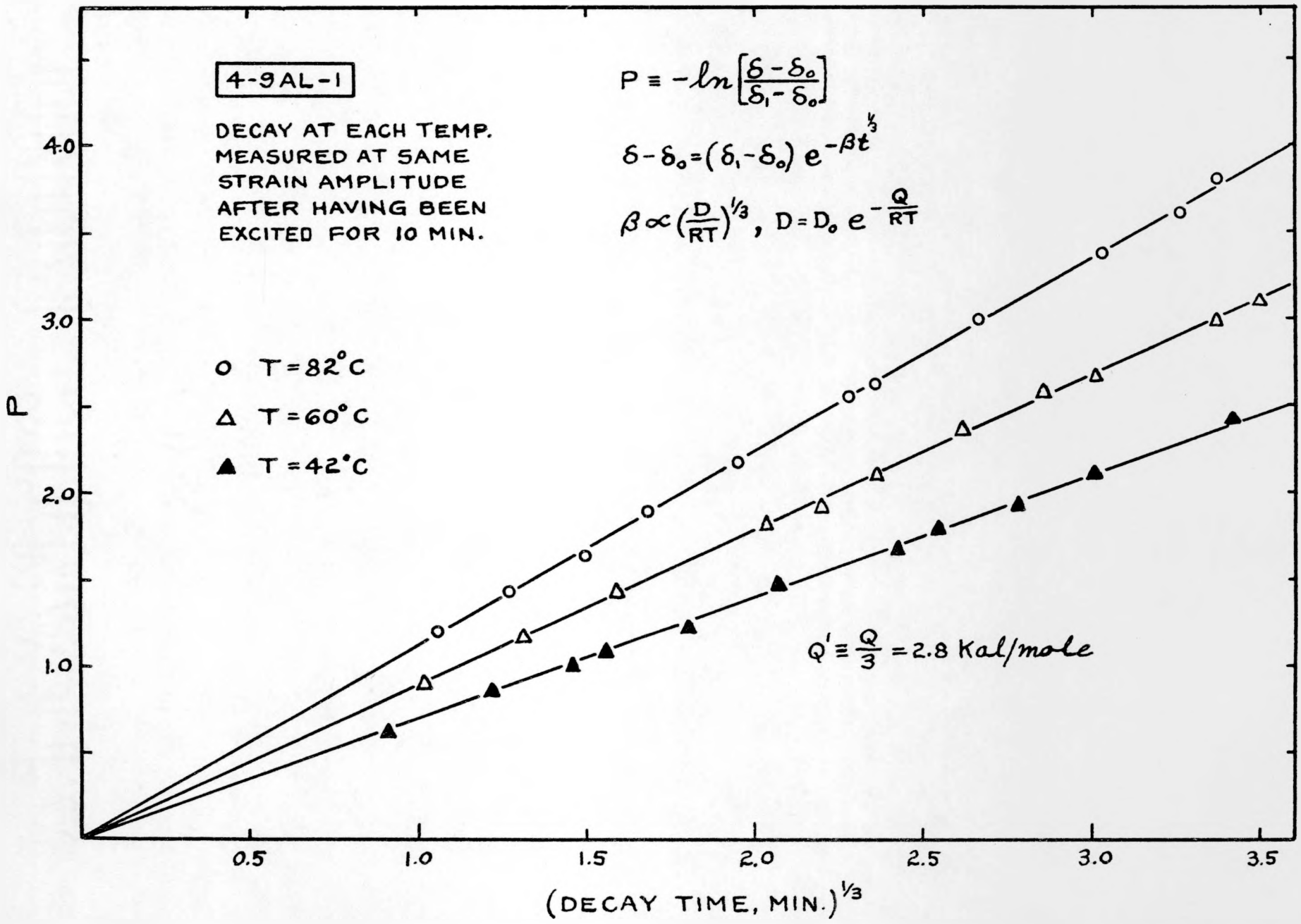
4-9AL-1
DECAY AT EACH TEMP. MEASURED AT SAME STRAIN AMPLITUDE AFTER HAVING BEEN EXCITED FOR 10 MIN.
$P \equiv -\ln\left[\frac{\delta-\delta_o}{\delta_1-\delta_o}\right]$
$\delta-\delta_o=(\delta_1-\delta_o)\,e^{-\beta t^{1/3}}$
$\beta \propto \left(\frac{D}{RT}\right)^{1/3}$, $D=D_o\,e^{-\frac{Q}{RT}}$
o T=82°C
Δ T=60°C
▲ T=42°C
$Q' \equiv \frac{Q}{3}$ = 2.8 Kal/mole
P
4.0
3.0
2.0
1.0
0.5
1.0
1.5
2.0
2.5
3.0
3.5
(DECAY TIME, MIN.)$^{1/3}$

FIG. 38